Master of Science by Research
University of Kent
The School of Physical Sciences

DEVELOPMENT OF ATP-PAGE FOR PROTEIN ANALYSIS

BY ELISABETTA BERTONI

Submitted in fulfilment of the degree of Master of Science by Research

October 2019

Table of Contents

ABSTRACT

This thesis reports the development of a new technique: adenosine triphosphate (ATP) polyacrylamide gel electrophoresis (PAGE). A widely used technique for the analysis of proteins and DNA, PAGE methodology has remained largely the same since its introduction. The aim of this research is to attempt to replace sodium dodecyl sulfate (SDS) with ATP, with the objective of yielding more comprehensive results, and widening the range of applications of this technique. From the literature, some proteins such as lysozyme and RNAse A have been found to give inconsistent results with SDS PAGE. Therefore, a streamlined method for these proteins would be valuable to achieve good, consistent results. Furthermore, an established ATP-PAGE could lead to applications within biochemistry: increased detail on the ability and quality of protein-protein interactions being seen from the gel itself. ATP could be used as a hydrotrope to allow solubilisation of otherwise poorly solubilising proteins, therefore expanding the applications of this technique. The work presented here aimed to characterise the proteins chosen first, and then the gels used. The ATP was replaced not only in the protein sample preparation, but also in the buffers used and within the gel structure. It was therefore necessary to also investigate how ATP affected the gels' properties. The proteins chosen for this project were glutathione-S-transferase (GST), bovine serum albumin (BSA), β - lactoglobulin (BLG), insulin (INS), RNAse A and lysozyme (LYZ). ATP is thought to interact with these proteins via hydrophobic interactions or by binding to the positive surface charges. Computational studies using "Chimera" software were successfully conducted to map the hydrophobic and positive surface areas and identify the proteins with the best chance of interacting: these were found to be insulin and RNAse A. Dynamic light scattering (DLS) and zeta potential studies were useful in providing insight into the behaviour of the proteins in solution, although some results were thwarted by protein agglomeration and poor sample preparation. Circular dichroism studies were conducted: these results showed ATP

presented peaks similar to β-sheet structures. This result was key into giving insight as to how ATP must be analysed with this technique. Rheometry was carried out to compare viscoelastic characteristics of polyacrylamide gels made in buffers containing ATP, sodium dodecyl sulfate (SDS) and only Tris-HCl. ATP gels which were left to polymerise overnight showed similar results to SDS gels. To visualise the changes in gel formation, scanning electron microscopy (SEM) was carried out. This showed relevant variations in the mesh formed by the crosslinking of acrylamide and bisacrylamide, core process of polyacrylamide gel formation. Most importantly, gel electrophoresis was tested under different conditions: native, SDS and ATP. The most successful results were seen with ATP samples in native gels, with otherwise difficult to visualise proteins seen. Similarly, ATP samples with ATP gels showed the most positive results, indicating ATP could be used as a replacement for SDS. However, there is need for further testing on different proteins, before this method may be used universally. Lysozyme was still poorly viewed with ATP-PAGE, therefore prioritising proteins with a high isoelectric point would be ideal.

ACKNOWLEDGEMENTS

Firstly, I would like to thank the University of Kent for a wonderful 5 years of learning opportunities and friendships.

I would like to express gratitude to Dr. Chris Serpell for the opportunity to take part in this research, and to the whole Serpell Research Group for being a constant source of support, ideas and laughter.

I would like to thank to Dr. Aniello Palma for his suggestions and guidance with the computational studies using the Chimera software, as well as different approaches to my project.

I would like to acknowledge Dr. Alison Edwards at the University of Kent at Medway for her invaluable help with Circular Dichroism.

Lastly, I would like to thank my wonderful family for the love and opportunity of pursuing my education abroad, and my dearest friends for the much-needed support.

LIST OF ABBREVIATIONS

% = Percentage

°C = Degrees Celsius

µL = Microlitre

µM = Micromolar

2D = Two dimensional

3D = Three dimensional

2-mercaptoethanol = β-mercaptoethanol

 - Potential = Zeta Potential

AMP = Adenosine Monophosphate

ATP = Adenosine Triphosphate

APS = Ammonium Persulfate

Beta LG = β - Lactoglobulin

BSA = Bovine Serum Albumin

CD = Circular Dichroism

CL = Cell Lysate

cm = Centimetre

Den = Denatured

DLS = Dynamic Light Scattering

DNA = Deoxyribose nucleic acid

EDX = Energy Dispersive X-Ray

G’ = Storage Modulus

G’’ = Loss Modulus

GSH = Reduced L-Gluthathione

GST = Gluthathione S-Transferase

HCl = Hydrochloric acid

INS = Insulin

kDa= Kilodalton

L-Dye = Loading Dye

LYZ = Lysozyme

mAmps = Milliamps

$Mg(OAc)_2$ = Magnesium acetate

Nm = Nanometre

PA = Polyacrylamide

PAGE = Polyacrylamide Gel Electrophoresis

PBS = Phosphate – buffered saline

PDB = Protein Data Bank

Red. = Reduced

RNA = Ribonucleic acid

RNAse= RNAse A

pI = Isoelectric Point

SDS = Sodium dodecyl sulfate

SEM = Scanning Electron Microscope

TBE = Tris borate EDTA

TEMED = Tetramethylethylenediamine

V = Voltage

CHAPTER 1: INTRODUCTION

The analysis of biological molecules is of paramount interest in the scientific world. Ranging from characterisation of protein standards to the comparison of DNA profiles in criminal cases, scrutiny of various biomolecules is essential. Proteins are a large class of molecules which play vital roles within the body: cell support, messenger and immune response among others.[1] Formed by subunits named amino acids, proteins are composed of specific sequences of amino which ultimately determine their structure and function. Within a human body, proteins are coded by protein coding genes, which are estimated to number 20,000.[2] Collating the human genome by mapping the proteins for which it codes – the proteome – has been of recent interest. This has been attempted using mass spectrometry, mainly for the advancement of biomedical research.[3] Specific regions of the proteome can be used as biomarkers to identify different diseases. In recent years this has been done to identify risks of cancer development, and to monitor the possible immune response to the proposed therapy.[4] These studies show how interlinked the function of proteins and the healthy functioning of the body is. To further this research, however, there must be a clear understanding of the structural composition of the proteins in question. Each of the proteins chosen in this project have a key function within the body. Some of these functions affect health, whereas others are involved solely in chemical processes.

Numerous methods exist for the characterisation of molecules. Characterisation involves determining concentration, purity, identity, shape, size and in the case of proteins, sequence of a sample in 2D and 3D structures. This information is key for determining the role or function of any molecule. Especially when researching efficiency of a molecule, characterising the results is vital for ascertaining the quality of the product. Therefore, the efficiency and reliability of all the methods listed above needs to be as high as possible and improving the analytical techniques will always be a necessity. For this reason, investigating different methods which may be more efficient is important. The most common methods specific for protein analysis can be seen in Figure 1.[5] These have been in use for many

years with little to no modification, as they yield good results. Electrophoresis is a method which contains several components, which may be interchanged. Below, a method for how it may be revised is described.

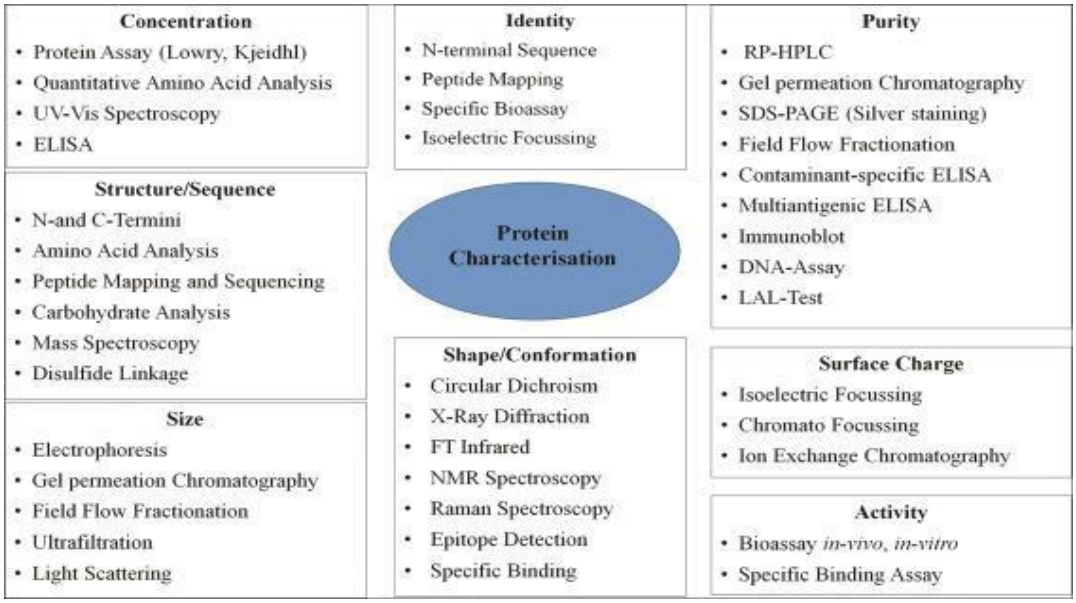

Figure 1: Widely used methods of protein characterisation, divided by property being analysed. Electrophoresis, the technique being used in this research, is crucial as it has various applications, such as size separation and purity. Furthermore, analysis of the shape and surface charge of the proteins sheds light on how effectively they will be separated in PAGE. This background information is necessary for method development.

METHODS AND APPLICATIONS OF ELECTROPHORESIS

The use of electrophoretic methods for analysing biological molecules has been a widespread technique for decades. Utilising the intrinsic charges found on the analytes, the principle of electrophoresis is defined as “the migration and separation of charged particles (ions) under the influence of an electric field”.[6] This may either happen using a gel slab medium (see Figure 4) - or a capillary tube - capillary electrophoresis, where the gel is contained within the tube. Both techniques will have an applied electric field. The migration velocity (w_k, cm/s) of the particle is proportional to the applied field strength. The distance travelled by the analyte molecule is used to estimate many different characteristics; the experimental value collected of degree of migration can be compared to a reference standard named electrophoretic mobility (μ). These values may uncover physical properties such as molecular weight[7], purity, subunit structure and, in the case of proteins, the amino

acid sequence.[8] Capillary electrophoresis is also used to sequence DNA and is the primary method of DNA analysis in Forensic Science. Similarly, the chain length of single and double stranded DNA may be estimated.[9] Furthermore, mobility values can be used to calculate molecular radius and electrophoretic mobility of the analyte, or the radius and total length of the polypeptide chain.[10] However, some variations of gel electrophoresis have been reported to be essential for other applications, such as medicinal chemistry.[4] Some variations of PAGE have been proven to be a valid detector in viroid research. Similarly, 2D Difference GE (2D-DIGE) – a technique created from PAGE- has been found to be useful in locating cancer biomarkers in the genome.[11] This is due to its high resolution, combined with a high sensitivity.[11] The main gel matrices for electrophoresis include the use of agar, agarose and most commonly polyacrylamide. These have been found to be essential when separating proteins, nucleic acids and DNA/RNA molecules above others.

Prior to the introduction of PAGE in the 1960's, commonly used methods included agar (formed by agarose and agaropectin) or only agarose gel electrophoresis. Both methods were considered effective, until it was understood the charges carried by these media interfered with the analysis of the molecules themselves. As mentioned before, the principle of electrophoresis is that of using the charges found on an analyte to form a flow of migration, from a negative electrode to a positive electrode. In turn, the distances travelled will give information on different physical properties. If, however, the gelling agents used carry an electric charge themselves, this may cause variations in the migration. For example, agaropectin was found to have a fixed negative charge, which caused a bulk liquid flow towards the cathode ("Electroendosmotic effect"-EEO).[12] Analogously, agarose carries a slight negative electric charge, due to the pyruvic acid and sulfate components[12].

Additionally, the pores formed through polymerization of the agarose monomers are considered too large for many analytes.[12] In comparison, PAGE does not undergo EEO, has variable pore sizes and does not carry specific charges which may let it react with the environment.[12] For these reasons it has become the most widely used method, as it also provides opportunity for easy customisation to different experimental needs. Since its

introduction in the 1970s, the method has progressed to using different modifications, such as SDS-PAGE, the setup can be seen in Figure 2.[13] This method separates proteins only by polypeptide chain length. SDS PAGE is useful for analysing a large range of protein size, as the concentration of acrylamide introduced will limit the pore size of the mesh created. This method allows for a wide range of experiments. However, some proteins below the size of 20 kDa are not separated correctly and require prior manipulation. Below 5 kDa results are poor but can yield an estimate of where the molecular weight lies between 1-5 kDa.[8]

SDS is a polar molecule with a polar hydrophobic head and non-polar alkyl chain, giving it amphiphilic properties, which allows it to have numerous applications such as in detergents, cosmetic and food products. This property allows SDS to bind to proteins and unravel them. The mechanism in which this occurs (Figure 3) is referred to as “beads on a string” due to the fashion as to which the micelles (the beads) bind to the protein (the string), in this case bovine acetyl coenzyme A (ACBP). The red dots are a representation of the hydrophobic tails that can be seen in Figure 3, whereas the green dots show hydrophilic heads.[14]

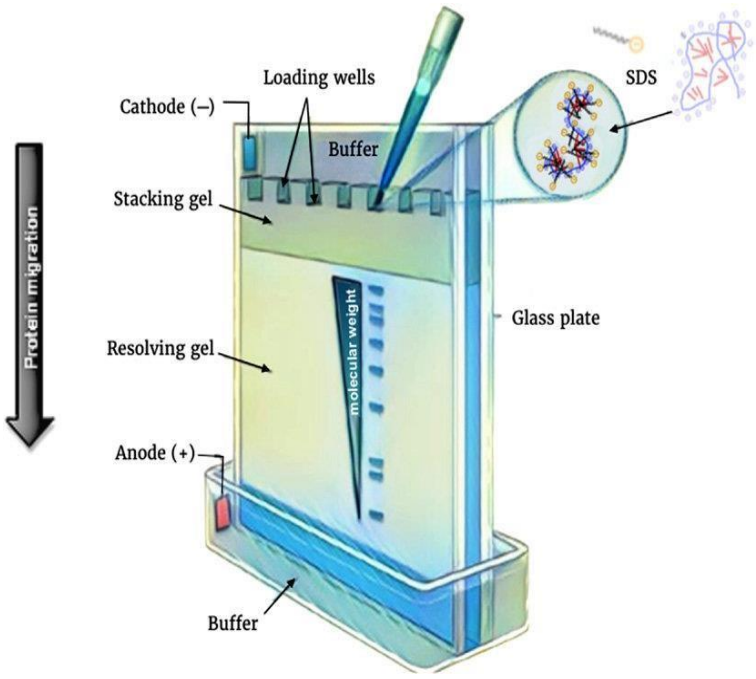

Figure 2: Diagram of typical SDS-PAGE setup. This research aims to replace SDS with ATP both in the gel structure, the buffers used, and within the sample. The objective is to yield more successful separation across all types of proteins, such as those with a small molecular weight.

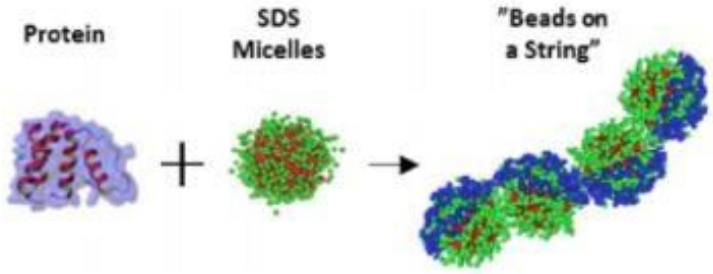

Figure 3: Micelle Formation of SDS on a protein as shown by Kachuck. The micelle attachment process described above leads to the unravelling of the protein, in this example case bovine acetyl coenzyme A (ACBP). This process is essential to the success of SDS-PAGE: macromolecules of all shapes and sizes are successfully separated and analysed.

ATP: ROLE AND FUNCTIONS

As discussed above, SDS-PAGE is a successful method, with the main caveat being the proteins are denatured in the process (Fig. 3). Investigating non denaturing pathways is therefore valuable. ATP is an essential chemical for the body. Besides its most widely known role in driving metabolic pathways, it provides the energy to perform functions necessary such as muscle movement, vasoconstriction, neuro and immuno-modulation.[15] It is involved in platelet aggregation during blood clotting, and research shows it is released in the lungs as a result of shock.[16] In combination with various antioxidants, ATP has been shown to be effective as radiation therapy to improve post-irradiation survival.[17] Additionally, ATP has a principal role in signalling for many diseases and infections to create an appropriate immune response, such as organ transplants and extracellular interactions between a host and tumour cell.[18] Recent studies have shown ATP concentration in the cell to be linked with neurodegenerative diseases, as they have been shown to occur as a consequence of a decrease in concentration of ATP[19] and cell fluidity, which declines with age. Similarly, a reduction in adenine nucleotides has been linked to depression and schizophrenia.[20] Moreover, it also functions as a transporter for molecules, cell signalling, molecule synthesis, and as a response mechanism between individual organs and the brain.

In a strictly chemical and physical context, the composition of ATP has been scrutinised to uncover if there are other functions linked to its structure. Characteristics such as polarity, hydrophilicity and lipophilicity have been studied to ascertain whether ATP may act as a surfactant, or if it may conjugate to form different conformations. Figure 4 shows the structure of ATP. Due to the phosphate groups having a pKa close to 0, at neutral pH ATP will carry a negative charge[21]; similarly, SDS is an anionic surfactant and therefore carries a negative charge. Charges present on the molecule may be stabilised using salts, most commonly that of Mg^{2+}.[22] The relative negative charge should allow for movement of any analyte towards the anode without causing denaturation, as the ATP molecules are expected to coat the protein without altering its conformation. This is postulated as ATP is a biological component found in high concentrations in the body, and if it were to be a denaturant, it would prevent proteins operating properly.

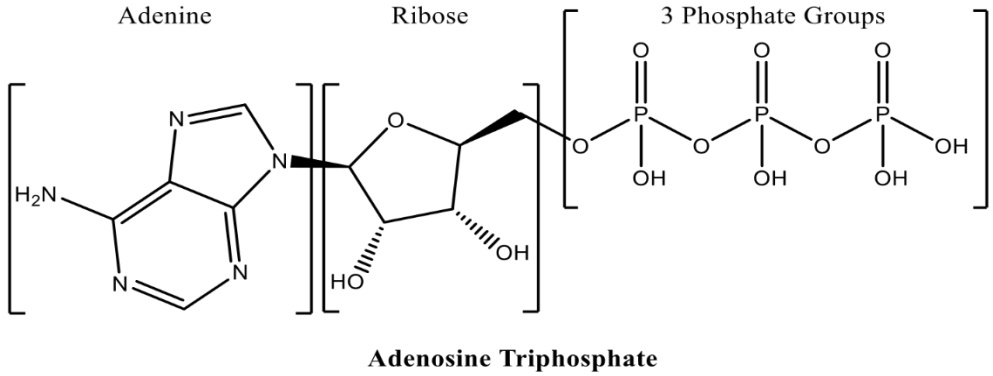

Figure 4: This figure describes the structure of ATP. At neutral pH, the phosphate groups carry a negative charge, similar to that of the non- polar alkyl chain found in SDS. This negative charge would be harnessed to allow protein movement in PAGE without altering the protein structure.

ATP AS AN AMPHIPHILE

Amphiphiles are molecules defined as containing both hydrophobic – non-polar - and hydrophilic -polar- regions.[23] In the case of ATP, the phosphate chain is negatively charged and hydrophilic. The adenine group, acting similarly to the polar group on an SDS molecule, is relatively hydrophobic. Amphiphilicity has been shown to be a necessary trait for surfactants, which are molecules which reduce interfacial tension, and tend to aggregate at

interfaces rather than in bulk.[24] Amphiphilic molecules may form larger organized aggregates. Among others, arrangements may be either in layers or micelles. From the literature, ATP tends to form layers as opposed to micelles: this has been described as "sandwiching" between dimers. On the other hand, SDS is known to form micelles, as it is formed by a much longer alkyl chain (Figure 5).[25] Provided it reaches its critical micelle concentration (CMC) of 8.0×10^{-3} mol/L[26] when in solution, SDS will form micelles.[27]

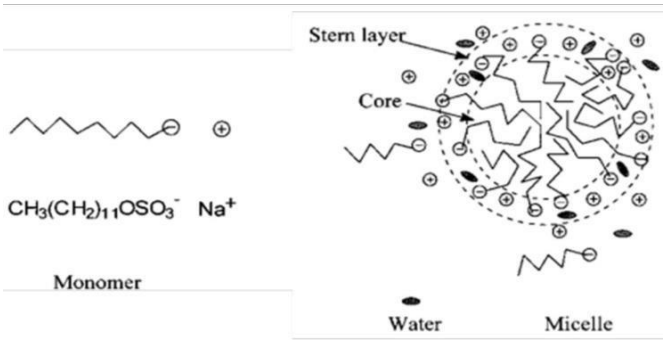

Figure 5: SDS micelle conformation. Good micelle formation at an identified CMC allows SDS to be widely used as a surfactant, and as seen above, the ability of SDS to form micelles and use these to denature proteins is a documented process.

It is thought ATP cannot form micelles as it is also a hydrotrope, meaning the role is to increase solubility. This increase may therefore interfere with the formation of a smaller organized structure such as micelles.[28]

ATP AS A HYDROTROPE

Hydrotropes are amphiphiles which cannot form micelles, but which may increase solubility of various molecules in water.[29] Typically, they are formed from a hydrocarbon ring and an ionic component.[29] Common hydrotropes may be seen in Figure 6 below, as discussed by Dhapte.[30] Although they may have many different arrangements, the same hydrotropic character may be seen in the ATP molecule: the ribose and adenine may take the place of the hydrophobic ring system, whereas the phosphate chain is the ionic counterpart. Hydrotropes differ from surfactants in that the hydrophobic region will not be sufficient to form organized structures such as micelles.[29]

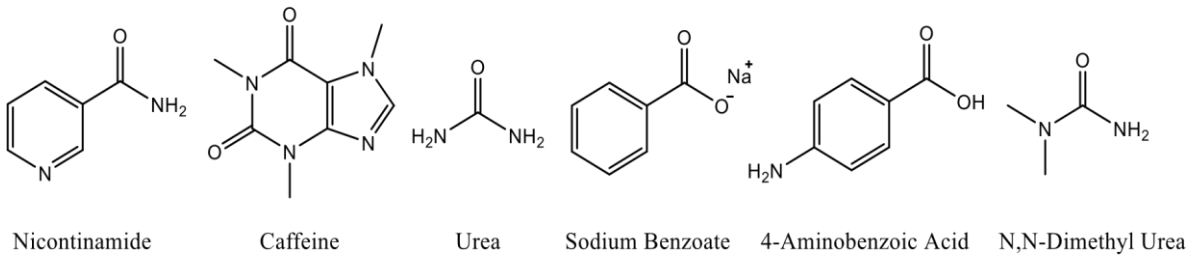

Figure 6: Commonly used hydrotropes. These molecules are used to increase solubility of other compounds in water. The similar structure of a hydrocarbon ring with an ionic component is seen with ATP: the ribose and adenine reflecting the ring and the phosphate groups as the ionic component. For this reason, ATP has been investigated in literature as a hydrotrope with some success.

Therefore, ATP is shown in the literature to be a hydrotrope but not a surfactant. The molecular structure difference between a hydrotrope and a surfactant remains unclear, and the varying factor remains the supramolecular arrangements it forms. When hydrotropes and surfactants are combined, the hydrotrope will smoothen the transition between phases. This combination has been shown to drive and combine the growth of two separate micellar phases.[29]

Within the cell itself, ATP has been reported to be present in high concentrations of 1 to 10 mmol/L[31] to maintain normal cellular function. As mentioned before, this is likely to occur to prevent proteins from aggregating, in addition to use as an energy source. According to findings published by Patel[5], the adenosine ring enhances the triphosphates' ability to stabilise proteins. On the other hand, the ribose ring forms clusters around other molecules to stabilise them in solution.[5] Though the exact process through which this occurs in unclear, due to this hypothesis it is thought ATP may act as a surfactant. ATP may attach to the surface of the molecule of interest in the same manner as how SDS attaches to the unravelled protein in SDS-PAGE. ATP would be able to form a cluster around the integral protein, giving it the charge needed for electrophoresis to occur. We reason that the protein should remain in the native state as ATP has not been shown to denature proteins in vivo, as this would cause many malfunctions in the body. Therefore, although it is not found in the literature, it can be hypothesised ATP in fact acts both a hydrotrope and a surfactant. There is little evidence as to how ATP's role as an amphiphile affects its other functions, however it is believed to be necessary for keeping the environment within the cell stable

and avoiding aggregation of other proteins.[32] In particular, it is seen to be a possible explanation as to why there is usually a higher concentration of it in the cell than needed. Depletion of ATP has shown to reduce mobility within the cytoplasm, which becomes less liquid.[17] Therefore, a high concentration of ATP is needed to maintain a dynamic, liquid environment.

ATP vs SDS

SDS, has been the preferred additive to PAGE since its introduction to the method. Acting as the denaturing component, SDS solubilises intracellular, folded, hydrophobic or precipitated proteins. However, it cannot be used in characterisation of proteins using mass spectrometry (MS), as it has been known to eliminate the protein signal from the spectra. Furthermore, it interferes with chromatographic analysis, either by reducing protein elution in HPLC or causing peak broadening and shifting. In MS, specifically Electrospray Ionisation (ESI), SDS has been seen to suppress signals, due to its interference with the ESI droplets and their surface tension. There is some evidence that refolding proteins may be possible, using non-ionic surfactants such as octaethylene glycol monododecyl ether (C12E8) and dodecyl maltoside (DDM), however there is no evidence to show it may reduce the issues with protein characterisation.[33] Similarly, a study has shown some enzymes may be renatured after SDS-PAGE.[34] However, this evidence shows that finding a good nondenaturing counterpart would be useful for the analysis of biomolecules. Especially when the analyte is of low molecular weight, analysing it as an unhindered molecule would increase reliability. As been discussed previously, ATP does not denature analytes or remove peaks from spectra. In a study conducted with direct transmission measurements of ATP and DNA in the 150 to 260 nm wavelength range, the researchers were able to distinguish both analytes and ascertain that the sugar-phosphate group which caused an unexpected peak increase.[35] Therefore, ATP will not cause the same interferences as SDS in characterisation of proteins or DNA.

AIMS OF THE PROJECT

The purpose of this research is that to create ATP-PAGE: polyacrylamide gel electrophoresis using ATP to provide negative charges to the sample, thus facilitating electrophoretic movement. The project will also trial ATP's cheaper counterpart, ADP. Developing ATP-PAGE would provide a substitute for most PAGE methods for the analysis of proteins and other macromolecules. It is expected that ATP will confer a stable, uniform charge without causing denaturation to the analyte. The method will be tested with different proteins with various molecular weights and isoelectric points (pIs). A pI is the pH at which a protein is neutral and will not migrate[36]. A wide range of proteins will be used to ascertain at what ranges of both properties ATP-PAGE may be effective. We will screen a panel of proteins with a range of isoelectric points (and thus negative charges) in solution. The hypothesis is that ATP should provide a negative charge to the protein thus covering the native charge. ATP has been trialled as a medium for gel electrophoresis within the Serpell group at the University of Kent.[37] Furthermore, SDS-PAGE trials and native gels will be done as a comparison with the ATP trials. Further applications, such as using cell lysate for affinity studies, will be tested in ATP-PAGE gels. Furthermore, for a complete overview of possible materials that may be used, adenosine monophosphate (AMP) will also be investigated instead of ATP. The effect of ATP on the proteins will be analysed by DLS, CD and zeta potential, and then compared to SDS and native proteins. As the effect of ATP on the gel architecture is unknown, rheology studies and SEM tests will be completed. Finally, gel electrophoresis analysis will be run on the SDS, ATP and native gels.

No matter how widely used a method is, no technique is perfect, and improvements could be envisaged. This could be to increase sensitivity, precision, reproducibility or simply to reduce cost. The method this research wishes to improve upon is a type of electrophoresis, specifically sodium dodecyl sulfate (SDS-PAGE). SDS-PAGE is commonly used as it has been proven to be reliable and reproducible. The roles of sodium dodecyl sulfate (SDS) are that of a surfactant thus increasing solubility, to separate the protein structure being analysed by unravelling it into subunits and to add a stable uniform charge,

which is essential for electrophoresis. This project asks whether it would be possible to add a uniform negative charge without denaturing the proteins.

CHAPTER 2: CHARACTERISATION OF ATP-PROTEIN INTERACTION

2.1: Introduction

Proteins are an essential component of living organisms, and each will have different properties and functions, which require certain chemical structures and properties. The proteins chosen in this project are widely available and inexpensive, and some have been thoroughly characterised. Furthermore, they show a wide range in size and isoelectric points, providing good insight as to how ATP interactions will vary with size and charge. Bovine serum albumin (BSA) and Lysozyme are also commonly used as standards in the literature. This chapter aims to explore the effects of ATP on the size, charge, and structure of these proteins, and compare them to their native state or with the addition of SDS. Specifically, it is essential to characterize proteins under ATP conditions to examine whether the structure and function remains the same as in their native state. As the ATP-protein engagement is proposed to occur through hydrophobic and electrostatic surface charge interactions, the propensity of each protein to undergo these will be evaluated through computational studies using Chimera software. This computerized method will also be used to visualise the secondary structures of the native proteins in terms of α- helix, β-strand and random coil presence. The size of the proteins under ATP conditions will be examined by DLS, to verify ATP does not affect their aggregation or folding. Similarly, the stability of their secondary structures to the addition of ATP will be tested with the Circular Dichroism. Lastly, the changes in surface charge will also be quantified and compared using ζ-potential studies, together with agarose gel electrophoresis. Another interesting approach considered to verify the functionality of the proteins post-ATP addition was that of binding assays. An initial method was developed for an RNA-RNAse A assay and can be found in the Appendix.

Due to time constraints, reliable data was not obtained, despite a few trials. The chosen proteins can be seen in the table below (Table 1), together with their pIs and molecular weights. The isoelectric points should give an estimation of the molecular weights of the samples and indicate how well the proteins are expected to travel down the gel.

Table 1: List of Proteins used in this project

Protein Name	Molecular Weight / kDa	Isoelectric Point
Insulin (Hexameric)	35	5.3
RNAse A	13.7	8.64
GST	29	4-5
Beta lactoglobulin	13	5
Bovine serum albumin	66	4.7
Lysozyme	14	10

2.1.1 Biological Applications of the Proteins Used in this Project

2.1.1.1: Glutathione Transferase

Glutathione transferase (Figure 7B) enzymes are widely found in the body and are classed into three families.[38] These enzymes work with the substrate reduced glutathione (GSH), catalysing its nucleophilic attack onto other substrates (Figure 7A)[39]. Their substrates include halogenonitrobenzenes, arene oxides, quinones, and α,β-unsaturated carbonyls.[40] They have peroxidase ability, and prevent H_2O_2 cell induced death.[41]

A

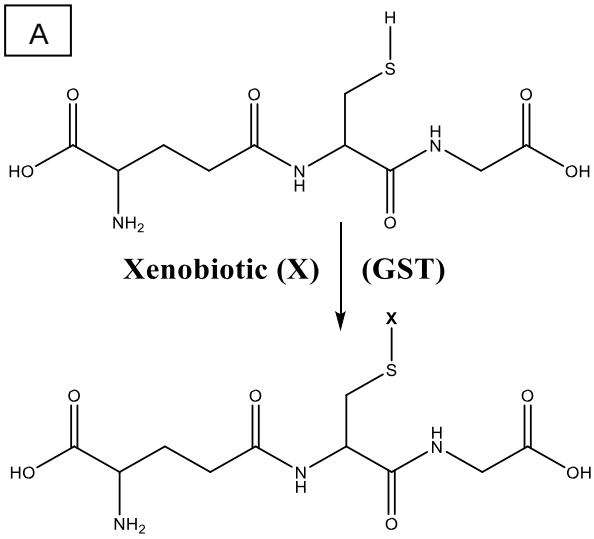

B

Figure 7 (A-B): Figure 7 A) Reaction scheme of GST-catalysed GSH conjugation with anticancer drug.

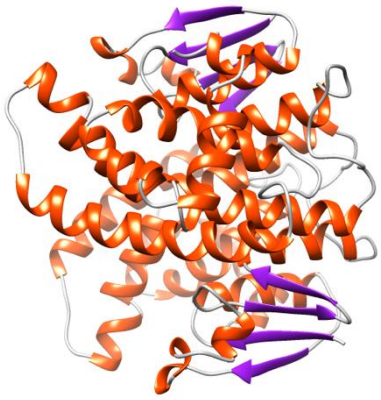

Figure 7 B): Ribbon structure of GST, PDB ID 1GNW. The α-helices are shown in orange and β-sheets in purple. As can be seen above from the predominance of orange, the majority of the GST structure is comprised of α-helices.

2.1.1.2: Bovine Serum Albumin

The globular protein Bovine Serum Albumin(Figure 8) functions biologically as a carrier for fatty acid anions and other simple amphiphiles in the blood stream.[42] In spite of the complexity in shape due to the loop linking and large size, the structure and dynamics of BSA can be easily studied making use of the intrinsic fluorescence rendered by the two tryptophan amino acid residues.[43] It is commonly used as a standard reference protein in characterisation studies due to its stability and easy availability.[44]

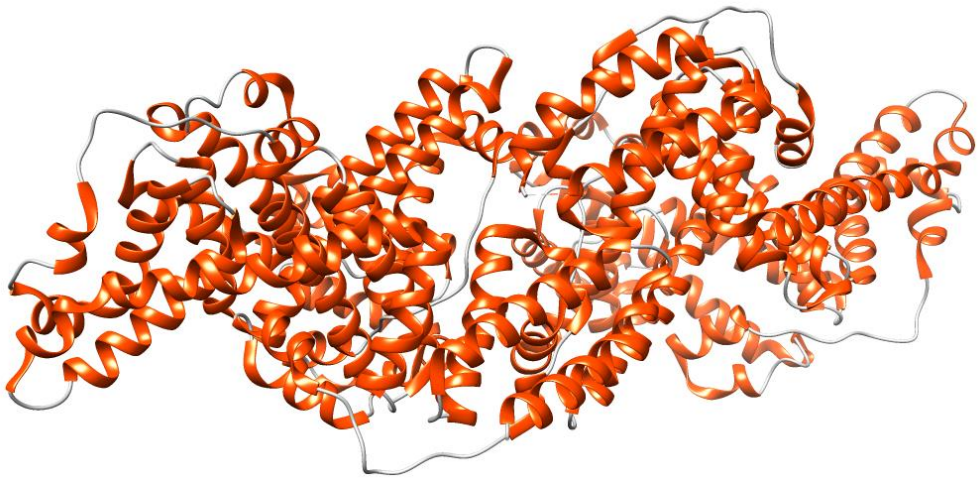

Figure 8: Ribbon structure of BSA. PDB ID: 3V03. The secondary structure analysis here shows α-helix presence (orange) entirely throughout the protein, joined by a few coils (grey).

2.1.1.3: β-Lactoglobulin

β-Lactoglobulin (BLG, Figure 9) plays a key role in hydrophobic ligand transport and uptake, enzyme regulation, and the neonatal acquisition of passive immunity.[45] The process under which BLG aggregates has been widely studied, due to the free cysteine which provides increased solubility in different solvents, with a preference for lower pHs.[46] At pH 7, BLG is found to undergo the Tanford transition.[47] This involves a conformational change worth noting for CD analysis.

Figure 9: Ribbon structure of BLG. PDB ID: 2Q2M. Unlike previous proteins, BLG contains a majority of β-strands (purple), followed by random coils (grey) and finally α-helix structures (orange) in the lower half of the protein molecule.

Numerous studies indicate that BLG possesses antimicrobial and antioxidant activities.[48] Furthermore, BLG also contributes to the defence against severe diseases. Sepsis and septic shock, which are often caused by bacterial infection, are currently treated by combining antimicrobial therapy to suppress further infections and antioxidant treatment to control oxidative stress within the mitochondria.[49] Additionally, there is evidence to show BLG is a promoter of cell proliferation until the protein is denatured.[50]

2.1.1.4: Insulin

Perhaps the most known function of insulin (Figure 10), is its ability to contribute to the processing and storage of sugars in the body.[51] In individuals with Type 1 diabetes (T1D) however, this hormone is lacking. Furthermore, it is a key antigen for the autoimmune islet destruction which also leads to T1D.[52] However, many non-diabetes related uses have been recently found. In critically ill patients with long term hospital stays due to heart surgeries or renal failures, intensive insulin therapy was proven to decrease mortality rate from 8% to 4.6% over a 12 month period, due to the controlled blood glucose levels.[52] In the 1950s,

insulin was used for “narcoanalysis”, a method where an individual’s higher mental functions are diminished by administering insulin or other drugs to act as a “truth serum” in criminal cases. This has been since discontinued due to ethical considerations. Furthermore, insulin has been used as a diagnostic tool for evaluating the levels of the growth hormone in adults.[53]

Interestingly, insulin has also been proven to be advantageous in cancer therapeutics. Introducing insulin intravenously in conjunction with anticancer drugs – Insulin Potential Therapy – has shown positive results when standard chemotherapy has failed. It has been shown to increase the number of tumour cells in the “S-phase”, which is the phase in which they are more responsive to chemotherapeutics.[54]

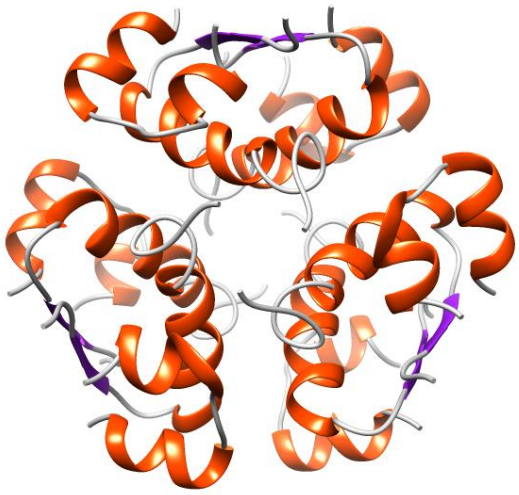

Figure 10: Ribbon structure of insulin hexamer. PDB ID: 3AIY. The hexameric structure is analysed here as it is the insulin used throughout the research. Each dimer has a large α-helix portion (orange), followed by coils (grey) and β-strands (purple) joining the helices at the back.

2.1.1.5: RNAse A

RNase A is an endoribonuclease with functions in RNA metabolism and regulation of gene expression[55] (Figure 11). It has been found to play important roles in diseases such as autoimmune diseases, renal insufficiencies, and pancreas disorders.[56] More recently, an anti-tumour activity was also reported for RNAses: this strategy aims to degrade cancer cells RNA, effectively leading to cancer cell death.[57] More generally, it can be used to

hydrolyse RNA from any protein sample, including removal of non-specifically bound RNA in assays or DNA strands.[56]

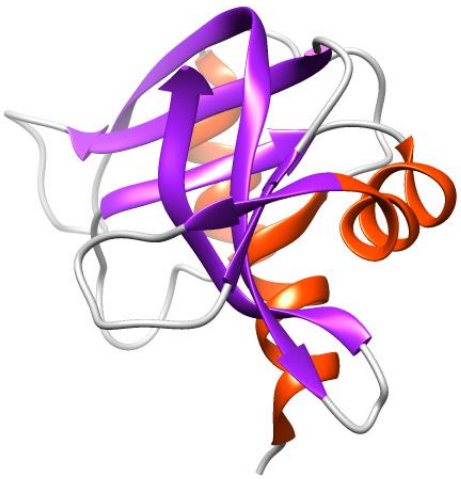

Figure 11: Ribbon structure of RNAse A. PDB ID: 3DH5. Here we see six β-strands (purple), two α-helices(orange) and seven coils (grey).

2.1.1.6: Lysozyme

Lysozyme (Figure 12) is widely used both in the food and the pharmaceutical industry. By preventing growth of unwanted organisms, it is used as an additive to prolong shelf life.[58] In medicine, it has been used both in antibiotic therapy and as pain reliever for cancer patients.[59] It is considered a pivotal component of intrinsic immunity, due to its ability to hydrolyse the peptidoglycan found in bacterial cell walls. Furthermore, it has been shown to modulate immune responses cause by various types of inflammation, such as in the intestines.[60] Addition of lysozyme to chitosan nanoparticles has seen to increase antibacterial activity, as the chitosan increases membrane penetration.[61]

Upon heating, lysozyme has been seen to form amyloids fibrils, and is therefore used to study amyloid formation. In some cases, individuals may suffer from lysozyme amyloidosis, a condition where the normally soluble protein aggregates and deposits into the body. In some reports, it was found extensively in the kidneys, causing renal failure, or the liver.[62] Therefore, studying when this aggregation occurs is essential for disease prevention. Examples of such studies include lysozyme crystals containing gold

nanoclusters create fluorescent probes for the early stages of protein aggregation, thus pinpointing when they could be reduced.[63] Similarly, magnetic nanoparticles have been shown to interact with lysozyme amyloid fibrils by reducing their length, increasing their diameter and partly changing the helical structure.[64]

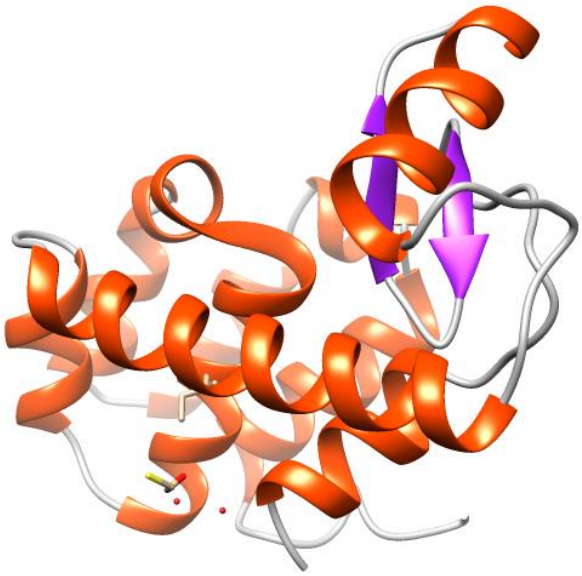

Figure 12: Ribbon structure of lysozyme. PDB ID: 253L. The secondary structure analysis shows mainly α-helix presence (orange), with two β-strands (purple) and some coils (grey).

2.1.2: Techniques

2.1.2.1 Dynamic Light Scattering

Dynamic light scattering (DLS) is used to estimate the size of a particle from the random movement of a particle in solution by measuring the laser diffraction on the solute surface. DLS measures fluctuations in scattered laser light; these fluctuations being caused by the Brownian motion of the particles. The variation in particle size will lead to different rates of movement. For example, larger molecules will move more slowly.

The Stokes-Einstein equation[65] is used to derive size from the speed of motion:

$$d(H) = \frac{kT}{3\pi\eta D}$$

where:-

$d(H)$ = hydrodynamic diameter

D = translational diffusion coefficient

k = Boltzmann's constant

T = absolute temperature

η = viscosity

Figure 13: Stokes-Einstein equation to derive the size of molecule from its speed of motion. This equation is part of the underlying calculations which provide the DLS results. Being aware of this terms of the equation helps to understand better how the analytical technique works.

Variables such as solvent temperature, viscosity and relative permittivity must be known for accurate results. The typical setup can be seen in Figure 14.[66] A common application, with regards to solutions, is to verify protein aggregation. Aggregates may be typically found between 10 and 100 nm. Depending on the size of the proteins, individual molecules would be in the 4 -10 nm range and aggregates would be 10 – 100 nm or larger. Aggregation is typically caused by non-specific interactions due to polarity of surface residues, net charge, and dipoles.

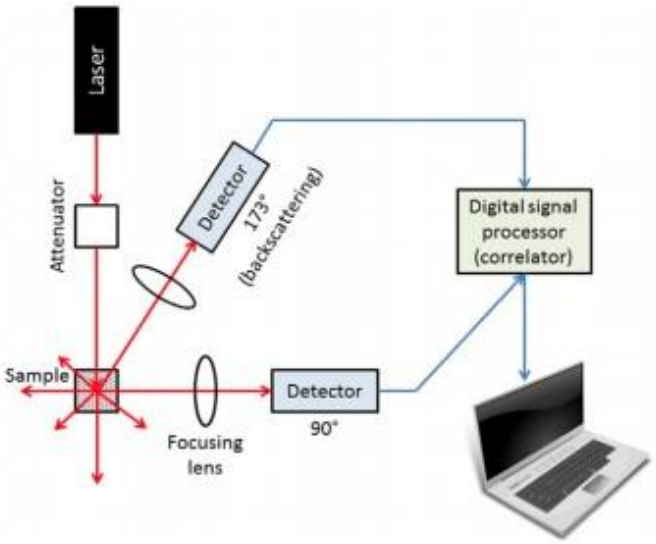

Figure 14: DLS set up. The software used was Anton Paar Kalliope. The sample is placed in a cuvette, then analysed by the detector. The data is then processed by the software and exported to Excel.

Some limitations have been found to arise from the sensitivity of this technique to solvent viscosity and temperature if not previously known. Moreover, DLS cannot distinguish populations close in size such as monomers and dimers, but can distinguish molecules with larger difference in form, such as monomers and trimers.[67] The effectiveness of DLS has been compared to another widely used technique to assess protein aggregation: resonant mass measurement (RMM). The latter measures the difference in density between the particle and the medium it is dispersed in. It was found DLS has a higher accuracy of measurement, albeit limited by the sample concentration.[66]

For this research, DLS is used to give insight on whether ATP is changing the diameter of the proteins. They are expected to retain a similar diameter to the native proteins, as this would prove the ATP is not denaturing the samples in any way. Unfolded proteins are expected to show a larger apparent diameter as they will unlikely hold a roughly spherical structure as the native state. A comparison of each protein under each condition (ATP, SDS and native) is therefore necessary to validate this. Samples treated with SDS are expected to show larger diameters, as they are unravelled.

2.1.2.2: ζ Potential

ζ - potential measures the potential difference between the mobile dispersion medium and the stationary dispersion medium attached to the particle submerged.[68] It does so by measuring the magnitude of electrostatic charge or repulsion between particles.[69] The zeta potential value will decrease as the distance from the molecule surface increases, as seen in Figure 15. Factors which may affect these values are pH, temperature, and sample concentration.[68] Generally, this technique is used to evaluate stability of the sample: results between >+/-30mV are considered stable. ζ -potential values smaller than these predict aggregation.

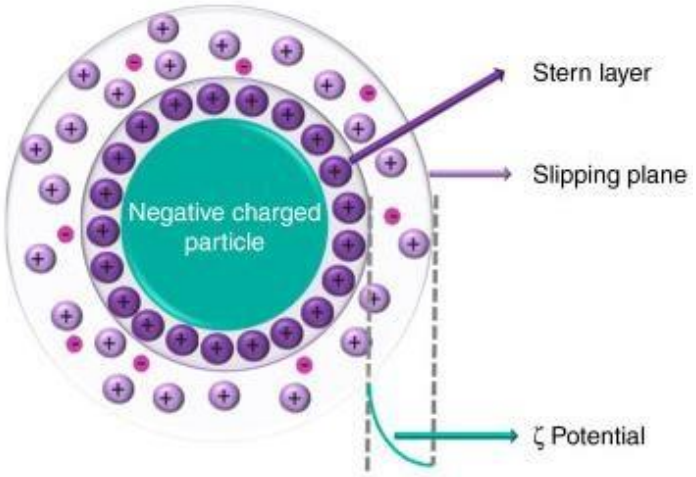

Figure 15: Illustration of ζ Potential compared to the particle surface. This measurement may be used to evaluate charge stability and magnitude of electrical charge. The green curve shows the decrease in ζ Potential as the distance from the molecular surface increases.

Due to protonation/deprotonation events, ζ potential tends to vary with pH. An example of how this happens, for a molecule with a pI of 7, is given in Figure 16.[68]

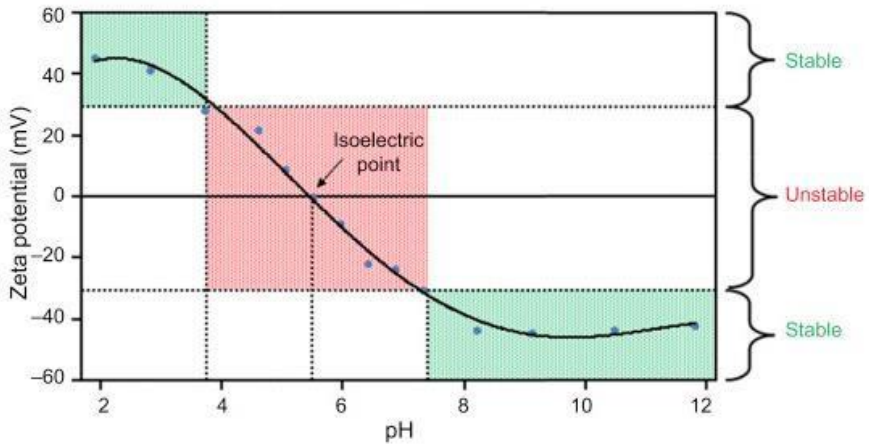

Figure 16: Changes in particle stability with increasing pH values. Particles with pI=7, at pH 4-8 will show unstable particles. Below 4 and above 8, there will be particle stability. This is due to the protonation and deprotonation which occurs at these pH thresholds.

2.1.2.3: Circular Dichroism

Circular Dichroism is widely used to probe secondary structures of proteins in solution, by measuring the difference in the absorption of left-handed circularly polarised light and right-handed circularly polarised light.[70] In CD, this polarisation will show ellipticity: the two circular components polarise in different proportions at an angle α, leading to birefringence (Figure 17).[71]

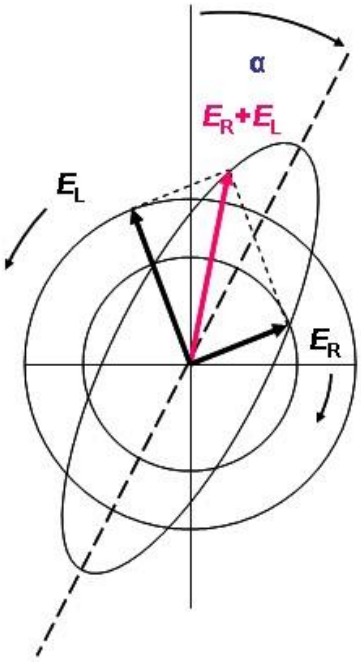

Figure 17: Illustration of the ellipticity of CD, which provides the difference in left and right polarised light. This is then used to estimate the structure of the proteins: whether they show α-helix, β- pleated sheets or random coil structures.

This occurs at wavelengths which are absorbed by the molecules in question.[71] CD provides an estimate on whether the proteins in the sample assume an α-helix, β- pleated sheets or random coil structures, as they show a characteristic spectrum for each type.[71] The α-helix percentage content of any protein can then be calculated using:

$$\%(ahelix) = \left({}^{-MRE - 2340}/_{3300}\right) x\ 100$$

The MRE is the mean residue ellipticity, which is defined as the observed molar ellipticity divided by the molar concentration of the protein multiplied by the number of amino acid residues.[72] This is used to quantify differences in protein conformations.

For the scope of this project, CD was chosen to verify the changes each protein undergoes under the three different conditions used. Ideally, the native and ATP secondary structures would remain very similar, if not the same. The SDS treated proteins would instead be expected to change structures, compared to their native counterpart, as they would unravel with the addition of the detergent. The differences would depend on the initial conformation but SDS has been found have increased α-helix content.[73]

2.2: Experimental

2.2.1 – CHIMERA

To evaluate hydrophobicity and surface charge on the protein, and therefore the potential extent of their interactions with ATP, computational studies were done using the Chimera software.

UCSF Chimera is a computational software used to visualise and analyse biological molecules.[74] From the crystal structure files retrieved from the Protein Data Bank (PDB), a map of hydrophobic areas and the positive or negative surface charges can be made. Furthermore, secondary structure analysis was completed. To do the latter, Chimera utilises a command named “Ksdssp” based on the Kabsch and Sander algorithm.[75] This algorithm defines protein sequences into helices, sheets and coils – referred to as bends in the research- by geometrical criteria. If not provided by the PDB data file, Chimera will automatically apply ksdssp to any file to generate the secondary structure information. Using x-coordinates of backbone atoms and the H-bond energy between the atoms, the α-helix and β-sheets are assigned first. Sheets build from antiparallel or parallel β bridges which combine into ladders and then into sheets. The atoms used as point of reference are typically N, Ca, C and O. Requiring a minimum of -0.5 kcal/mol bond energy, 3 residue helix and beta length, the command writes as following[76]:

ksdssp [-c cutoff] [-h helix_min] [-s strand_min] [-S file] [-v]

The hydrophobic surface tool creates instead a colour coded representation of the most and least hydrophobic areas, where red are the most hydrophobic and blue the least hydrophobic. To ascribe these, the Kyte-Doolittle hydrophobicity scale (command name **kdHydrophobicity**)[76] is used. The scale assigns each amino acid a value based on its relative hydrophobicity or hydrophilicity. The residue's value is given by the sum of the amino acids included in the sequence and plotted in the midpoint. Therefore, for a sequence of 7 amino acids, the scale will assign a value to each of these, sum them and plot the value at amino acid 4. From these same files, the Coulombic surface interaction can be assessed (command: coulombic), where the red colour shows negative surface charges (-10 threshold), whereas blue areas are positively charged (+10 threshold). The tool is named Coulombic Surface Colouring as it is calculated based on Coulomb's Law, applying the electrostatic potential to the binding ability:

$$\varphi = \sum [\frac{q_i}{(\varepsilon d_i)}]$$

Where:

Φ = Electrostatic potential

∑ = sum

q = charges on the atoms

d = atomic distances. Default value 1.4 Å

ε = dielectric constant, to account for solvent screening. Default value of 4.0

From the electrostatic potential calculated, the molecule is mapped by colour, with red showing negatively charged areas, white neutral and red positively charged areas.

The hydrophobicity of each protein was quantified using the "Grand Average of Hydropathy" (GRAVY) scale on an online GRAVY calculator website or the "ProtParam" tool on the ExPasy portal[77].

2.2.2 – ZETA POTENTIAL & AGAROSE GEL ELECTROPHORESIS

Zeta Potential ζ - potential studies were conducted using the Anton Paar Particle Sizer Litesizer 500 instrument and the Anton Paar Kalliope software. Identical samples as the Dynamic Light Scattering studies were used, with the concentrations at 2 mg/mL and pH of 8.8. Native samples were diluted to this concentration using MilliQ water and filtered using a 1 nm syringe filter. ATP samples were diluted using a 10% ATP filtered solution. For SDS samples, these were denatured and reduced to mimic the conditions these would be used in with a denaturing SDS PAGE. To achieve this, they were diluted to the desired concentration using 10% SDS, followed by the addition of β-mercaptoethanol (2 µL) and heated to 95°C in the thermocycler for 5 minutes. For the lower pH experiments, the same samples were instead diluted in PBS buffer at pH 7.8.

Alongside the ζ potential (in mV), electrophoretic mobility will also be included, and is retrieved from the same file with the zeta potential results. This term quantifies the ability of a solute to move towards the cathode or the anode, which is proportional to the surface charge of the molecule and inversely proportional to size.[78] This ability is used to calculate the zeta potential using the Smoluchowski equation[79]:

$$\zeta = \frac{4\pi\eta}{\varepsilon} f(\kappa\alpha) \cdot \mu_e$$

Where: ε = *Dielectric constant* η = *Viscosity of medium*

$f(\kappa\alpha)$ = *Debye function* ζ= *Zeta potential* μ_e= *Electrophoretic mobility*

Figure 18: Smoluchowski Equation for zeta potential. Electrophoretic mobility is the directly measured parameter from which the ZP value is derived. It quantifies the ability of a solute to move towards the cathode or anode. This value is proportional to the surface charge and inversely proportional to size. Quantifying these values therefore provides evidence for how these may change under different conditions, in this case addition or removal of ATP.

Agarose Gels

The protocol followed for this was based on that outlined by Lonza.[80] The ATP agarose gel was made by mixing ATP disodium salt tetrahydrate Tris Lower Buffer (60 mL) ,1.5M Lower Buffer: Tris base (90.8 g, 0.74 mol), ATP (2 g, 0.007 mol), up to 500 mL (fill to 400 mL and adjust to pH 8.8 with HCl) with agarose (0.6 g), and heating in the microwave for 1 minute. This was then poured in the "Owl Easycast B1" agarose electrophoresis system (Thermo Fisher) to cast and covered with a sheet of paper to prevent dust collecting on it. Once set, 20 µl of each ATP protein sample were loaded onto the gel. This was then set to run at 100V, 50mAmps for 3 hours. It was then stained in Coomassie Blue overnight and destained the following day for a minimum of 4 hours. The Coomassie Blue stain was made by dissolving Coomassie Brilliant Blue (1 g) in a solution of methanol (500 mL), glacial acetic acid (100 mL) and MilliQ water (400 mL), stirred for 4 hours and filtered. The Coommassie Destain was made using methanol (500 mL), glacial acetic acid (100 mL) and diluting to 1L with MilliQ water.

2.2.3 – Dynamic Light Scattering

The samples were made to concentration of 2 mg/mL. Native samples were diluted to this concentration using MilliQ water and filtered. ATP samples were diluted using a 10% ATP filtered solution. For SDS samples, these were denatured and reduced to mimic the conditions these would be used in with a denaturing SDS PAGE. They were diluted to the desired concentration using 10% SDS, followed by the addition of 2-mercaptoethanol (2µl) and heated to 95°C in the thermocycler for 5 minutes. The DLS instrument used was an Anton Paar Litesizer 500, which was also used for the zeta potential measurements. 5 measurements were done, each of 60 runs. The settings used were of Smoluchowski apporoximation, disposable cuvettes and the refractive index of proteins provided by the Anton Paar Kalliope software.

2.2.4 – CIRCULAR DICHROISM

The samples were made to concentration of 0.1 mg/ml. Native samples were diluted to this concentration using MilliQ water and filtered. ATP samples were diluted using a 10% ATP filtered solution. For SDS samples, these were denatured and degraded to mimic the conditions these would be used in with a denaturing SDS PAGE. They were diluted to the desired concentration using 10% SDS, followed by the addition of β-mercaptoethanol (2 µl) and heated to 95°C in the thermocycler for 5 minutes. These were then analysed at 20°C in a 1mm path length quartz cuvette with wavelength range 190nm to 290nm.

2.3: Results & Discussion

In this section, the results of the protein characterisation will be presented and discussed. Firstly, the computational analysis aimed to show the hydrophobicity studies, using the Chimera software methodology outlined in section 2.2.1. In the images below, in the hydrophobicity sub section, the proteins' front and rear view are showed with blue, white and red shaded areas. These represent hydrophilicity (blue), neutral (white) and hydrophobic (red). The relevance of this lies on the hypothesis that ATP binds to the protein via hydrophobic interactions. Therefore, the proteins with a more prevalent red shading would interact best with the ATP. From the results below, it can be seen most of the proteins have a good balance of blue, red and white, with some showing more blue areas. Hence, the only protein which would show a preference for ATP's hydrophobicity is However, another aspect that was qualitatively measured was the Coulombic surface colouring, which shades in different colours positively, negatively charged, and neutral areas. Although the results are shown in a similar colour scheme, they have a very different meaning: blue represents positive charge, white neutral charge and red a negative charge. Thus, as ATP is relatively negatively charged due to its phosphorus tail, proteins with a foremost positive

charge will show higher affinity for binding to it. Proteins such as GST, RNAse A and lysozyme are therefore expected to be good candidates for this.

2.3.1 – CHIMERA

Hydrophobicity Studies

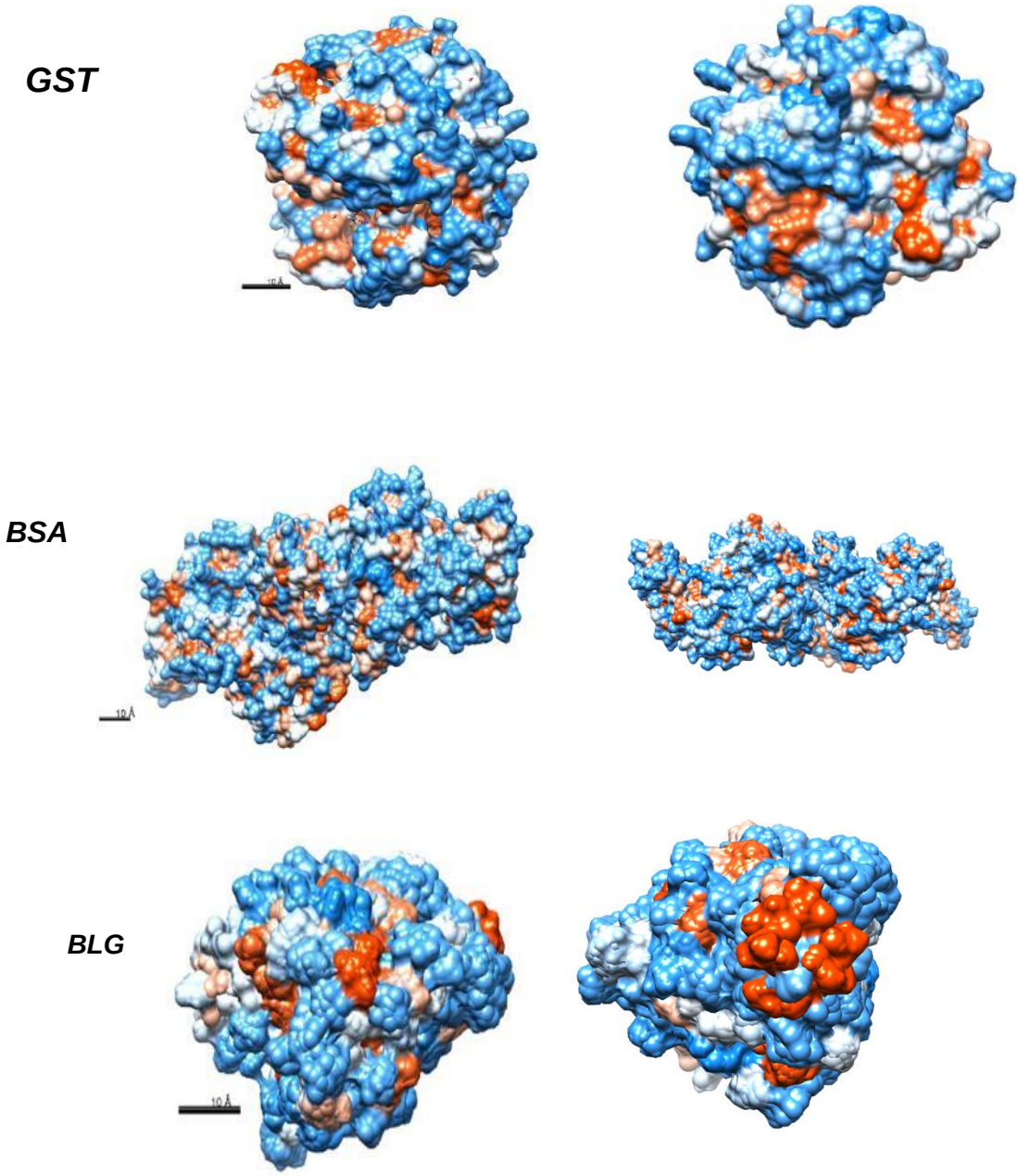

Figure 19A: Chimera hydrophobicity studies assigned using the Kyte-Doolittle scale. On the left, front view of the protein and on the right, the rear view. Blue shaded areas indicate most hydrophilic, white is at 0.0 and red are most hydrophobic. The scale is of 10Å.

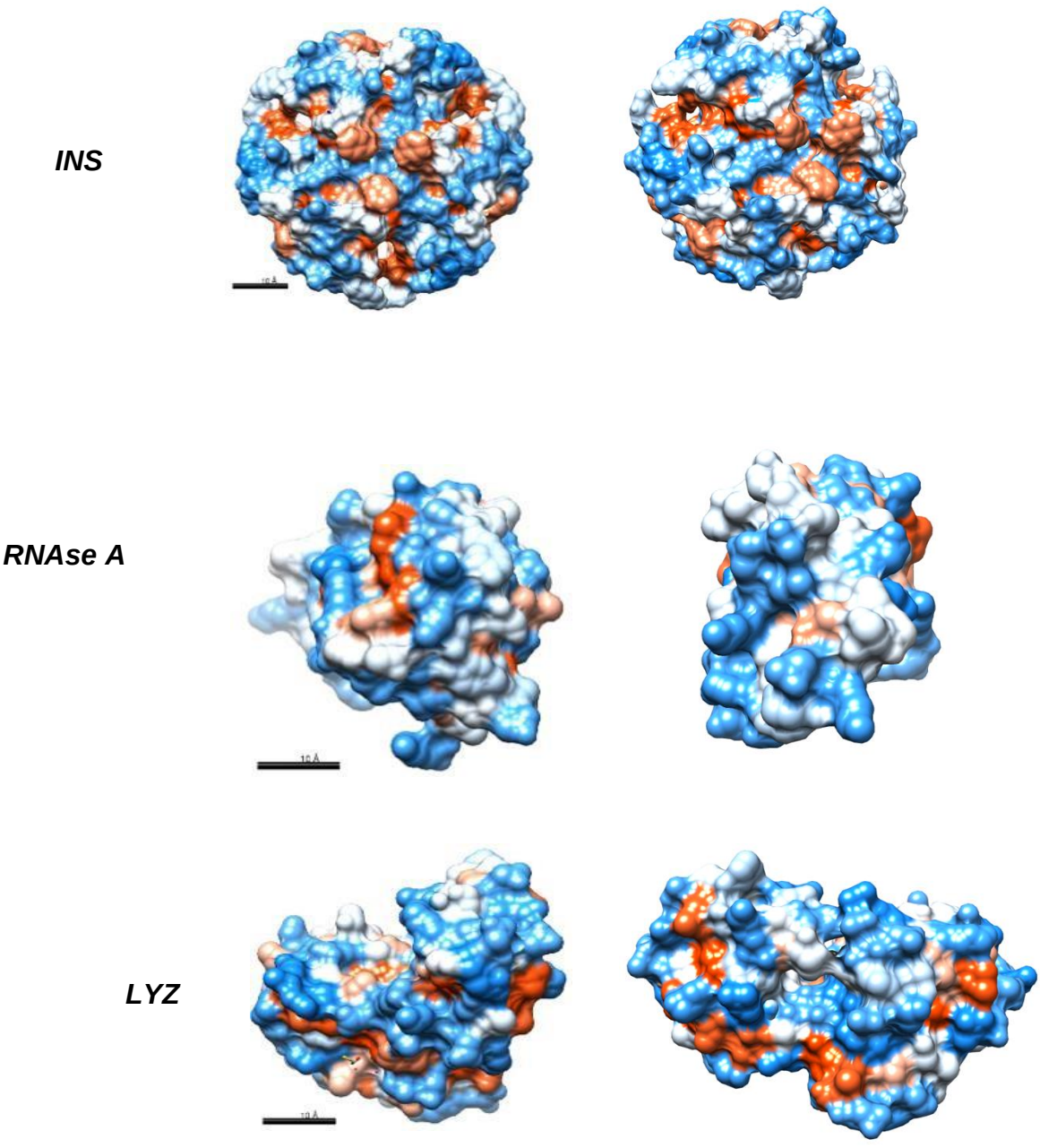

Figure 19B: Chimera hydrophobicity studies assigned using the Kyte-Doolittle scale. On the left, front view of the protein and on the right, the rear view. Blue shaded areas indicate most hydrophilic, white is at 0.0 and red are most hydrophobic. The scale is of 10Å.

Coulombic Surface Colouring

GST

BSA

BLG

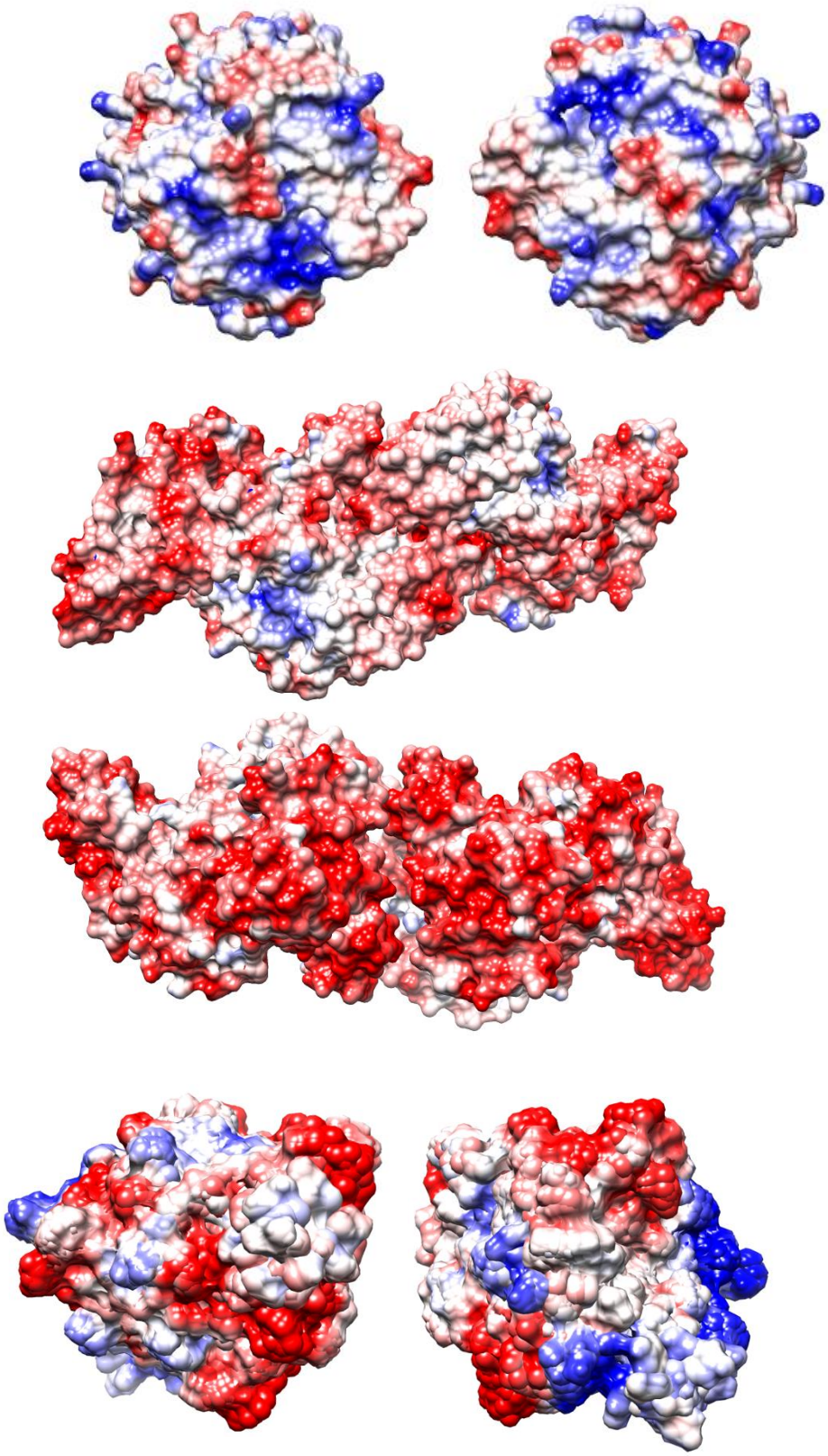

Figure 20A: Chimera Coulombic surface coloring studies assigned using the "Coulombic" command described above. On the left or top, front view of the protein and on the right or bottom, the rear view. Blue shaded areas indicate positive charge, white is at 0.0 and red is negatively charged. Therefore, a very negatively charged protein such as BSA is expected to bind to ATP less effectively.

INS

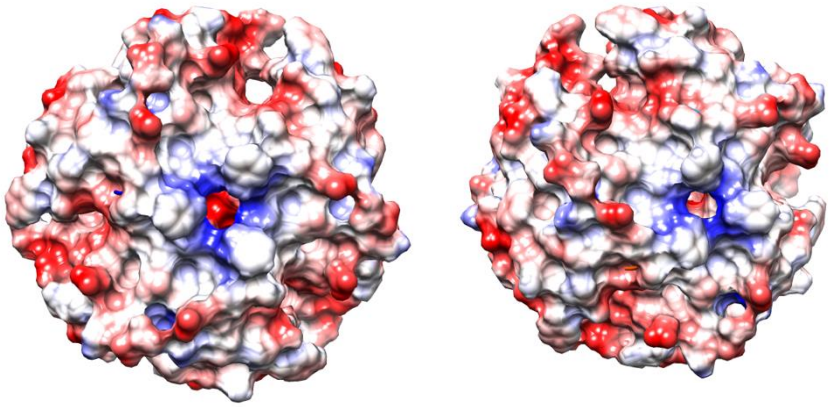

RNASE A

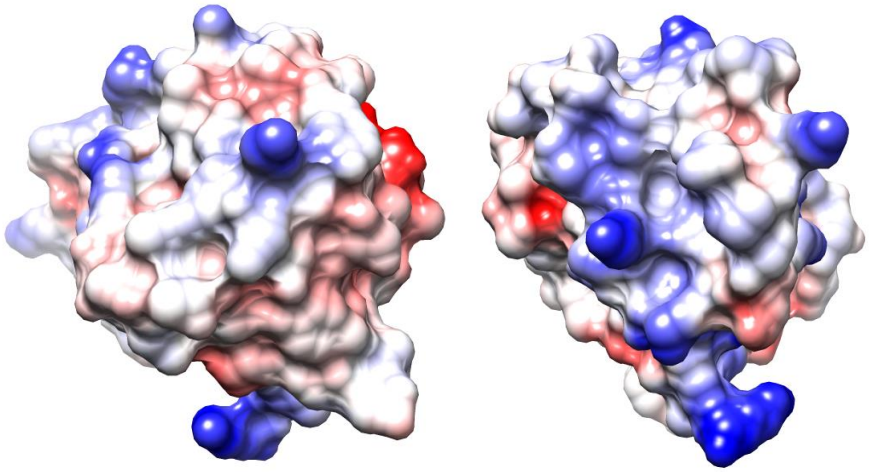

LYZ

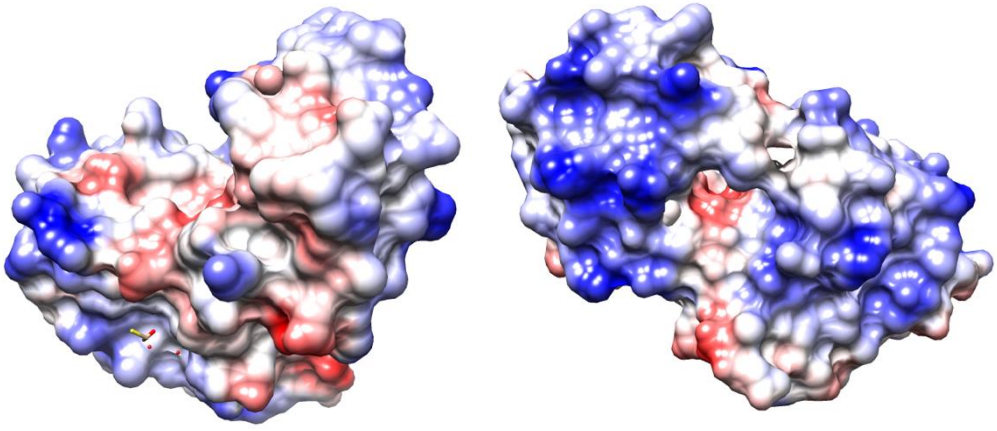

Figure 20B: Chimera Coulombic surface colouring studies assigned using the "Coulombic" command described above. On the left or top, front view of the protein and on the right or bottom, the rear view. Blue shaded areas indicate positive charge, white is at 0.0 and red is negatively charged. Therefore, a very positively charged protein such as lysozyme is expected to bind to ATP more effectively.

Table 2:

Overview of the data collected from Chimera to evaluate propensity to interact with ATP.

Protein	*Calculated Diameter (nm)*	*Gravy Scale*	*Hydrophobicity*	*Surface Charge*
GST	4.41	-0.39	Negative	Positive
BSA	14.6	-0.42	Negative	Negative
β-LG	5.07	-0.10	Negative	Negative
INS	5.1	0.19	Positive	Positive
RNAse A	3.4	-0.21	Positive	Positive
LYZ	4.1	-0.15	Positive	Positive

On the hydrophobic interaction maps, blue areas mark hydrophilic regions, whereas the red areas are most hydrophobic. Table 3 above describes some of the characteristics of the proteins used. These were evaluated to ascertain which proteins would interact best with ATP, i.e. those with either substantial positive charge or hydrophobic patches on their surface. Furthermore, the diameters calculated using Chimera were needed as a comparison with the observed values from the DLS studies. The Gravy scale values were collected to have complementary data to the Chimera hydrophobicity studies. The Gravy scale is a measurement of hydrophobicity of amino acid residues, which can therefore be used to calculate hydrophobicity of a proteins. Showing relatively positive Gravy values, together with mostly positive charges seen on the Chimera maps indicate that insulin, RNAse A and lysozyme should interact best with the ATP negative phosphate tail. However, the other proteins could still interact well with ATP. Lysozyme, for example, although positively charged, has four strong disulphide bonds which may lead to a more compact native structure. Smaller structures will migrate faster down a gel. Furthermore, the surface area available for ATP binding may be limited. Lysozyme has ATP induced amyloidosis, which could hinder the interaction and good analysis with electrophoresis.[32] Negatively charged proteins in the native state will migrate without the addition of ATP.

2.3.2 – MEASUREMENT OF PROTEIN CHARGE

2.3.2.1 ZETA POTENTIAL

Table 3: Results of Zeta Potential studies (in mV) at pH 8.8 with standard deviation errors (STDEV).

Protein	Native	STDEV	ATP	STDEV	SDS	STDEV
GST	-23.75	0.346	-9.03	0.346	-15.39	0.346
BSA	-6.93	0.346	-3.79	0.346	-0.20	0.346
BLG	-23.73	0.346	-1.72	0.346	-2.77	0.346
INS	-19.73	0.346	-1.02	0.346	-5.80	0.344
RNAse A	-0.25	0.346	-1.06	0.346	-1.54	0.346
LYZ	-0.81	0.346	-1.96	0.346	-8.59	0.346

ζ potential values were collected at the pH of the sample buffer used (8.8) and in a PBS buffer of 7.8, to evaluate the changes at the same pH level of the body. Lower pHs were intended to be analysed as well – 3 and 5 – however due to time constraints this was not done. Analysing these proteins under ATP conditions is essential to verify it is providing the negative charge needed for electrophoresis. Furthermore, the comparison with proteins in SDS will evaluate the extent of negative charge being provided. For PAGE analysis, a higher amount of negative surface charge should provide more satisfactory results. The first pattern which may be seen from Table 3 is the increase in values with ATP addition. The addition should cause a decrease in ζ potential due to the increased negative charge. A possible reason for the opposite occurring is the ATP carrying cations other than its own charge via secondary ions. Typically, a value close to zero indicates the solution is close to aggregation. However, the point of interest of the values below is that with most of the ATP

samples the values become increasingly more positive, albeit remaining negative. Generally, the native state proteins values are the closest to the stability range of -30mV. The proteins in SDS show a relevant increase in zeta potential compared to the native state samples. The sharpest decreases can be seen from native to ATP sample. Specifically, from -23.75 in native GST to -9.03 in ATP GST and similarly from -23.73 native BLG to -1.72 ATP. These are likely due to the first four proteins' isoelectric points being well below the pH of 8.8, all ranging between 4-5. An isoelectric point below the solution pH will lead these proteins to being protonated and so gaining positive charge. There are however two exceptions, RNAse A and lysozyme, which have a pI of 8 and 10 respectively. With the first protein there is a decrease from –0.25 in native state to -1.06 in ATP and a further decrease to -1.54 in SDS. With lysozyme, there is a decrease in -0.81 in native state to -1.96 in ATP and further down to -8.59 in SDS. The variations seen across the proteins are largely due to the surface charge they naturally have (Table 2); these will either interfere or promote ATP binding and the subsequent surface charge.

Table 4: Zeta Potential results (in mV) of samples at pH 7.4.

Protein	Native	STDEV	ATP	STDEV	SDS	STDEV
GST	-25.06	0.347	-3.01	0.345	-13.63	0.347
BSA	-10.9	0.347	-4.01	0.347	-4.00	0.347
BLG	-6.90	0.347	-1.08	0.347	-8.81	0.339
INS	-7.20	0.347	-4.70	0.347	-5.00	0.347
RNAse A	-4.60	0.347	-4.70	0.347	-25.73	0.347
LYZ	-0.28	0.347	-4.50	0.347	-10.06	0.329

In comparison to the values seen at pH 8.8, the samples at pH 7.4 show a similar pattern but to a smaller extent. The decrease from GST native to GST ATP is present (22.05 mV difference) although larger than seen in Table 3 (-14.72 mV). A similar decrease between GST SDS across the two pH experiments is also seen. Besides the GST, the remaining proteins show more similar results between native and ATP conditions. This is a promising result, as the pH is closer to the isoelectric points. Further investigation at lower pH would be required to ascertain whether the trend of increasing zeta potential with ATP continues. In terms of surface charge, it does show a more positive charge. However, it would be challenging to determine whether this may only be due to the ATP already binding to the protein surface, whilst still providing the negative charge required for PAGE analysis. The two outliers of RNAse and lysozyme behave differently once more, with the native values being the most positive across the three conditions. The SDS results are the most negative and closest to the stability range. This may justify the challenge in visualising these proteins in ATP-PAGE. A low pH, for example of 3, might be needed to provide enough negative charge.

2.3.2.2 Agarose Gels

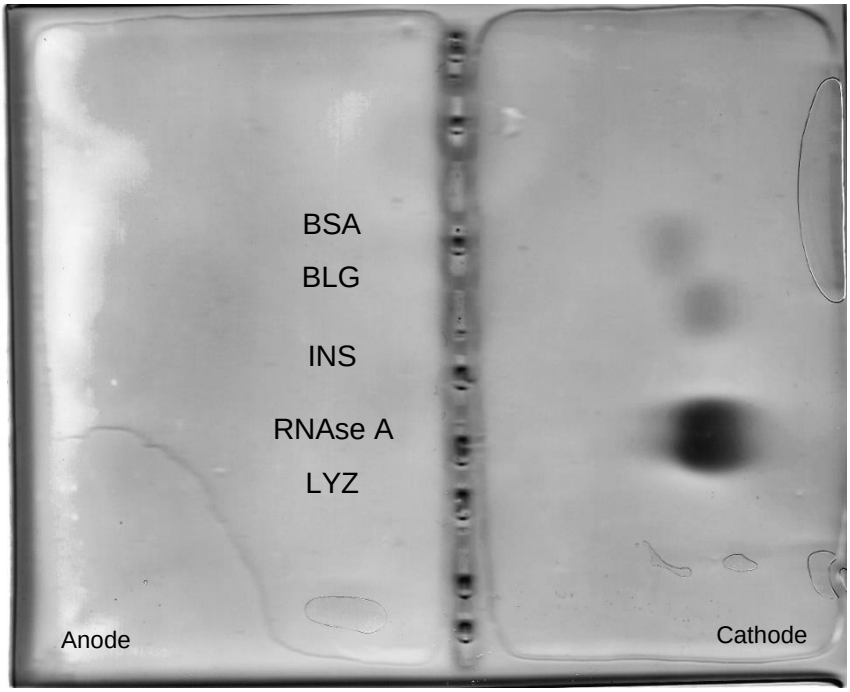

Figure 21: 1% Native Agarose Gel. Cathode is on the right, anode on the left. The samples were only diluted with MilliQ water and loading dye. Only three of the six proteins are seen on this gel: insulin RNAse a and lysozyme. These are the most negatively charged, and in fact have clearly moved towards the cathode. Repeats of this trial using higher concentrations would be necessary but was impossible due to time constraints.

To verify the ζ potential values collected aligned with the theory of ATP providing negative charge to the proteins, Native proteins were run on 1% agarose gels. With this method, proteins should clearly move from the centre of the gel towards the anode or the cathode. Negatively charged proteins should therefore move towards the cathode (right hand side of the gel). A native agarose gel experiment was performed (Figure 21): from this gel, only three out of the six proteins can be seen. The agarose trial was done in native conditions to provide a control sample. From the Chimera studies, the proteins which are mostly positively charged were found to be glutathione transferase, bovine serum albumin and beta lactoglobulin. Hence, it is expected they would not have moved towards the cathode. The

bands that are seen in the gel are those corresponding to insulin, RNAse A and lysozyme; the mostly negatively charged proteins. It is possible the other samples' concentrations were too low for appropriate visualisation. This experiment would need to be repeated at higher concentrations.

2.3.3 – DYNAMIC LIGHT SCATTERING

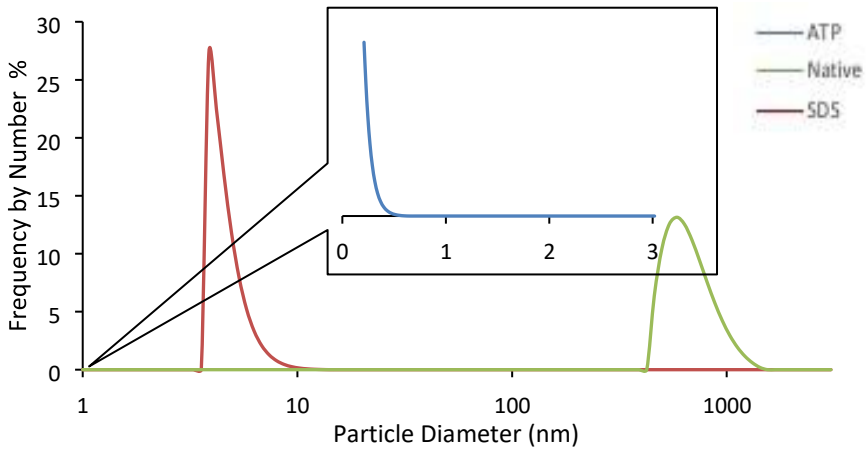

Figure 21: GST Dynamic light scattering, frequency by number (%). The red peak represents GST in an SDS solution, blue peak is in an ATP solution and the green peak is the protein in its native state. The results show an unexpectedly small peak for ATP, which usually are indication of no data. The very high hydrodynamic radius seen for the native protein could be explained by aggregates formed, as seen in literature. In future, this test would benefit from repetition. Due to lack of time and protein availability due to high cost, this was unable to be done.

The DLS data is shown here via frequency by number. The spectra by intensity, volume and all correlation functions may be found in the Appendix. Although the proteins used in these samples are well known, the results presented in this section are not of good quality. This is mainly due to poor sample preparation, as most of the data shown for ATP suggests strong protein aggregation. In future, better testing conditions for DLS – including sample concentration or a different solvent – could yield more satisfactory results. Protein conformation is affected by many factors, such as type of solvent, as well as ionic strength.[81] Therefore, these parameters could be explored to get results more consistent with literature. Another important factor to consider is that DLS can be sensitive to how compact a protein is – the Chimera studies (Fig 7B and Figure 12) give some insight as to which proteins would be negatively affected by this property, as they could show as having a larger

diameter due to being densely arranged. An example of a more compact protein would be GST or BLG – the quaternary structures leave little to no gaps between each other. On the other hand, insulin's hexamer shows there are some apertures between the dimers. In Figure 21, the particle sizes for native GST, ATP GST and SDS GST may be seen. The apparent particle size for ATP is rather small, with a peak at 0.5 nm. The GST treated with SDS can be seen at around 6 nm, whereas the native protein has a peak at nearly 900 nm. It is unlikely this peak is representative of the true size. The peak at 900 nm suggests the sample aggregated. In literature, native GST DLS studies show high molecular weight aggregate formation, found at around 300nm. Although this is still lower than the peak at 900nm seen in Figure 21, the discrepancy could be due to this aggregation occurring to a higher degree. Assuming the diameter of GST is of 4.41 nm (Table 2) the protein in this case does not show native properties. Values below 0.5 nm typically are proof of no data. With the addition of ATP, the proteins may have hydrolysed into amino acids. However, when confronting this data with the computational studies in Figure 19, it is clear the interaction with ATP was limited by the mostly negative protein surface. Therefore, the disparity in DLS results is explained for GST[82].

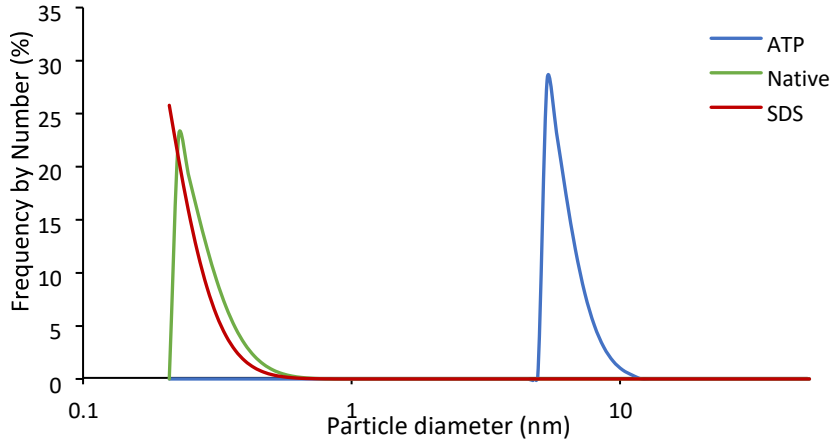

Figure 22: BSA DLS, frequency by number %. The red peak represents BSA in an SDS solution, blue peak is in an ATP solution and the green peak is the protein in its native state. Similar to the GST results, the SDS peak at 0.5nm is indicative of no reliable result. In literature, BSA DLS studies included the sample being treated with NaCl to reduce electrostatic interactions. Including this in future tests may give more desirable results.

Table 2 shows the measured diameter of native BSA to be 14.6 nm. From the data above in Figure 22, the ATP peak is the closest to this value, with a peak at around 9 nm. This is a desirable result, likely due to the good interaction between ATP and BSA provided by the largely positive and hydrophobic protein surface. In Figure 22 a native peak can be seen; however, this is much smaller than the known diameter of BSA showing only 0.5 nm length. This incongruency with calculated results may be due to sample concentration, however due to time constraints and low protein quantities this experiment could not be repeated. The SDS-protein also shows a peak at 0.5 nm, which shows no reliable data.

As mentioned above, ionic strength can play a part in DLS – in literature, NaCl was added to the sample to reduce electrostatic interactions[81]. Not having this addition to the sample may have affected these native results. From literature, native BSA treated with NaCl showed a peak at 9nm. This would be a closer result to the ATP treated BSA, showing again that BSA does respond well to the ATP addition.

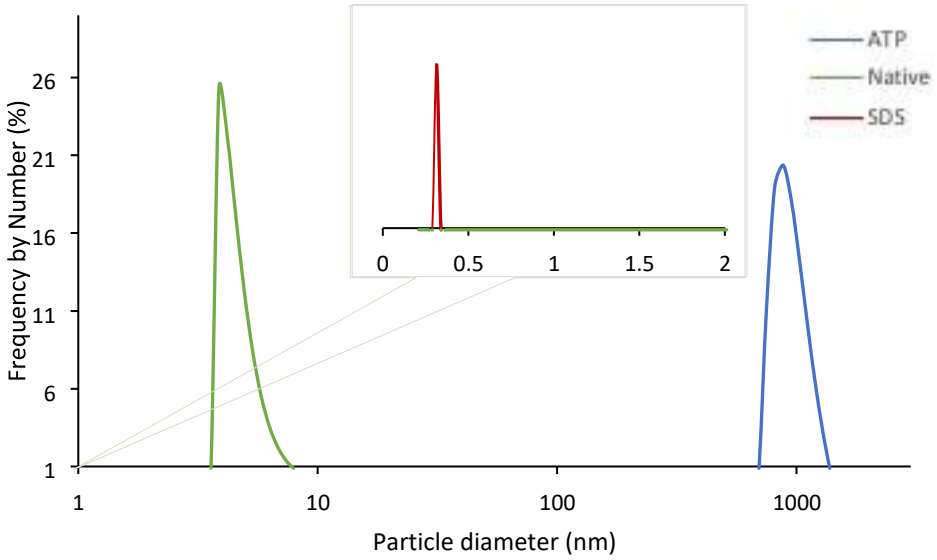

Figure 23: BLG DLS, frequency by number %. The red peak represents BLG in an SDS solution, blue peak is in an ATP solution and the green peak is the protein in its native state. Literature reports particle diameters akin to the value seen above for the native sample, and similar issues with solutions becoming cloudy, which interferes with DLS analysis. This could explain the shifted peak seen for the ATP sample. The smaller diameter with SDS is expected as it would have been denatured by the SDS.

Figure 23 shows BLG is largely split into a concentrated positive area and negative area adjacent to it. However, it is largely hydrophilic, so a good ATP interaction is not

expected here. Figure 23 represents the BLG results: a small SDS peak at 0.4 nm, a native protein peak at 9 nm and a very large ATP peak at 1000 nm. With the calculated diameter being 5.07 nm (Table 2), it Is clear the SDS peak is too small and the ATP peak much too large. The SDS peak may be explained by the denaturing process. With regards to the ATP, a peak this shifted is more likely due to an artefact rather than truly representative of the size. Possible reasons for this artefact are both low concentrations and protein aggregation.[83] In literature, BLG has been extensively studied with regards to the thermal denaturation process it undergoes. These studies are often combined with DLS analysis. Due to the thermal denaturation, as BLG is globular, the hydrodynamic diameter is expected to change with temperature and pH variations. Takata[84] showed the hydrodynamic radius varied with pH and that the BLG solution became opaque between a pH of 4 and 6. As this was the pH range our protein solutions were at, this explains what was assumed to be protein aggregation when the solution became cloudy. The radii seen also jumped from 3nm to 90nm prior to transitioning to the milky solution. These then decreased again to 3nm with a pH increase. Although our studies were not pH dependent, the results seen in figure 23 of a hydrodynamic radius of 9nm indicate that in the native state, the pH was laying at around 5. As this was the case for the SDS and ATP solutions, the opaque phase would have affected these results, explaining the shifted ATP peak. Further method development would be needed with samples at a much higher concentration, such as 25 mg/mL, and an interesting future study would be to repeat this characterisation with a pH dependence, across the pH scale.

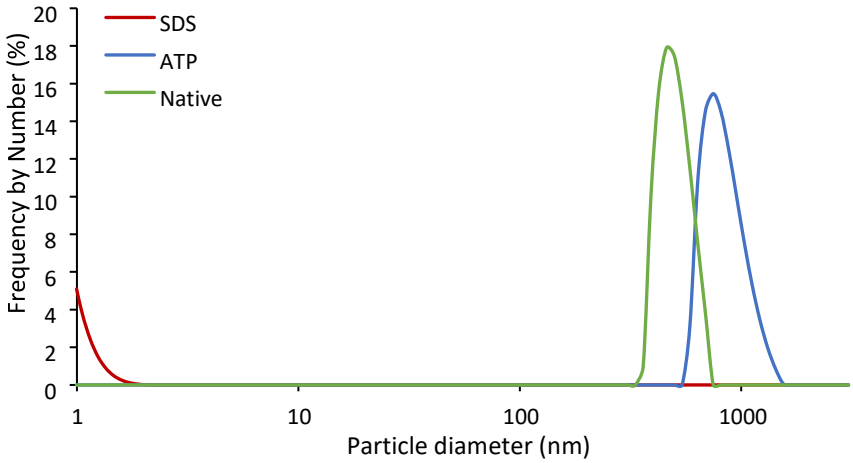

Figure 24: Insulin DLS, frequency by number %. The red peak represents insulin in an SDS solution, blue peak is in an ATP solution and the green peak is the protein in its native state, they are lower than those seen in the literature. As the SDS results are also poor, albeit indicative of denaturation, repetition of this test would be advisable for clearer results. Similarity in ATP and native results is very promising of the good interaction between ATP and insulin.

Insulin shows a largely positive surface area (Figure 19): a good interaction with ATP would be expected. Figure 24 shows ATP and native peaks close together, although the sizes of 900 and 1000 nm are much too large, as the calculated diameter is of 5.1 nm (Table 2). Literature, however, shows diameters close to 40μm (40,000nm) for native state insulin[85]. Therefore, the ATP and native peaks seen above in Fig. 24 may be acceptable, but indicative of low sample concentration. However, the close proximity of the peaks may be promising. In contrast, the SDS peak is at around 1 nm, which is also much too small. This experiment would benefit from trials with higher concentrations as suggested above. Furthermore, literature shows sonication was used prior to analysis, which could also improve results.[85]

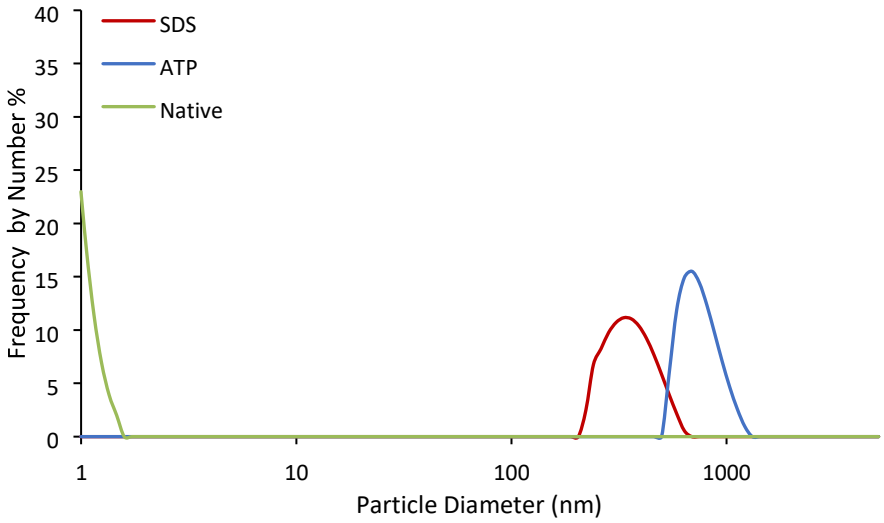

Figure 25: RNAse A DLS, frequency by number %.%. The red peak represents RNAse A in an SDS solution, blue peak is in an ATP solution and the green peak is the protein in its native state, they are lower than those seen in the literature.

RNAse and lysozyme are outlier proteins due to their isoelectric points. As these samples were in a solution at pH 8.8, the proteins being effectively measured by DLS would have been protonated thus with added positive surface charge. Figure 25 shows a native peak at 1 nm, smaller but consistent with the calculated diameter of 3.4 nm. In literature, this was experimentally reported as 2.0nm, therefore this result does align with what expected.[86] The SDS peak shown is large, at over 300 nm, similarly to the ATP peak at nearly 800 nm. These peaks are again likely subject to aggregation or precipitation effects, although no literature comparisons were found. Proteins precipitating out of solution are especially seen with the addition of SDS: a cloudy solution would interfere with the DLS analysis and show peaks of aggregation or other precipitates. Furthermore, they could be seen as artefacts of extremely large size compared to the other protein peaks. Conducting DLS experiments at a more acidic pH to match the pIs of these proteins would be an interesting approach. Examining the effects of these conditions on ATP interactions would be valuable.

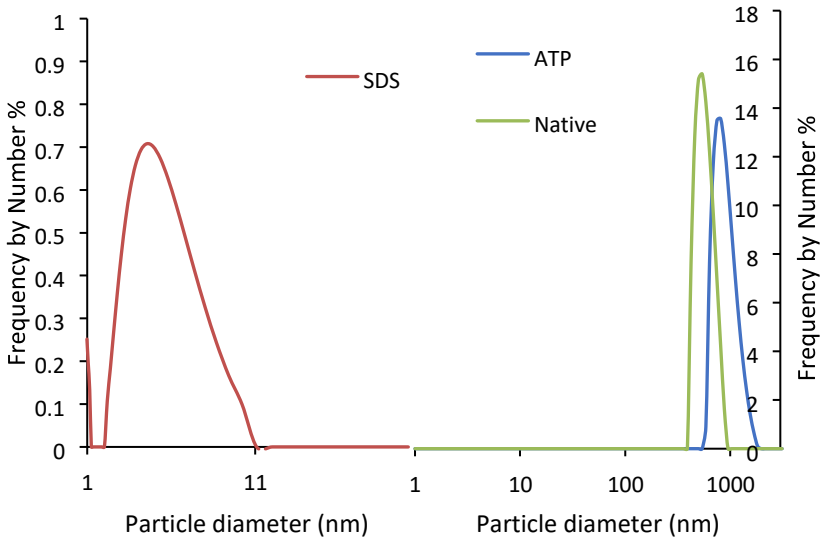

Figure 26: Lysozyme DLS, frequency by number %. %. The red peak represents lysozyme in an SDS solution, blue peak is in an ATP solution and the green peak is the protein in its native state, they are lower than those seen in the literature.

Lysozyme has a calculated diameter of 4.1 nm (table 2). Figure 26 above shows an SDS peak at around 3 nm, native and ATP at over 800 nm. The smaller peak for SDS would be reasonable as the SDS would denature the lysozyme, causing it to reduce in diameter. With regards to the protein-ATP sample, ATP is known to induce amyloidosis in lysozyme, explaining the large aggregates. The native peak at 800 nm may also be due to aggregation. In literature[87], DLS analysis of lysozyme has been conducted in a NaOAc/AcOH solution to ensure electrostatic equilibrium. The absence of this in the methodology used here could explain the aggregates seen in the native and ATP peaks. In research, varying the buffer solution's pH and ionic strength has been used to analyse lysozyme's DLS analysis. Therefore, this would be a worthwhile parameter to vary, to ascertain if the native or ATP peaks would then alight more with the calculated diameter. However, the nearly overlapping of the native and ATP peaks could be a promising result with regards to ATP being non denaturing post protein binding.

2.3.4 – CIRCULAR DICHROISM

Circular dichroism was used to evaluate whether the addition of ATP (Figure 27) affected the protein secondary structures. The ATP signal would ideally be subtracted from the spectra obtained, however due to the low protein signal yielded, the spectra discussed below include the ATP signal. Figure 28 shows an example of a CD spectrum where the ATP baseline was subtracted. Table 5 summarises the α-helix and antiparallel β-sheet percent content in the samples listed, calculated from the CD spectra.

Table 5: α-helix and/or Antiparallel β-sheet % content calculated from CD spectra.

PROTEIN	NATIVE		ATP		SDS	
	α-helix	β-sheet	α-helix	β-sheet	α-helix	β-sheet
GST	7.1	31.9	0.0	47.7	10.0	27.4
BSA	55.0	4.4	53.4	36.6	43.5	3.3
BLG	70.3	11.6	0.9	50.3	55.7	6.1
INS	18.9	28.1	22.0	17.0	31.2	20.5
RNAse A	47.6	0.0	57.3	22.9	36.0	19.4
LYZ	32.4	19.7	0.0	79.1	60.0	0.2
ATP Control	N/A		0.0	58.8	N/A	
SDS Control	N/A		N/A		4.9	37.8

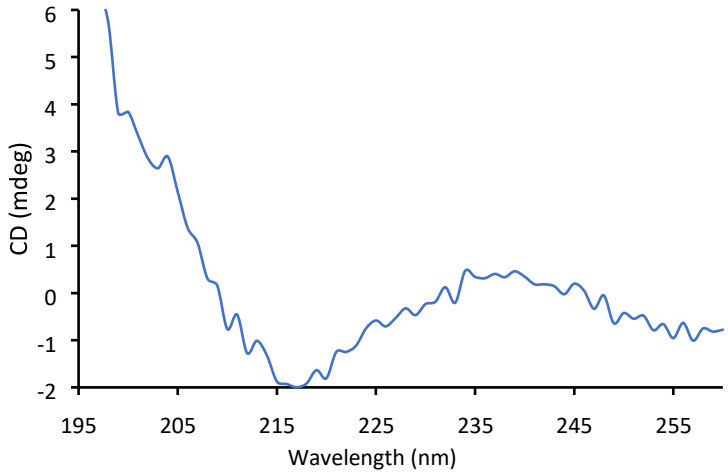

Figure 27: ATP circular dichroism control spectrum. The results above and the results in Table 5 indicate a β-sheet conformation (58.8%).

The control spectrum for ATP was taken to visualise the apparent conformation of ATP, to then subtract it from the protein CD analysis. Subtracting this peak allows us to compare the ATP-protein sample to the native and SDS-protein samples without the interference of the ATP. As discussed below however, the protein concentrations used were too low, meaning the results obtained were objectionable. Repetition of this investigation would be fruitful for future work. Due to time constraints and materials, this was not feasible at the time. Nevertheless, results from Figure 27 and Table 5 indicate ATP has a predominant β-sheet conformation (58.8%).

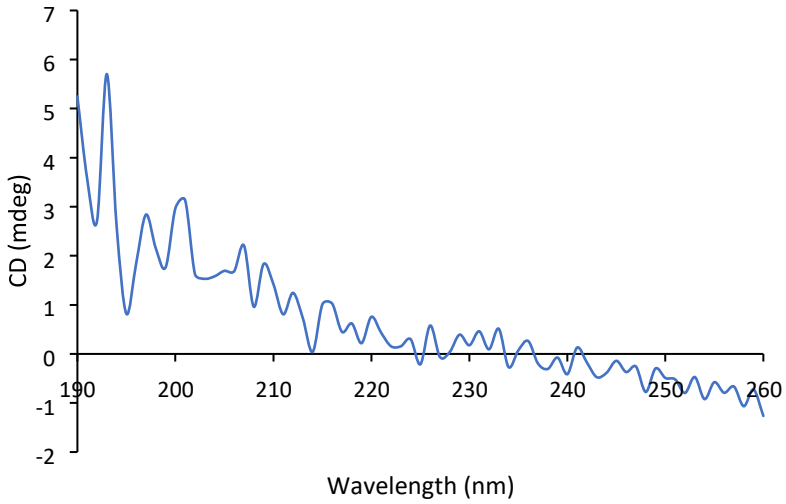

Figure 28: GST ATP spectrum with ATP signal subtracted. The irregular lines of the peak show the protein concentration was far too low, compared to the smooth lines seen in literature for CD and below for some of the other proteins. Visually, on its own it is difficult to attribute a specific conformation to this graph, however it is more in line with pleated sheets. Combined with the results in Table 5, a clear preference for the β pleated sheet arrangement is seen. Due to the poor result, this is the only protein-ATP sample shown separately from the other samples.

With the glutathione transferase in ATP (Figure 29), there is an apparent loss of α-helix content, and an increase in antiparallel β-sheets. This is likely due to the ATP curve showing a similar structure to β-sheets. In SDS, GST increases its α-helix content and decreases in β-sheet conformation (Table 5). Figure 29 shows the juxtaposition of the CD signals under each condition: there is a significant change in protein structure across these conditions, with the water/buffer baseline subtracted. This could be due to low concentrations. However, the possibility of the sample changing to random coil structure or

a combination of all of these is noteworthy and would not be shown by the results below. In fact, the signal shown is more likely to be an average of all the structures it may undergo.

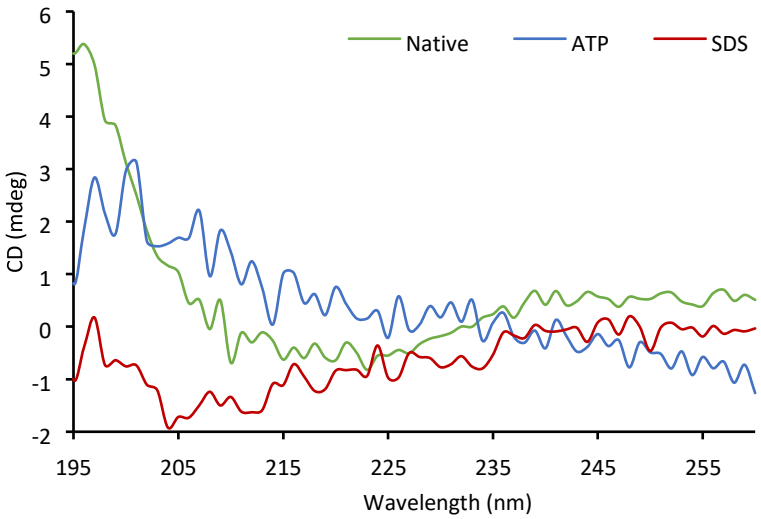

Figure 29: Graph showing GST circular dichroism results. The GST native signal is in green, GST-ATP in blue and GST-SDS in red. The native sample has a large peak at the 195nm mark, showing the mainly β-sheet conformation of GST in the native state (31.9%). With the addition of ATP, the signal varies considerably in shape, possibly due to low protein concentration. Calculated values in Table 5 however show this remains the favoured conformation, with 47.7% presence.

Although the GST-ATP peak does not overlap as hoped, the calculated values in table 5 show the main conformation is still β-sheets (47.7%), with no α-helix content. With SDS, these numbers balance out due to the denaturing process to 10% and 27.4% respectively, showing the conformation changes more significantly. The GST-native peak is consistent with literature[88], therefore the percentage compositions calculated from figure 29 can be taken as reliable. However, repeating these tests with higher protein concentrations would achieve clearer CD spectra.

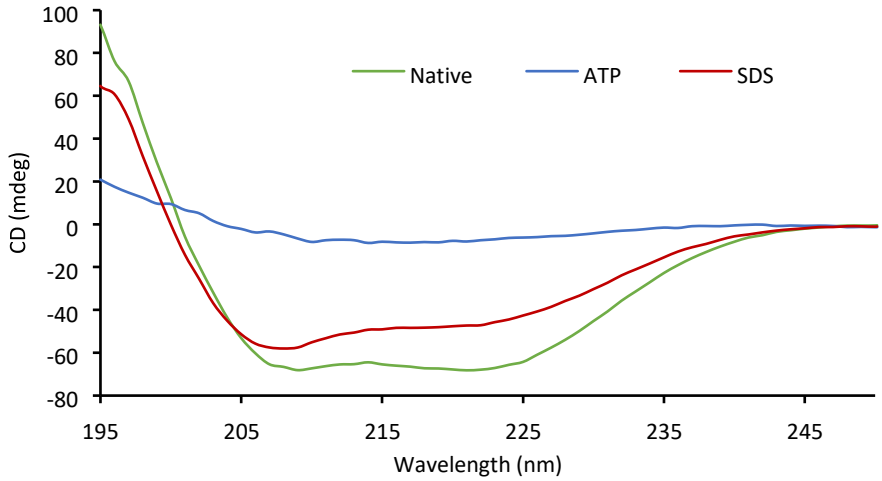

Figure 30: Graph showing BSA circular dichroism results. The BSA native signal is in green, BSA-ATP in blue and BSA-SDS in red. Here, the BSA-native and BSA-SDS results show a very similar peak shape, indicating despite denaturation, BSA will keep a prominent α-helix conformation (55% and 43.5% respectively). The smooth lines indicate the concentration was high enough, however for BSA-ATP the generated peak is much flatter than expected, indicating increasing concentration would be advised.

In the case of BSA, the conformational changes were minimal, although the ATP signal was at a lower intensity, thus not being discernible in Figure 30 as the other peaks. There was a slight decrease in α-helix percentage from the native state protein to the ATP protein; this was seen in larger quantities with the SDS treated protein (Table 5). Regarding the β-sheet content, the addition of ATP created a large increase of 32.2%, which was likely due to ATP containing a high percentage of β-sheet conformation (58.8%). The interaction between ATP and BSA was also considered more reliable, as the Chimera studies (section 2.3.1) showed that process would be favourable due to the large positively charged surface area. On the other hand, treating the protein with SDS lead to a decrease of 1.1% in comparison to the native protein. Variations between these two conditions are to be expected due to the denaturing effect of SDS. Literature reports results very similar to these: results in phosphate buffers too showed the peak at 195nm, two dips and increase at 205nm and the increase at 225nm[89], with a final increase at 235nm until it plateaus. This is consistent with the secondary structure being manly α-helix, as reported in literature[90] and seen in figure 8. The increase in ellipticity between BSA-native and BSA-SDS at 205nm is also consistent with literature being reported.[91]

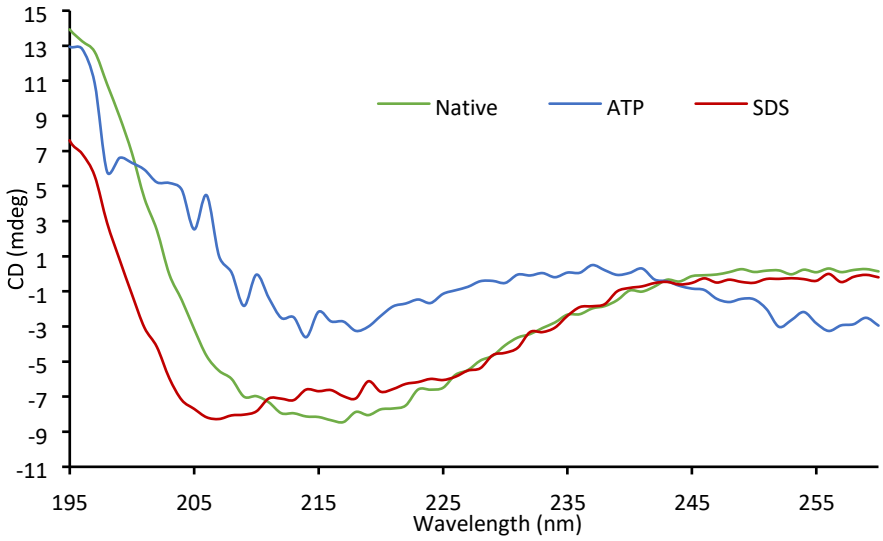

Figure 31: Graph showing BLG Circular Dichroism results. The BLG-native signal is in green, BLG-ATP in blue and BLG-SDS in red. Here, the native BLG-SDS spectra follow a very similar shape, with the SDS peak shifted to 205nm from 215nm, representing the denaturation process. Although the ATP peak does not overlap precisely with the others, the trough of the peak is also at 215nm, such as BLG-native.

β-lactoglobulin (Figure 31) showed the largest structural change after the addition of ATP, with a 69.4% decrease in its α-helix and 38.7% increase in β-sheet content (Table 5). The variation in α-helix percentage is represented by the disparity between ATP and native peaks in figure 31; similarly, the 70.3% in native state and 55.7% in SDS result in a closely related peak. A weak interaction with ATP was expected: the hydrophobic surface map (Figure 19, Section 2.3.1) showed a highly hydrophilic protein. However, the strongly positively charged centres also seen may have counteracted this and provided the path for the contact to occur. The increase in β-sheet content with SDS treatment is likely due to the surfactant containing a high percentage of this conformation type. Comparison with literature shows the native[92] and SDS results are consistent, with BLG-native spectra in water showing the similar troughs at 215nm, between -7 and -8 mdeg. The comparable trough for BLG-ATP is also at 215nm, however at a much lesser extent. This is possibly due to the BLG-ATP concentration being too low, as can be seen by the uneven lines (fig. 30) and uneven shape of its spectrum. The initial peak at 195nm is consistent with all three samples, as well as the sharp decrease until 215nm, where it then increases once more

until around 225nm. BLG-native and BLG-SDS here overlap steadily until 255nm, whereas BLG-ATP starts decreasing once more at 240nm. These trends are indicative of the heavy preference for of α-helix conformation[93]. Interestingly, the calculated BLG-ATP values (Table 5) do not show this preference, as in fact there is nearly no α-helix (0.9%) compared to β-sheet (50.3%). As BLG is in nature a predominantly β-sheet structure (Figure 9), this could signify ATP has a positive impact on keeping the native state protein shape.

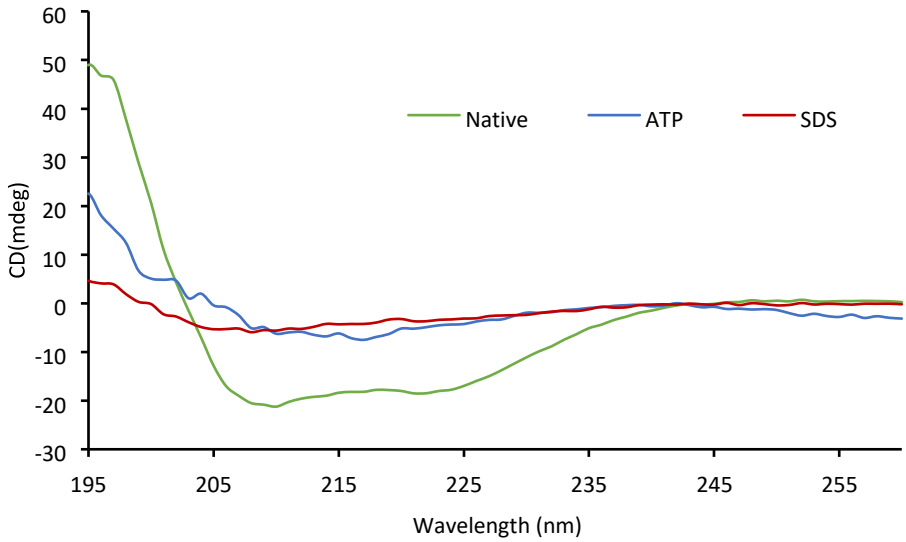

Figure 32: Graph showing insulin CD data. The insulin-native signal is in green, insulin-ATP in blue and insulin-SDS in red. Insulin-native showed an ideal, smooth spectrum in line with literature results. Comparatively, the other two spectra are difficult to analyse. This is possibly due to the protein concentration being much lower or the signal being interfered with by the addition of ATP and SDS.

Figure 32 illustrates the insulin CD response. Across the three sets of data, the native and ATP response is more similar in terms of α-helix and β-sheet conformation, with 18.9%, 22% and 28.1% and 17% respectively (Table 5). The enhanced signal seen in figure 32 for the native protein is due to a higher protein sample concentration. This intensified peak leads to the shapes of the other two peaks being more difficult to interpret. However, the similarity in values indicates the secondary structure has remained similar. This can be supported by the Chimera results, where the maps showed a largely positively charged insulin tetramer (figure 19) with multiple hydrophobic areas. From the literature[94], native insulin is shown with similar results: peak at 195nm, decrease until 205nm, subsequent slight increase at 215nm, another decrease at 225nm followed by a final increase at 235nm which plateaus afterwards. This is consistent with insulin's strand A and B α-helical

conformation. The hexamer used here would also have α-helix bonds between the dimers, explaining the strong α-helix percentage in Table 5, spectrum shape in Figure 32 and corroborated by the Chimera studies in Figure 10. The presence of β-sheet within the insulin trials, seen in Table 5 results, is due to the ATP (see Figure 27). With the help of the calculated results in Table 5, if focusing on the α-helix percentage, the native secondary structure has remained more so with insulin-ATP. This is considered a good interaction, as it did not show the same denaturation as SDS, which is the purpose of the ATP addition after all.

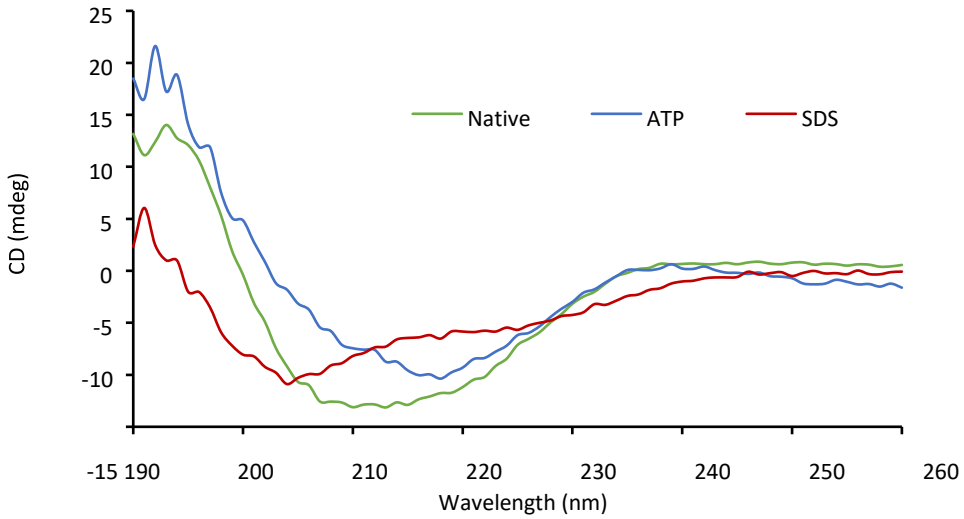

Figure 33: Graph showing RNAse A circular dichroism data. The RNAse A-native signal is in green, RNAse A-ATP in blue and RNAse A-SDS in red. Despite the spectra not overlapping completely, the shape of these overall is promising. Increasing protein concentration would yield smoother curves. The results above are consistent with computational studies in Figure 11, which show twice as much of a α-helix preponderance compared to other structures; however, combined with significant β-sheets and random coils. Similar peaks for RNAse-ATP show an optimal result in terms of ATP not changing the native structure.

RNAse A (Figure 33) is one of the smaller proteins analysed. In both ATP and SDS conditions, the α-helix content remains similar: 47%, 56% and 36% (Table 5). However, the β-sheet conformations increase significantly from the native state. With the ATP, there was an increase of 22.9%, and with the SDS, it increased by 19.4%. The ATP peak is likely showing the ATP's β-sheet contribution, therefore increasing the RNAse A β-sheet actual conformation. In figure 33, the spectra have generally the same shape, divided as the other

spectra in three main areas: an initial peak at 195nm, a concave curve between 205nm and 220nm and the final, mostly overlapped increase and plateau after 235nm. This is consistent with a predominant α-helix, as supported by the computational analysis shown in Figure 11 and in literature[95]. Different studies have shown RNAse A to have this ratio of α-helix, β-sheet and random coil, in decreasing proportions[96]. The RNAse A-native and RNAse A-ATP spectra are extremely similar with the main difference being the downward shift of the ATP in wavelength and higher ellipticity. This is likely due to the ATP signal. The Chimera studies Figure (19) showed the positively charged surface was concentrated on one protein side, and the hydrophobic area was less prominent. Consequently, the ATP interaction may be limited.

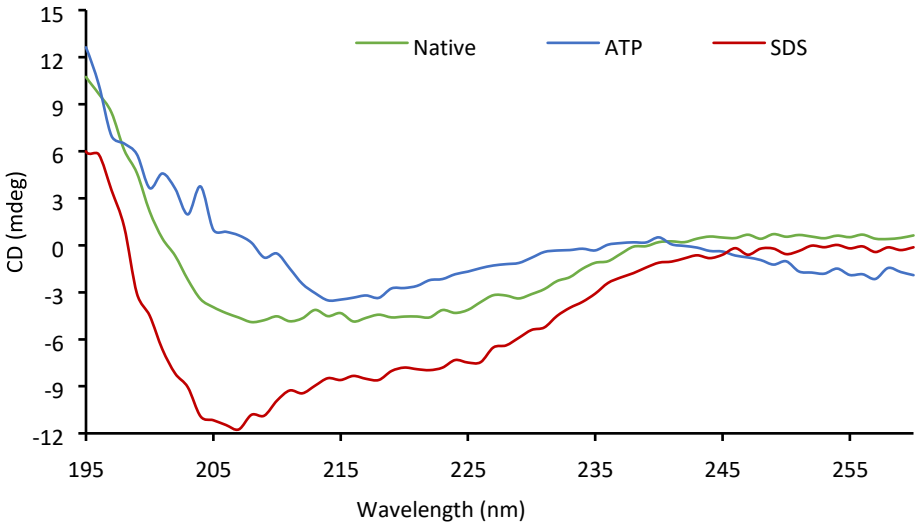

Figure 34: Graph showing lysozyme CD results. The LYZ-native signal is in green, LYZ-ATP in blue and LYZ-SDS in red. The uneven lines are due to too low of protein concentration in the sample. The spectra show similar results for LYZ-native and LYZ-ATP and strong difference with LYZ-SDS. However, literature[97] shows lysozyme is mainly α-helical, which is not discernible here from the ATP spectrum. Results in Table 5 also show nearly no α-helix conformation for LYZ-ATP. A possible reason for this is that sample heating is required for the ATP-induced thermal unfolding.

Comparably to β-lactoglobulin, lysozyme showed a noticeable decrease in α-helix content and increase in β-sheet conformation: 32.4% and 59.4% respectively (table 5). From the literature, studies have shown that ATP induces thermal unfolding of hen egg lysozyme[98], leading to a rich α-helix intermediate structure. Figure 34 instead shows the opposite: however, the ATP samples used were not heated prior to CD analysis. The need for heating to provide a conformational change is possibly due to lysozyme's largely

negatively charged surface not allowing for a good interaction with ATP. Furthermore, lysozyme contains strong disulphide bonds: these are unlikely to break with solely the addition of ATP and therefore lysozyme will retain its β-sheet structure. With SDS, the β-sheets are removed nearly completely, as the 19.7% presence seen in LYZ-native decreases to 0.2% with LYZ-SDS (Table 5). On the other hand, LYZ-ATP shows a strong increase from 19.7% to ~79%, likely from the ATP β-sheet conformation; this shows some of the native secondary structure is retained. Future work including heating of the LYZ-ATP sample at different temperatures would be a suitable investigation to achieve a conformation akin to the native protein.

2.4: Conclusion

Chimera proved to be a valuable characterisation tool to elect which proteins would interact best with ATP, although it could not predict experimental results. From the hydrophobicity studies and Coulombic surface analysis (seen in Fig. 19 and 20), the proteins expected to engage best with ATP were insulin, RNAse A and lysozyme. The secondary structure analysis (Fig. 7-11) was a valid baseline comparison for the Circular Dichroism analysis, as it helped show when the results were consistent with literature. The GST trials need to be repeated as the concentration is too low, however the calculated results in Table 5 do align with the structure seen in Figure 7. It also served as a valuable comparison with the other characterisation techniques.

ζ.-potential and DLS results needed repetition, as the results are not the most desirable, due to low concentration or aggregation. As discussed in previous sections, different buffers for DLS samples could also yield better results. Addition of NaCl in some cases has helped stabilise the solution and prevent it from becoming cloudy, which severely inhibits good results, as seen above. Furthermore, repeating zeta potential at a pH 3 could help establish the relationship between pH and ATP interaction.

Furthermore, CD quantified the conformational changes caused by the different treatment conditions of the proteins, as can be seen in Table 5. The most promising results were seen with BLG, insulin, RNAse and lysozyme. For some, methodology changes such as heating

of the sample or changes in pH and buffers could yield more desirable results. Interestingly, three of these proteins were expected to generate better results from the Chimera studies. With these proteins, the secondary structures with ATP were very similar to the native state samples. This was the desirable outcome, as the aim of the project is to develop ATP-PAGE as a method that does not denature proteins. The possible applications with biochemical assays would be many and having an improved PAGE result without denaturing the protein in any way could help reduce material expenditure. However, the CD results also suggest that with some samples, ATP has not kept the protein's native conditions. To further investigate this, samples with higher concentrations could prove useful.

CHAPTER 3: CHARACTERISATION AND ANALYSIS OF POLYACRYLAMIDE GELS

3.1: Introduction

This chapter concerns the characterisation and analysis of different polyacrylamide gels. To begin building ATP-PAGE, gels were polymerised firstly. The gel integrity was compared to native and SDS gels. Physical properties such as viscosity, elasticity and internal structure were measured via Rheometry and SEM. Subsequently, gel electrophoresis conditions were optimised. Native and SDS PAGE was also carried out,

3.1.1: Gel Electrophoresis

Gel electrophoresis is a widely used technique for separation of biomolecules. In the context of this project, it is used to separate and analyse different proteins. Each protein was examined under three conditions: with SDS, ATP or in the native state. PAGE is the main tool for ascertaining the validity of the addition of ATP as a substitute for SDS. This technique will be able to qualitatively confirm the extent of the protein migration when ATP is added. With the addition of SDS, proteins travel longer distances due to the negative charge applied, combined with the denaturing effect. With ATP, the negative charges should have a similar effect, although to a lesser extent due to the fact the proteins will not be denatured. Proteins with an isoelectric point higher than the pH of the gel (6.8-8.8) will be protonated and thus create a positive charge on them, which will slow their movement down.

3.1.2 Rheology

Rheology is the study of the flow of matter. Due to the nature of how polyacrylamide gels are formed by mixing a polymer solution and a cross-linking agent (see Figure 35[99] below), the liquids essentially undergo a state transition to solid-like state.[100]

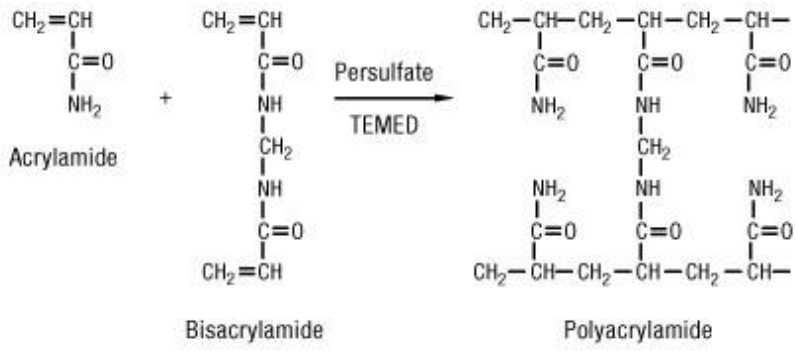

Figure 35: Crosslinking mechanism which forms polyacrylamide gels. The ratio of the reagents dictates pore size and gel rigidity. TEMED acts as the catalyst for this reaction.

To analyse the inevitable change in properties as it changes from a liquid to a viscoelastic solid, rheology has been used to determine various characteristics, such as the shrinking process the gel will undergo over time.[86] The rheometer works by measuring the way in which a sample responds to an applied force, in this case shear strain, applied by a metal plate. When analysing gels, the elasticity of the gel will be determined by the storage modulus (G'), whereas the viscosity is measured through the loss modulus (G''). In terms of Rheometry, viscosity is defined as the material's resistance to deformation dependant on time and temperature.[101]

Viscosity (G"), is a ratio calculated from the "stress" divided by the "shear rate". Elasticity, or G', is instead "stress" divided by "strain".

The equations used by the rheometer are as follows:

$$G' = \frac{\sigma}{\gamma} = \frac{M \times K_\sigma}{\theta \times K_\gamma}$$

Where: θ= angular motor deflection (radians) σ= Stress (Pa) γ = strain

K_σ = stress constant K_γ= strain constant M= torque (in N/m)

$$G'' = \frac{\sigma}{\gamma} = \frac{M \times K_\sigma}{\Omega \times K_\gamma}$$

Where: Ω= motor angular velocity (rad/sec) σ= Stress (Pa) γ = strain

K_σ = stress constant K_γ= strain constant M= torque (in N/m)

For the scope of this project, SDS, ATP and native gels were examined, as the consequence of adding ATP into the structure of the gel is unknown. As SDS gels are widely used, obtaining a quantification of the changes in physical characteristics of the gel variations. This is essential to corroborate the worth of ATP-PAGE, as changes in the rheology may affect the electrophoresis results. Large deviations from the SDS gels could show the ATP is affecting the gel structure negatively, and ideally, the elasticity and viscosity of ATP gels would be similar to those of SDS gels.

3.1.3: Scanning Electron Microscopy (SEM)

Scanning electron microscopy reveals information on the specimen's surface, by scanning the sample using a focused, high energy electron beam (Figure 36).[87] This interaction creates electronic signals which are eventually converted into the processed image. See Figure 37 for a typical SEM setup.[102] To avoid sample charging, it is essential the sample is thoroughly dried. This technique has been widely used to characterise polyacrylamide gels, such as to analyse the consequences on the gel architecture after freeze drying.[103] SEM is useful to determine particle shape and distribution of particles, so to determine surface morphology. The process works as follows: an electron beam is directed towards a sample, where it will interact with atoms within it. These atoms, found at different depths, will produce different signals which are then detected and used to produce the image. Due to the various depths the beam can reach, the image produced is representative of the morphology.

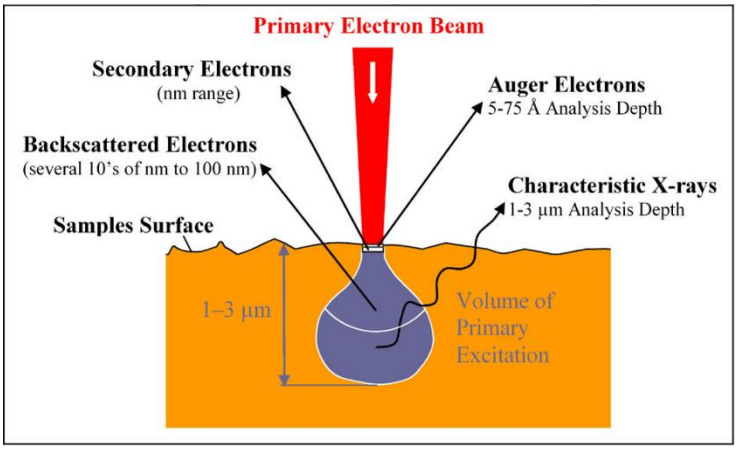

Figure 36: Schematic representation of the electron beam range and interaction with sample surface and atoms.

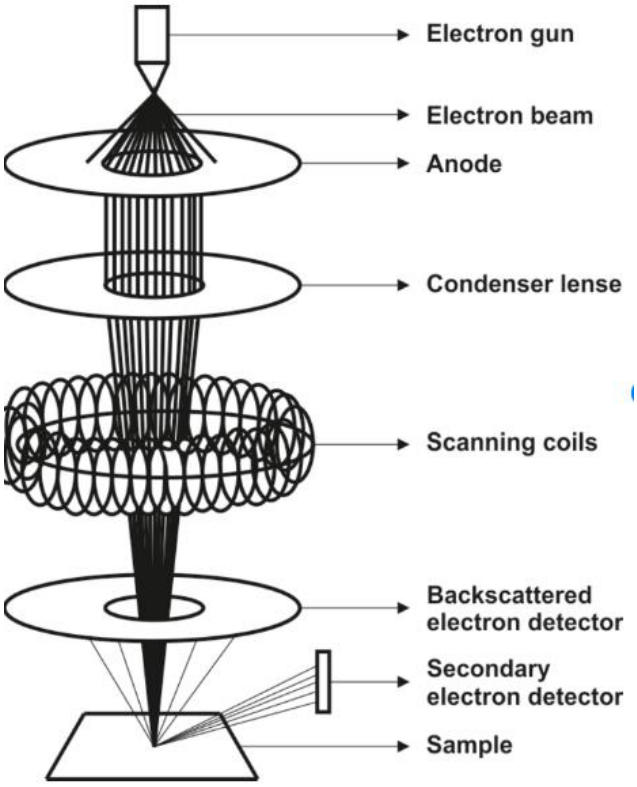

Figure 37: Schematic representation of the typical SEM setup. The electron beam source can be seen at the top, with the different electron detectors at the bottom, slightly above the sample plate. As mentioned above, the electron beam will separate into different electron scattering, which will each need a specific detector in order to yield a good surface morphology image.

3.2: Experimental

3.2.1 SDS PAGE

The experimental procedure followed for the SDS data collection was based on the Laemmli Protocol[104], with a 12% acrylamide gel, formed by a resolving gel layer below and a 4% stacking gel above. The proteins analysed thus far are bovine serum albumin (BSA), lysozyme, gluthathione transferase, RNAse A, and beta lactoglobulin. Insulin, due to its very low molecular weight (5.8kDa) compared to the other proteins, was analysed separately from other proteins, to avoid it possibly running too far down the gel. For dilution series, samples were diluted in 1:2, 1:4, 1:8 and 1:10 ratios to find optimum concentration. Secondly, a denaturation series was done, with each sample made under different conditions: the first, containing a sample buffer which included β-mercaptoethanol and was heated to 94°C in the thermocycler machine. The second, containing only the sample buffer was heated. The third, containing only loading dye was kept at room temperature. Lastly, the fourth, a native control. To make the gels, which were usually made in pairs, the method used was the following. For the resolving gel layer, 2.66 mL (0.44 mol) of acrylamide:bisacrylamide 37.5:1 solution were added to a 15 mL centrifuge tube, followed by 2.7 mL of MilliQ water and 1.15 mL of 1.5M lower buffer. These were shaken lightly before the addition of TEMED (6.6 µL, 0.06 mol). After the thawed 40% APS was stirred on the vortex stirrer, 52 µl (0.14 mol) of this was added to the solution and mixed by hand lightly. This was then poured into the glass plates. For the stacking gel, acrylamide (0.44 mL) were added into a 15 mL centrifuge tube, followed by 2.92 mL Milli Q water and 1.15 mL of 1M upper buffer. After mixing, 6.6 µL (0.06 mol) of TEMED were added prior to 52 µL (0.14 mol) of 40% APS. This solution was then lightly mixed and poured into glass plates and a plastic comb inserted. This was then left to polymerise.

<u>Gel Buffers:</u>

1M Upper Buffer: Tris base (60.5 g, 0.5 mol, 0.001 M), SDS (2 g, 0.007 mol, 0.014 mM) up to 500 mL water (fill to 400 mL and adjust pH with HCl, around 80 mL needed for pH 6.8)

1.5M Lower Buffer: Tris base (90.8g, 0.74 mol, 0.00148M), SDS (2g, 0.007 mol, 0.014 mM), up to 500 mL (fill to 400 mL and adjust with HCl, around 50 mL for pH 8.8)

For Running Buffers:

10x Stock: Tris (30 g, 0.2 mol, 0.0002 M), Glycine (144g, 1.91mol, 0.00191 M), SDS (2 g, 0.007 mol, 0.007 mM) to 1L

3.2.2 NATIVE PAGE

The method used for native gels followed the same steps as above, without the addition to SDS to either gels, samples or buffers. To make the gels, which were usually made in pairs, the method used was the following. For the resolving gel layer, 2.66 mL (0.44 mol) of acrylamide:bisacrylamide 37.5:1 solution were added to a 15 mL centrifuge tube, followed by 2.7 mL of MilliQ water and 1.15 mL of 1.5M lower buffer. These were shaken lightly before the addition of 6.6 µL (0.06 mol) of TEMED. After the thawed 40% APS was stirred on the vortex stirrer, 52 µL (0.14 mol) of this was added to the solution and mixed by hand lightly. This was then poured into the glass plates. For the stacking gel, 0.44 mL acrylamide were added into a 15 mL Falcon tube, followed by 2.92 mL Milli Q water and 1.15 mL of 1M upper buffer. After mixing, 6.6 µL (0.06 mol) of TEMED were added prior to 52 µL (0.14 mol) of 40% APS. This solution was then lightly mixed and poured into glass plates and a plastic comb inserted, and then left to polymerise. The samples were not denatured in any way and were prepared by adding loading dye to the protein solution. Reverse polarity gels were also tested, with the same procedure as above, but with the electrodes plugged in in reverse into the electrophoresis machine (ie, red electrode in black socket and viceversa).

Gel Buffers:

1M Upper Buffer: Tris base (60.5 g, 0.5 mol, 0.001 M), up to 500ml water (fill to 400ml and adjust pH with HCl, around 80ml needed for pH 6.8)

1.5M Lower Buffer: Tris base (90.8 g, 0.74 mol, 0.00148 M), dilute up to 500ml (fill to 400ml and adjust with HCl, around 50ml for pH 8.8)

For Running Buffers:

10x Stock: Tris (30 g, 0.2 mol, 0.0002 M), Glycine (144 g, 1.91 mol, 0.00191 M) to 1L

Lower Acrylamide Percentage Gels: 8% and 10%:

For the 8% resolving gel layer, 3.2 mL of acrylamide:bisacrylamide 37.5:1 solution were added to a 50 mL Falcon tube, followed by 8.5 mL of MilliQ water and 4 mL of 1.5M lower buffer. These were shaken lightly before the addition of 4 µL of TEMED. After the thawed 40% APS was stirred on the vortex stirrer, 40 µL of this was added to the solution and mixed by hand lightly. This was then poured into the glass plates and left to polymerise.

For the 10% acrylamide gel, 2.5 mL of acrylamide:bisacrylamide 37.5:1 solution were added to a 50 mL Falcon tube, followed by 5 mL of MilliQ water and 2.5 mL of 1.5M lower buffer. These were shaken lightly before the addition of 2µL of TEMED. After the thawed 40% APS was stirred on the vortex stirrer, 20 µL of this was added to the solution and mixed by hand lightly. This was then poured into the glass plates and left to polymerise.

3.2.3 ATP PAGE

The gels were cast following the same procedure as the SDS PAGE gels, however every buffer containing SDS was replaced with ATP. For the resolving gel layer, 2.66 mL (0.44 mol) of acrylamide:bisacrylamide 37.5:1 solution were added to a 15mL Falcon tube, followed by 2.7 mL of MilliQ water and 1.15mL of 1.5M lower buffer. These were shaken lightly before the addition of 6.6µL (0.06 mol) of TEMED. After the thawed 40% APS was stirred on the vortex stirrer, 52 µL (0.14 mol) of this was added to the solution and mixed by hand lightly. This was then poured into the glass plates. Therefore, the gels were cast containing ATP, as well as the sample and the running buffers. The first concentration tested, based on literature, was 8 mM[5]. Next, 4mM, 16mM, 2mM and 1mM were trialled. For the 8mM 1x running buffer, 1.507 g of ATP was used with 100 mL of the 10x native

stock, and diluted to 1 L. The resolving gel buffer contained 2.075 g of ATP. The 4, 2 and 1mM buffers were diluted accordingly from the 8mM stock. The 16mM buffer was made fresh by using 3.015 g of ATP in 1x native buffer diluted from a 10x stock.

Magnesium, when used[105], was included by addition of magnesium acetate at 4, 8 and 16mM concentrations, with 0.85 g, 1.71 g and 3.4 g of magnesium acetate tetrahydrate added to the ATP 1x running buffers. For the resolving buffers of each concentration, 0.04 g, 0.08 g and 0.16 g of $Mg(OAc)_2$ were added. A 5ml sample buffer stock was prepared by adding the same amounts of ATP and $Mg(OAc)_2$, plus adding 70% glycerol, loading dye and diluting to 5 mL with deionized water.

For all trials, the base protocol followed that of a Tris-Glycine Polyacrylamide gel. For the native buffer recipe, Tris base (Merck), Glycine (Merck) and MilliQ water were used. SDS purchased from Thermo Fisher was used for the SDS trials. All products were used without further purification and used to make 10x stock solutions of running buffers and lower and upper gel buffers. PageRuler Prestained Protein Ladder (ThermoFisher) was used across all trials to give an indication of the distance moved by the proteins. The electrophoresis system used was a Mini Protean Tetra Cell (BioRad). For native gels, the buffers were made the same apart from the addition of SDS. For ATP/AMP gels, a direct molar equivalent substitution with SDS was done.

For the stacking gel buffer, 1M upper buffer was made mixing 60.5 g Tris and 2 g SDS, diluting to 500 mL with MilliQ water and then adjusting to pH 6.8 using HCl. Resolving gel buffer consisted of 1.5M Lower Buffer. This was made mixing 90.8 g Tris and 2 g ATP, diluting to 500 mL and adjusting to pH 8.8. The running buffer is made from a 10x Stock consisting of 30 g Tris, 144 g Glycine, 15 g SDS to 1 L, which is then diluted to 1x running buffer. The 4x sample buffer was made up of 0.5M Tris (1 mL), 10% ATP (1.6 mL), 50% Glycerol (5 mL), and loading dye.

Gel Buffers:

1.5M Lower Buffer: Tris base (60.5 g, 0.49 mol, 0.001 M), ATP (3 g, 0.01 mol, 0.02 mM) up to 500 mL (fill to 400 mL and adjust with HCl, around 50 mL for pH 8.8)

For Running Buffers:

10x Stock: Tris (30 g, 0.2 mol, 0.0002 M), Glycine (144 g, 1.91 mol, 0.00191 M), ATP (26 g, 0.05 mol, 0.05 mM) to 1 L

Lower Acrylamide Percentage Gels: 8% and 10%:

For the 8% resolving gel layer, 3.2 mL of acrylamide:bisacrylamide 37.5:1 solution were added to a 50 mL centrifuge tube, followed by 8.5 mL of MilliQ water and 4 mL of 1.5M lower buffer. These were shaken lightly before the addition of 4 µL (mol) of TEMED. After the thawed 40% APS was stirred on the vortex stirrer, 40 µL (mol) of this was added to the solution and mixed by hand lightly. This was then poured into the glass plates and left to polymerise.

For the 10% acrylamide gel, 2.5 mL of acrylamide:bisacrylamide 37.5:1 solution were added to a 50 mL Falcon tube, followed by 5 mL of MilliQ water and 2.5 mL of 1.5M lower buffer. These were shaken lightly before the addition of 2 µL of TEMED. After the thawed 40% APS was stirred on the vortex stirrer, 20 µL of this was added to the solution and mixed by hand lightly. This was then poured into the glass plates and left to polymerise.

3.2.4 AMP PAGE

The gels were cast following the same procedure as the ATP PAGE gels outlined in section 3.2.3, however every buffer containing ATP was replaced with AMP. Therefore, the gels were cast containing AMP, as well as the sample and the running buffers. For the 8mM 1x running buffer, AMP (2.921 g, 0.007mol) was used with 100 mL of the 10x native stock, and diluted to 1 L. The resolving gel buffer contained 0.0146 g of AMP (0.004 mol). As with the ATP trials, magnesium was added to investigate whether it would activate the AMP further and so improve the gel results. This was done at 4 and 8mM concentrations, with 0.753 g (0.005mol) and 1.4 g (0.01mol) of magnesium acetate tetrahydrate added to the

respective AMP 1x running buffers. For the resolving buffers of each concentration, 0.003 g (0.002 mol) and 0.006 g (0.004 mol) of $Mg(OAc)_2$ were added. A 5ml sample buffer stock was prepared by adding the same amounts of ATP and $Mg(OAc)_2$, plus adding 70% Glycerol, loading dye and diluting to 5ml with deionized water.

3.2.5 SAMPLES

The SDS trials consisted of a combination of different denaturing conditions applied to the same protein. In each trial, the first sample entailed a mixture of protein (5 µL), sample buffer (2 µL) (Sample Buffer 4x: 0.5M Tris (1 mL), 10% SDS (1.6 mL), 50% Glycerol (5 mL), loading dye) and beta-mercaptoethanol (1 µL), with heating to 92°C using the thermocycler. The second sample included loading dye (3 µL), 70% glycerol (2 µL), protein solution (5 µL) and heating to 92°C. The third sample had protein (5 µL), loading dye (3 µL) and 70% glycerol (2 µL), but at room temperature. The final sample was only native protein (5 µL) and 70% glycerol (2 µL). This sample was included as a control. Denaturation running times for RNAse A and lysozyme denaturation were changed. Prolonged runs (1 hour) in the thermocycler lead to the aggregation of these proteins, hence the poor results on the gels. These two proteins were therefore only run in the thermocycler for 5 minutes.

The AMP and ATP samples were prepared by following the SDS Sample Buffer components and replacing it with the same percentage of ATP and AMP. A stock solution was made of these, which included 0.5M Tris (1 mL), 70% glycerol and ATP (0.03g, 0.05 mM) in 5mL water for the ATP sample buffer and 0.5M Tris (1 mL), 70% glycerol and AMP (0.02 g, 0.05 mM) in 5 mL water for AMP.

The native samples were always diluted with MilliQ water to the required concentration and then mixed with glycerol to weigh them down for loading.

Cell Lysate samples were diluted from the stock with MilliQ water to required concentrations (1:2, 1:4, 1:8 and 1:16), and enough ATP buffer to reach 10 µL.

3.2.6: Rheology Studies

The software used was Anton Parr RHS. After software has initialized, the measuring unit “CP/PP7” is inserted: this is a cone plate geometry, profile 7 (bob, beaker) 2.3 x 0.5mm. After this, the motor was adjusted, as well as the auto zero gap, the temperature (25°C) and then the system brought down to 1mm distance from the sample plate. The gels used for these studies were cast using the procedure outlined in section 3.2.1, 3.2.2 and 3.2.3. The parameters set in the software can be seen below. The gels analysed were SDS, native and ATP 12% gels. Two ATP sample gels were examined as one was analysed directly after polymerisation, whereas the second was left to polymerise overnight before analysis. This was done to ascertain whether a longer polymerisation time affects the structure and therefore PAGE results.

Table 6: Parameters for RheoCompass Software

Waiting, Resting and Running Time	5 minutes
LVER limit	3%
Tolerance	0.03
Smoothing Range	0.01
Angular Frequency	10 rad/s
Variable X Sheer Strain	Default
Variable Y G’ Storage Modulus	Default

3.2.7 – Scanning Electron Microscopy (SEM)

The samples consisted of SDS, ATP and Native 12% acrylamide gels, prepared as outlined in sections 3.2.1, 3.2.2 and 3.2.3. After polymerisation was completed, 4cmx4cm sections of the gels were placed under vacuum overnight to dry appropriately for SEM use. The following day, 1 cm x 1 cm pieces were placed onto carbon sticky tabs attached onto metal sample holders. The samples were then analysed with the SEM under different orientations by Luke Alesbrook, to visualise the surfaces as well as the cross sections.

All of the images were taken in either Secondary Electron (SE) mode or Backscatter Electron (BSE) 3D mode. Those taken in SE mode have less defined borders, as the image is taken more superficially (Fig 38A, for example), compared to BSE mode, which will reach deeper in the thickness of the sample (Fig. 39A) Th SEM was operating under 1 Pa. The magnification is shown underneath each image with a scale bar. The operating voltage was 10KV with single frame imaging and a 5 µm dwell time.

3.3: Results & Discussion

3.3.1 – RHEOLOGY STUDIES

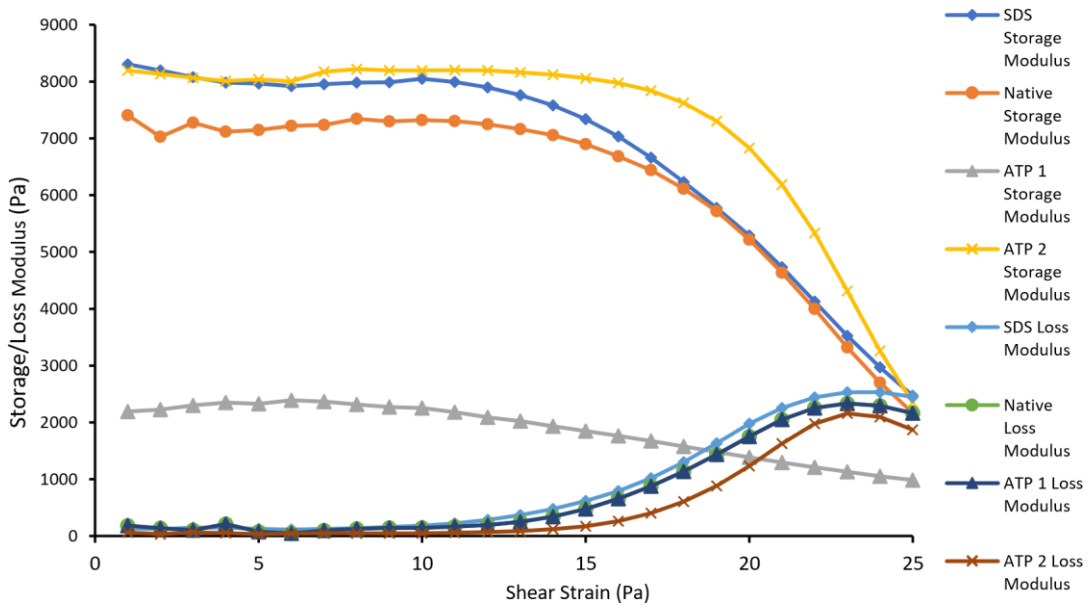

Figure 36: Amplitude Sweeps for SDS, Native and ATP 1 & 2 Gels. Amplitude sweeps show the behaviour of a sample and are used to ascertain the linear viscoelastic region. This is the range at which analysis can be performed without sample destruction. The graph above shows these results as a function of shear strain (Pa) vs Storage and Loss Modulus (G'/G").

Rheometry was chosen to investigate whether ATP would negatively affect the gels. If the gel was poorly polymerised, protein migration would be hindered. The amplitude sweeps (Figure 36) were performed to narrow down the region to be analysed such that the sample will not be destroyed. This region is called the "Linear Viscoelastic Region" (LVER). To find the best region to continue the analysis, three points are taken from the region where

there is most plateauing. The results are taken from this region as it represents a constant response to increasing shear strain.[106] The three points chosen are then averaged and used for the frequency sweep. For native and SDS gels, the LVER equalled 0.133. With ATP1 and ATP2 (the former gel used right after polymerisation, the latter allowed to polymerise overnight), LVER was found to be 0.0562 and 0.562. It is important these are before the point of interception, as this is the strain point, after which the gel's viscous characteristic[91] will overtake elasticity. The amplitude and frequency sweeps are then repeated in the LVER. The storage moduli (G') – top of the graph – represent the elastic response of the sample. The storage modulus is also an indication of the gel's ability to store deformation energy and is related to the extent of cross-linking present.[107] A higher storage modulus therefore shows a higher degree of cross-linking present. Thus, for the gels being analysed here, it will show whether the addition of ATP to the structure hinders cross-linking and so protein migration. Poor gel architecture would affect PAGE results as the proteins would not be able to separate by molecular weight. If these results are poor, we would exclude adding ATP to the PAGE gels and instead consider solely native gels with ATP-protein samples for future work. The loss moduli (G") shows instead the viscosity of the gel. From fig 36, we can see all four samples showed similar viscosity, with al lines overlapping. We can see a steady line between 0-12 Pa/Hz, until 15 Pa/Hz where it then increases When the G' is larger than G'', the sample has gel or more solid like structure, as elasticity would need to be higher than viscosity. Otherwise, the sample would be a fluid.

The results in Figure 36 show the following trends: there is a strong overlap between the loss moduli of the SDS, native and ATP 1 gels. ATP 2 results show a less strong but still good result, indicating the viscosity of all the samples is mostly similar. This is expected for a gel-like structure, within the LVER.[108] Within the storage moduli, there are consistent results with SDS, native and ATP1 gels between 7000-8500 Pa. ATP2's loss modulus is much lower, at 2000 Pa. The interesting point here is the proximity to its storage modulus data and the crossing between the two at 19 (Pa or Hz), unlike the others which do not cross until 25 (Pa/Hz). Therefore, ATP2 has a higher viscosity in comparison to its elasticity;

the overnight polymerisation in the refrigerator (at around 4°C) could have caused the gel to lose this elasticity. Although a longer polymerisation was expected to yield a more thorough cross-linkage, the colder temperature causes more rigid gels, as seen in Fig 37.[109]

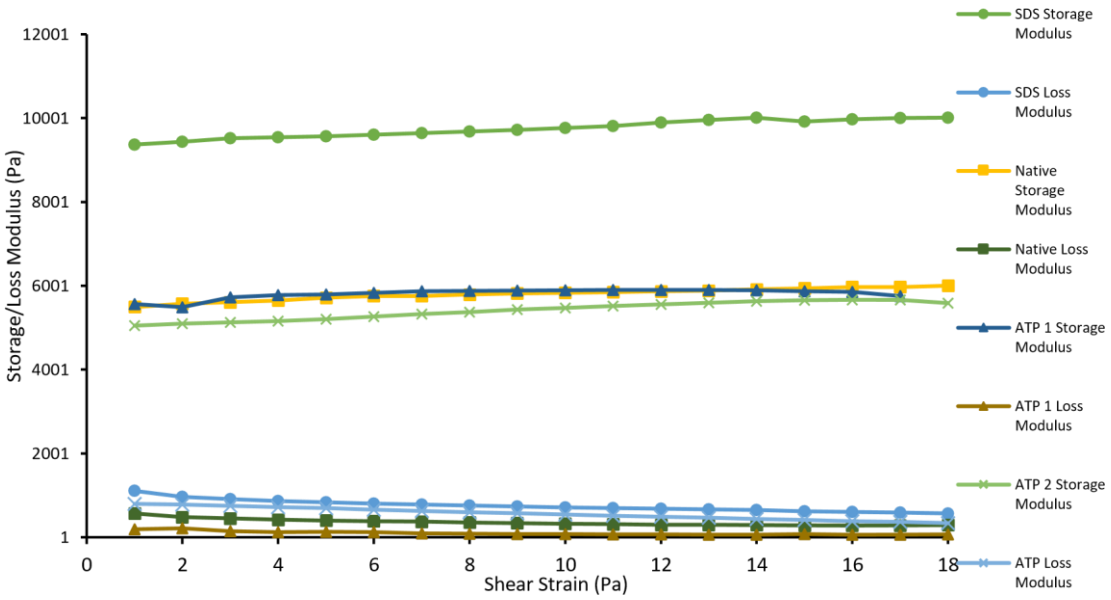

Figure 37: Frequency Sweeps for Native, SDS and ATP1 & ATP2 Gels. Frequency sweeps describe the viscoelastic properties of a sample over time. This is usually represented as a function of Frequency (Hz) vs G'/G''.

Following the amplitude sweeps, the frequency sweep (Figure 37) is conducted in the LVER found previously. These results show a uniform storage and loss modulus response, with the exception of the SDS storage modulus. However, this is to be expected. With SDS being a surfactant, it will contribute greatly to providing elasticity to the gel. It has been shown to increase both viscosity and elasticity, until a maximum SDS concentration is reached at $8x10^{-3}$ mol/L, after which it will have a sharp decrease.[92] The concordance between the other results shows ATP is not hindering these characteristics. This is a promising result with regards to the effects of the ATP, as they are otherwise unknown. Collecting rheology data, in conjunction with SEM will provide further information on this matter.

3.3.2– SCANNING ELECTRON MICROSCOPY (SEM)

3.3.2.1 12% Polyacrylamide Native Gels

In Figure 38, the results for the 12% native gel SEM and EDX analysis can be seen. The SEM analysis (38A & 38C) shows the surface characteristics of the gel, which is expected to look like a mesh of pores as formed by the polyacrylamide. In the images above, the surface seems porous at 50 μm, whilst the cross section at 25 μm shows long and narrow fissures. The porous structure of a PAGE gel is essential for protein movement; however, the uneven surface may be a result of the drying process outlined in section 3.2.7. As drying under vacuum occurs, particles from the buffer may sediment on top of the gel, causing the gel to look opaque. Some sedimentation can be seen in Figure 38A, with white deposits of varying size and shape. The hypothesis that these could be superficial sediments could be supported by their absence on the cross-section surface (Fig 38C). Had there been compositional flaws, they would be present throughout the sample architecture. However, the cross-section surface would have been expected to have a similar round porosity as the top surface. Instead, the narrow troughs seen above (Fig 38C) could be a result of the drying process, where the gel contracted, shrinking[110] slightly as it lost hydration.[111]

Concurrently to the SEM, EDX analysis was also completed on the gel samples. The results are shown above in Figure 38B and Figure 38D. Each of these is the EDX breakdown for the area analysed in the figures above. Therefore, Fig. 38B matches to Section 9 outlined in 38A and Fig. 38D to Section 8 outlined in 38C. Some elements are, as expected, seen in high proportion in both images, such as carbon and oxygen. The increased presence of these in Figure 38B – 12.2 eV compared to 0.7 eV for carbon, and 7 eV compared to 0.6 eV for oxygen - is reasonable as this is the upper surface of the sample. Similarly, a higher proportion of chlorine in Section 9 of 2.2 eV compared to 0.4 eV found in Section 8 may also be ascribed to the cross-section being less exposed to the

drying effects, which may cause deposit formation, as well as contamination from the drying or the SEM machine itself, such as the electron source. Molybdenum also is completely unexpected from the sample and so likely to be a trace contaminant from the machine.

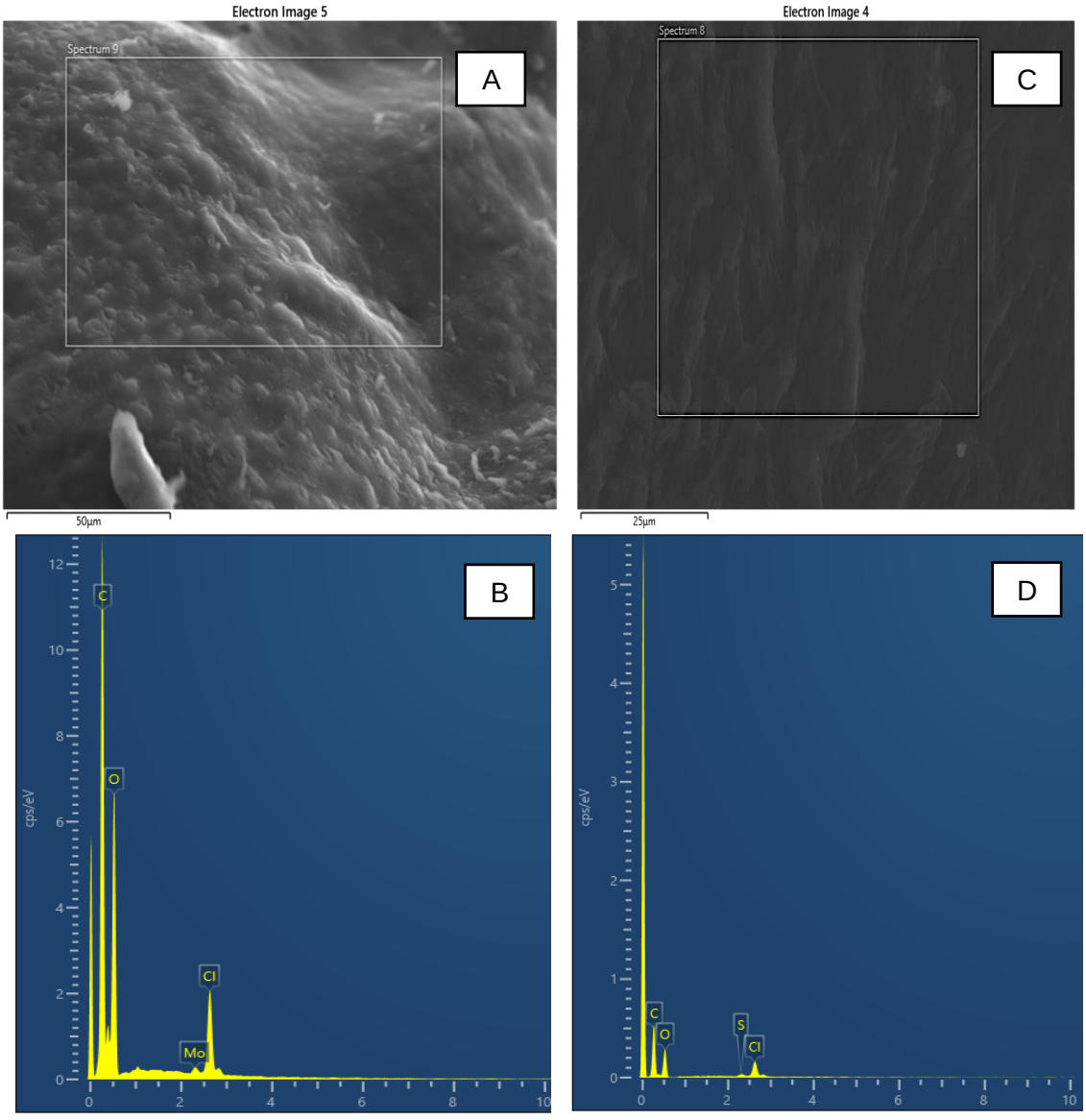

Figure 38 (A-D): 12% Native Polyacrylamide Gel SEM Images. Figure 38 A) highlights the topography of the Native Gel, whilst Figure 38 B) shows the EDX Spectrum of the Spectrum 9 area. Figure 38 C) shows the structure of the cross section of the gel, whilst Figure 38 D) has the corresponding EDX spectrum for Spectrum 8 seen in the previous figure.

3.3.2.2 12% Polyacrylamide ATP Gel

ATP polyacrylamide gels were also analysed using SEM, to further explore the extent to which ATP could be a viable substitute for SDS. The topography seen in Fig 39A is a much more complex structure than that seen in Fig 38A, with the prior showing long, narrow filaments forming interconnecting knots in a similar geometry to a chain. This has been seen before in polyacrylamide gels when subject to freeze drying, swelling in buffers and under vacuum[110]. However, the cross-section which can be seen to the right of the outlined area of Spectrum 27 shows a much smoother surface, with only some striations. The intricate surface could therefore also be a result of drying effects; the scale of 500 µm is also indicative this may be the case. Figure 39C further zooms into the surface, showing thick, uneven trenches that are also shown to be a result of drying.[111] In literature, drying effects such as shrinking and cracking are inevitable unless two main methods are implemented: either the gel is soaked in ethanol and glycerol[112], then placed between glass plates, or the gel may be placed between two acrylic plates.[111,113]

Figure 39E is the cross section of the gel. This was an interesting angle to examine as it showed how deeply into the gel the drying effects will cause disruption on the surface. Although it cannot be discerned if the mesh is present in the entirety of the gel thickness, the upper and lower layer clearly show the pattern. The white areas which can be seen on the bottom façade are precipitation products of the disodium salt contained in the ATP.

In Figure 39B, the EDX results for Spectrum 27, Electron Image 13 (Fig. 39A) are reported. The peaks present in highest proportion are those of carbon and oxygen, as expected. However, although the sample analysed contains a large amount of nitrogen (within the ATP and the Tris-Glycine, TEMED and APS) this is not encountered in the EDX. This is due to the limitation of EDX: it is not able to detect elements with an atomic number below 10.[114] This would also apply to Fig 38B & 38D. Again, here, nitrogen is not visualised on the spectra. Figure 39B also shows some small peaks (0.2 eV magnitude) for phosphorus, aluminium, silicon and sulphur. In comparison to the carbon peak at 3.9 eV, it is reasonable to hypothesise these elements were background noise.

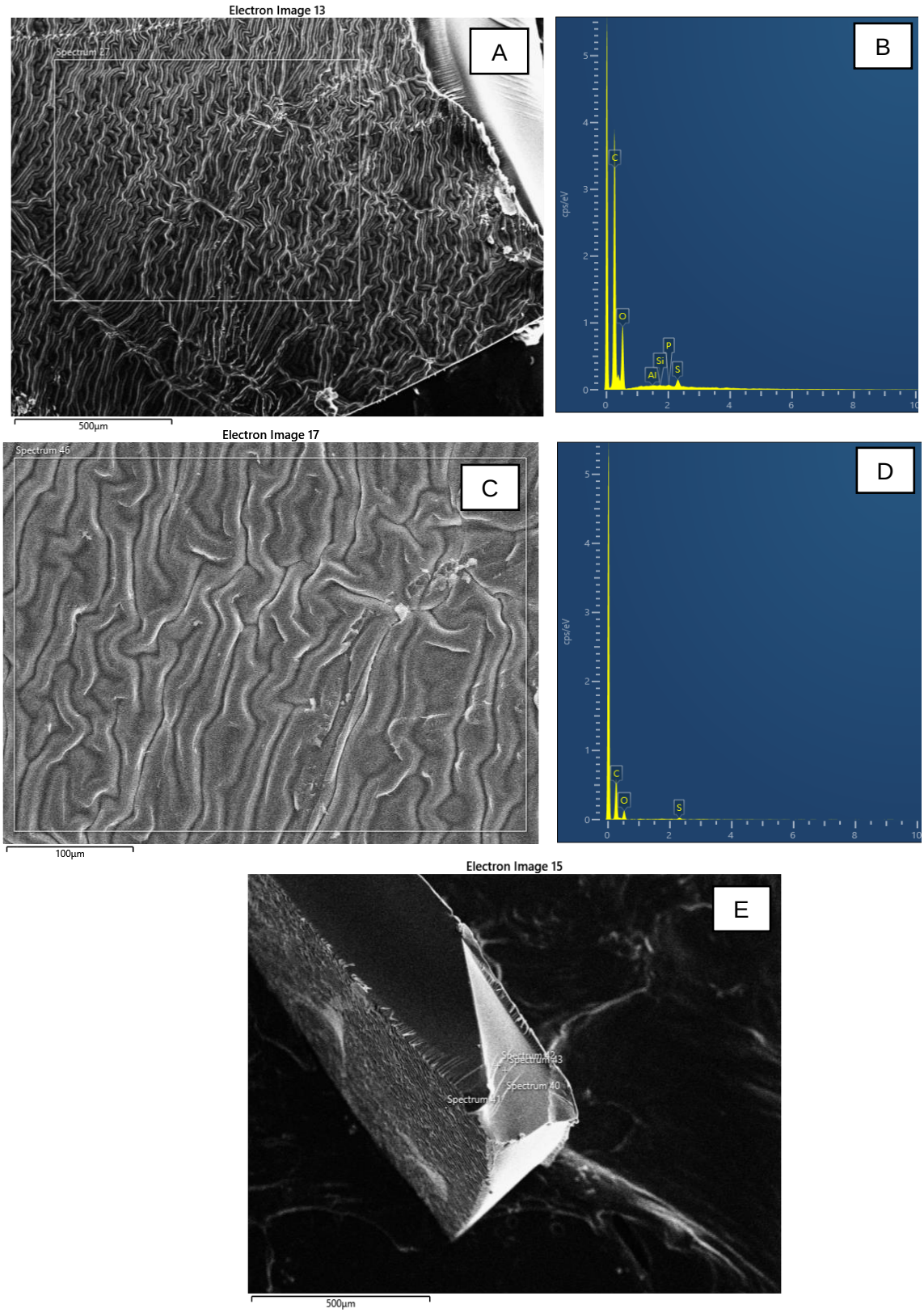

Figure 39A-E: Fig.39A shows the morphology of the upper surface of 12% polyacrylamide ATP gel at 500 µm. Fig 39B is the EDX analysis for Spectrum 27 seen on Fig 39A. Figure 39C is a closer look at Spectrum 27 from 39A at 100 µm. The accompanying EDX results are seen in Fig. 39D. Figure 39E shows the entire cross-section and depth of the gel, which gives good insight as to how the architecture varies throughout the gel, due to factors such as drying.

With regards to the aluminium, this may be a small peak formed as a result of the aluminium stub the sample is placed upon. Figure 39D does not show any peculiarities, with the exception of the peaks being much smaller in comparison to Figure 39B. For example, the carbon peak is 3.9 eV (Fig. 39B) compared to 0.7 eV in Figure 39D. This may be due to the latter spectrum showing the elemental composition deeper within the sample, where drying effects may have caused structural disruption, showing the same elements with less intensity.

3.3.2.3 12% Polyacrylamide SDS Gels

As the viability of ATP-PAGE is being ascertained in contrast to the widely used and established SDS-PAGE, comparisons of the SEM-EDX data with SDS-PAGE gels were necessary. Unlike the previous samples (Fig 38A, 39A), the cross-section seen in Figure 40A shows a mesh of trenches throughout the thickness of the gel, at 250 µm scale. Although the corresponding EDX spectrum for Spectrum 15 (Fig 40B) – the area most central within the gel thickness – shows no unexpected results, with only relatively small peaks for carbon and oxygen (0.7 and 0.2 eV), there are a lot of precipitates seen on the surface and within of the gel. Interestingly, other expected components, such as sulphur, were not seen in Figure 40B. As a component of SDS itself, it would have been reasonable to expect to see it within the gel architecture. A possible explanation for this is that the SDS is found to precipitate at temperatures below 16ºC.[115] Therefore, as the gels dried overnight at a colder temperature, particles of SDS may have precipitated out of the gel and sedimented on top of the gel surface. This hypothesis is further supported by the presence of sulphur in Figure 40D and 40E. The prior is an analysis of the top surface of the gel (Spectrum 24, Figure 40C), whilst the latter is of an aggregate (Spectrum 25, Figure 40C). Although the peaks of sulphur here are small (0.1 eV or less) it may regardless be indicative of a portion of this precipitate. Figure 40E shows other elements not encountered previously with this sample, such as silicon and potassium. As they are not present in other EDX spectra of Figures 38 and 39, the source of these could have been the SDS specifically.

Furthermore, SDS is known to precipitate easily when combined with potassium.[116] The presence of this on the EDX spectrum Fig 40E could therefore further support the aggregate on Spectrum 25.

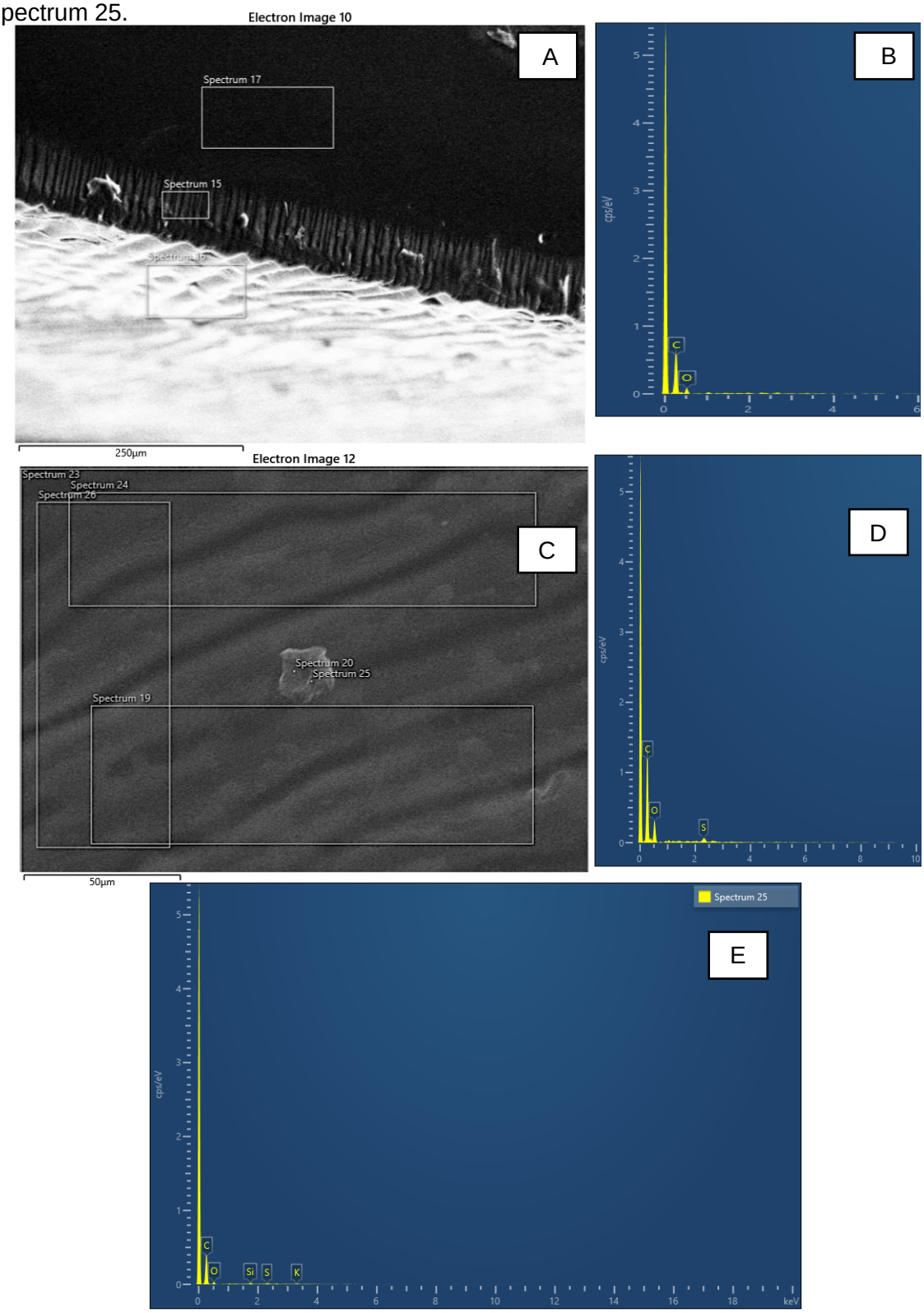

Figure 40 (A-E): 12% Acrylamide SDS Gels. Figure 40 A) captures the cross section showing the architecture across the thickness of the gel - the EDX elemental analysis for Spectrum 15 is shown in Figure 40B). Figure 40 C) show a possible aggregate formed during the gel drying process. Figures 40 D) and Figure 40 E) show EDX spectra of different areas of the Figure 40 C), Spectrum 24 and Spectrum 25 respectively.

3.3.3 SDS POLYACRYLAMIDE GEL ELECTROPHORESIS

SDS PAGE was conducted to assess how the SDS interacts with each protein, and to compare with the ATP interactions. The denaturation conditions used showed varying results as expected. The proteins overall migrated further in the SDS gels compared to native or ATP PAGE. This result was expected as the proteins undergo thermal denaturation and reduction via β-mercaptoethanol. With single chain proteins, reduction will increase their molecular weight to a small degree. Multiple polypeptide chains such as insulin should have lower molecular weights than in their native state.

Glutathione S-Transferase

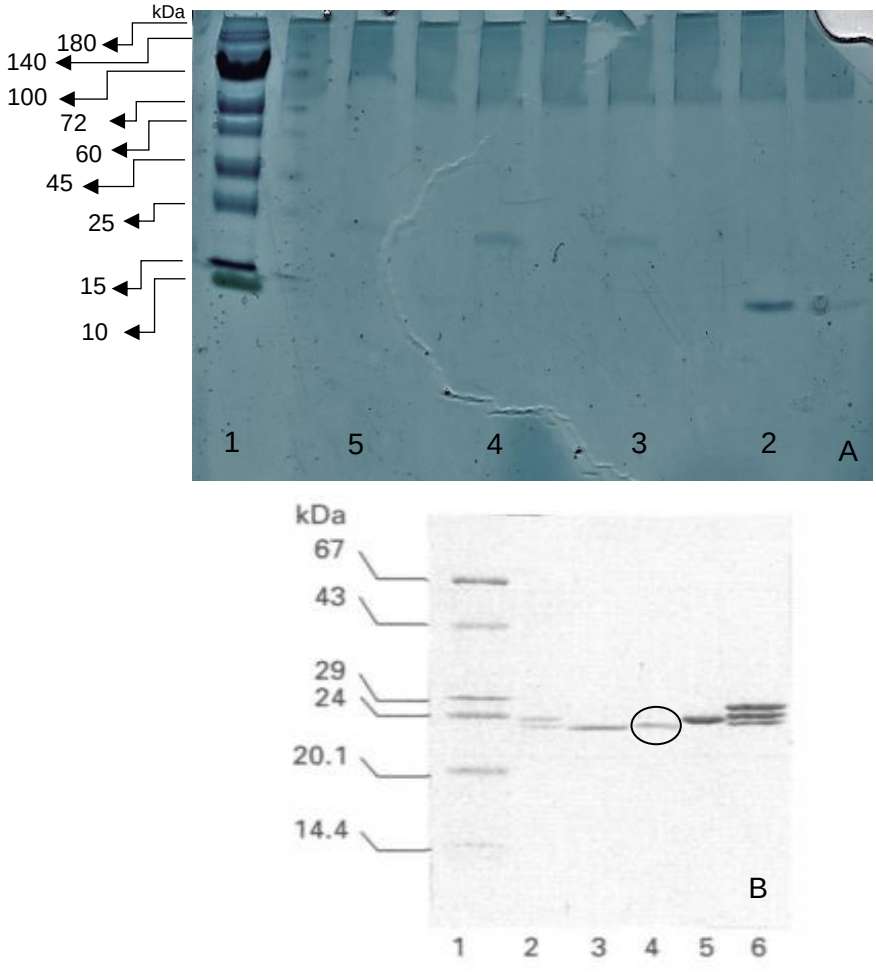

Figure 41: 12% SDS-PAGE of GST (Figure 41A) under different conditions. Lane 1: Molecular weight ladder. Lane 2: Reduced and denatured sample. Lane 3: Only denatured sample. Lane 4: Native protein + loading dye. Lane 5: Native protein. Figures 41B[117] is the corresponding literature comparison. The native sample for GST in (B) is in Lane 4 (highlighted) and is shown at ~24 kDa.

In Figure 41A, we can see the SDS-PAGE trials for Glutathione s-transferase. From the image, we can see immediately some issues with the results. Firstly, the molecular weight ladder in Lane 1 did not run to the bottom of the gel. Although we can see from literature (Fig 41B) this can happen, it is important to note. This likely occurred due to overloading in the well or short running time for the electrophoresis. Nevertheless, the bands seen in Figure 41A are in good correspondence to the literature results, with the native sample (Lane 5) band at ≈25 kDa. For reference, Table 1 showed the molecular weight from literature of GST is 26 kDa. Samples which underwent solely reduction or denaturation (lanes 3 and 4, Figure 41A) showed similar results, with bands also at ≈25 kDa.

On the other hand, the sample that had been denatured and reduced (lane 2, Figure 41A) showed a band much lower than the others. This is expected, as the process of denaturation and reduction would cause the protein to unravel, thus migrating further down the gel. The band here is seen at the last band of the molecular weight ladder (lane 1, Figure 41A), which represents 10 kDa. Therefore, thermal denaturation and reduction by β-mercaptoethanol causes a large conformational change in GST: the results in the figure above show at least 10 kDa difference. For the purposes of this project, this is relevant as it will serve as a comparison with the ATP-PAGE results. As GST is expected to interact well with ATP due to the overall positive charge and hydrophilic surface (Figure 19A, 20A and Table 2), SDS-PAGE results will help identify to what extent ATP-PAGE could be a suitable replacement.

Bovine Serum Albumin

BSA has been widely used as a reference band on SDS-PAGE gel, prior to the introduction of pre-mixed molecular weight markers. The molecular weight of BSA is commonly documented as 65-67kDa (Table 1) and usually appears as a single band on SDS gels (Figure 43B). However, from the literature[118], it has also been reported as two

bands. This was also seen in this project (Figure 42A), where the samples in lane 2 and 3 show two clear bands above the 72kDa marker and around 40kDa. As these samples were denatured and reduced respectively, it is a reasonable assumption to make that separation into two bands is due to this process. In Figure 42B[118], Panel A, the sample in lane 1 was also reduced and denatured, with two bands visible at 100kDa and 50kDa. Although the difference between the two bands is larger in Figure 42B, this is accredited to the fact the gel used in this project was at a higher polyacrylamide percentage (12%) compared to that used in the literature. Therefore, a larger protein such as BSA (Figure 22) would migrate slower through a higher percentage gel. A longer run time could have given further separated bands. As BSA also has a mainly negatively charged surface (Figure 19A), it would have more difficult migrating towards the negative electrode. From the Chimera studies, it is also postulated BSA will not interact as well with ATP, as the mostly negative and hydrophobic surface (Figure 19A and 20A) would not allow for successful hydrophobic interactions with the ATP, or strong attraction between ATP's negative phosphate groups and BSA's surface.

B – Lactoglobulin

The third protein analysed with a denaturing SDS-PAGE was β-lactoglobulin, one of the main components of cow's milk. In literature, it is reported to have different quaternary structures depending on the pH.[119,120] Above a pH of 5, it can be seen as an octamer, with a molecular weight of 140 kDa[121] (Figure 43A). Between a pH of 3-5, it shows a dimer conformation of 34 kDa (43B), and below this it can be found as a monomer at 17kDa (Figure 43A and 43B). The results in Figure 43A show the octamer and monomer conformation in lanes 3 and 5. As lane 5 contains the native protein, this is reasonable. However, lane 3's samples are thermally denatured; therefore, the protein molecular weight is expected to decrease, thus lower bands should be seen on SDS-PAGE. It may be that a higher temperature is required for denaturation to occur completely. Nevertheless, the

monomers seen in lane 2, 3 and 5 (Fig 43A) are consistent with the literature results in Figure 43B. Results in Lane 3 show three distinct bands, with the octamer and monomer at the correct molecular weight stage. The middle band, however, is slightly higher than expected for a BLG dimer (43-55 kDa in Figure 43A compared to 34 kDa in Figure 43B)[122]. However, as this band is seen again in further results, it may be reasonable to assume it is a dimer band, as BLG may assume both conformations at similar pH. The denatured and reduced sample in lane 2 (Fig 43A) shows the lowest molecular weight, however it is still aligned with the molecular weight of the monomer (17 kDa).

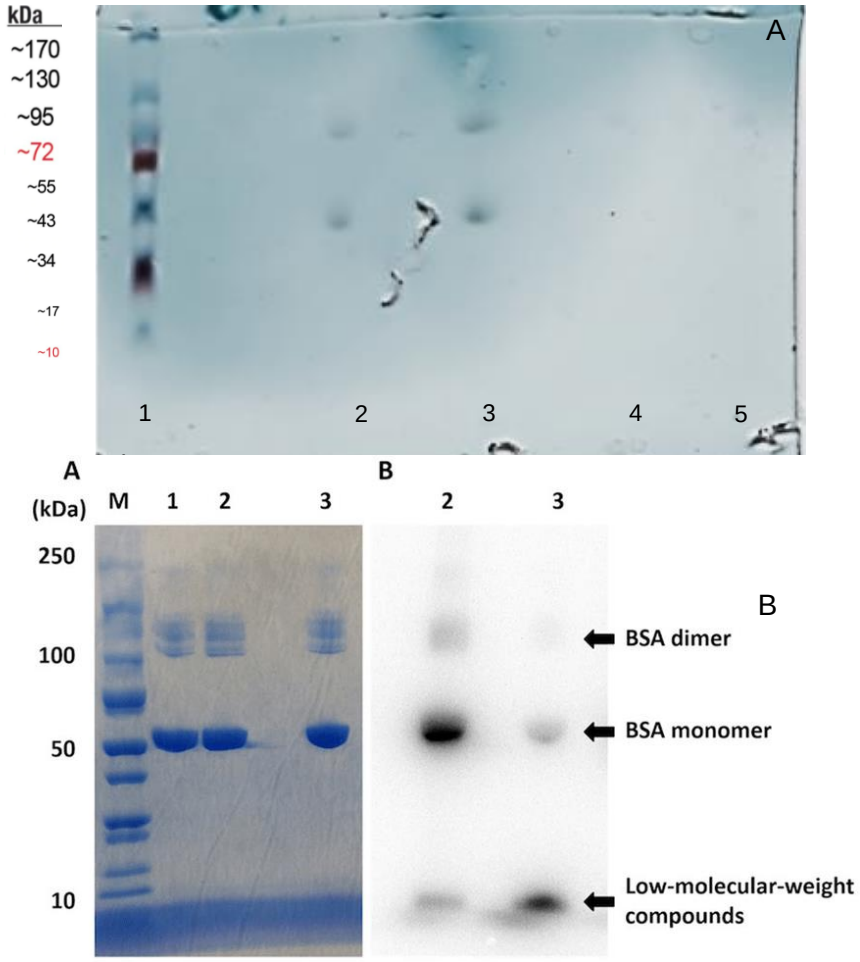

Figure 42: 12% SDS-PAGE of BSA (42A). under different conditions. Lane 1: Molecular weight ladder. Lane 2: Reduced and denatured sample. Lane 3: Only denatured sample. Lane 4: Native protein + loading dye. Lane 5: Native protein. Figure 42B shows a comparison image from literature of BSA.[118] Details of this image are: panel A was stained using Coomassie blue, panel B with radiography. Only panel A is of interest, but the annotation and panel B were kept for ease of understanding. Lane 1 is native BSA and is the lane used for comparison here. Lane M shows the molecular weight ladder.

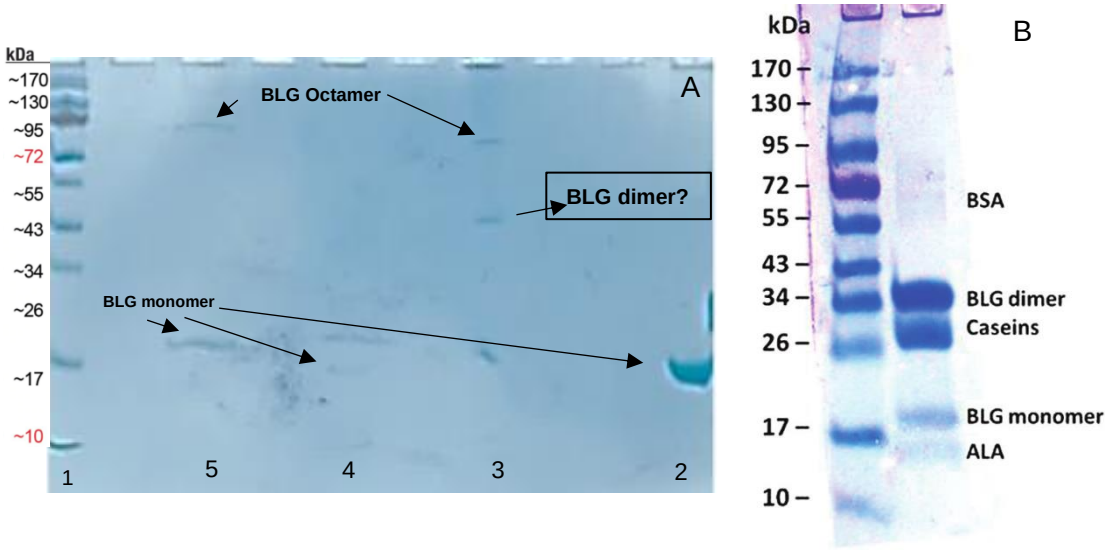

Figure 43: 12% SDS-PAGE of BLG (43A). under different conditions, showing monomer and octamer[121] conformations. Lane 1: Molecular weight ladder. Lane 2: Reduced and denatured sample. Lane 3: Only denatured sample. Lane 4: Native protein + loading dye. Lane 5: Native protein, seen at 17 kDa, compatible with a BLG monomer. Figure 43B shows a comparison image from literature[122]. Here a band for the BLG monomer (circa 17 kDa) and dimer (34 kDa) can be seen.

Insulin

As mentioned previously, the insulin used throughout this project was an insulin hexamer. As observed in literature[85,123], the addition of zinc provides for stability of the hexameric structure. For this reason, it is stored within the body as a zinc-insulin hexamer[124] until it is required. Due to higher molecular weight of the hexamer (one insulin monomer is around 6kDa, as seen in Figure 44B, therefore a hexamer would weigh ≈36kDa), the bands for the native samples (lanes 4 and 5, Figure 44A) would be expected to be seen around the 35kDa mark. However, no strong bands can be seen here. This could be due to the sample concentration being too low. On the other hand, two robust bands can be seen in lanes 2 and 3 (Figure 44A), where the samples were reduced & denatured or only denatured, respectively. The protein in these samples would have lower molecular weights due to the denaturation process, as seen with the bands between the 10-15 kDa molecular weight marker. As literature (Figure 44B) confirms the monomer weighs 6kDa, the results in Figure 44A could therefore be showing a dimeric unit. The addition of the zinc could have

increased structural stability enough for the architecture not to break down further to a monomer.

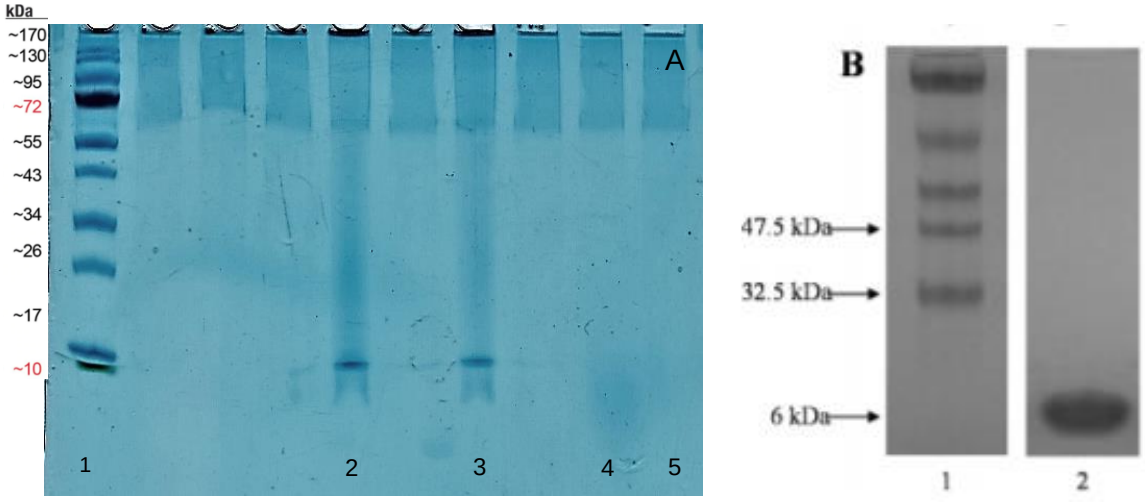

Figure 44: 12% SDS-PAGE of Insulin (44A). under different conditions. Lane 1: Molecular weight ladder. Lane 2: Reduced and denatured sample. Lane 3: Only denatured sample. Lane 4: Native protein + loading dye. Lane 5: Native protein. Figure 44B shows a comparison image from literature[125]. Lane 1 is a molecular weight ladder and Lane 2 is insulin native sample. The low MW indicates the insulin here was not a hexameric structure.

RNAse A

RNAse A is one of the smallest proteins used in this project, with a molecular weight of 13.7 kDa (Table 1). From Figure 45A, the results seen across the lanes are rather consistent. Despite the reduction and thermal denaturation, all bands seen show similar molecular weights to the native sample in lane 5, as well as the literature comparison (Figure 45B)[126]. The surplus band seen next to lane 5 was likely caused by the sample being pipetted into the well too quickly, which can often lead to some of the sample moving into the neighbouring well. Furthermore, the wave-like pattern seen with the band in lane 3 is frequently a result of letting the loaded gel sit in the electrophoresis tank for too long before running the gel. In this case, the results are still consistent with the literature. Bands at even lower molecular weights are likely not seen due to the limitation of SDS-PAGE with lighter proteins. For proteins below 10kDa, literature recommends a different protocol[127,128], which first, demands a higher acrylamide concentration in the gel. To visualise the potential

band of denatured and reduced RNAse A, increasing acrylamide percentage would be valid future work to explore.

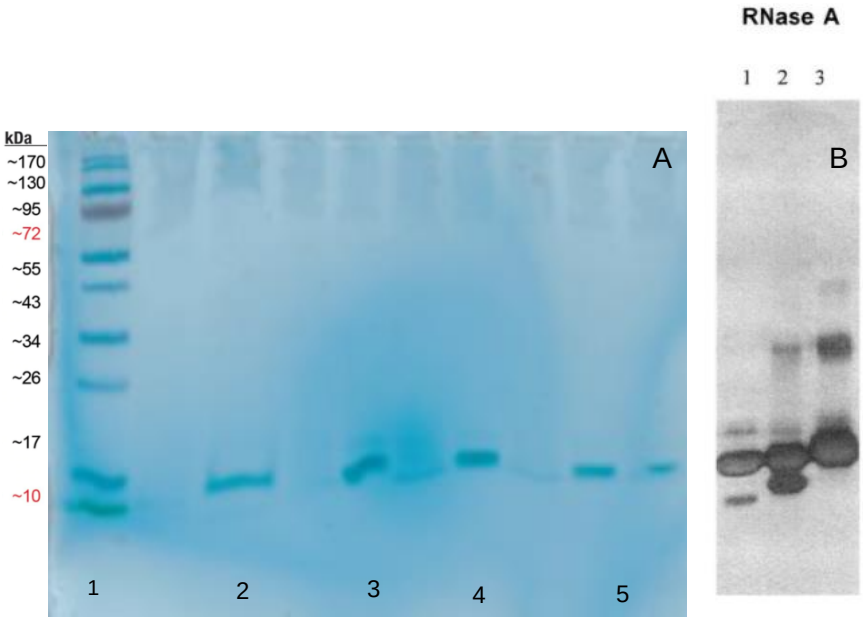

Figure 45: 12% SDS-PAGE of RNAse A (45A). under different conditions. Lane 1: Molecular weight ladder. Lane 2: Reduced and denatured sample. Lane 3: Only denatured sample. Lane 4: Native protein + loading dye. Lane 5: Native protein. Figure 45B shows a comparison image from literature[126]. Lane 1 represents the native protein sample.

Lysozyme

Lysozyme is a very widely represented protein in SDS-PAGE literature. With a molecular weight of 14.4 kDa (Table 1), the result seen in Figure 46A are nicely aligned with the literature results seen in Figure 46B. As with RNAse A above (Figure 45A), the denatured/reduced/denatured and reduced samples in lanes 2, 3 and 4 would have been presumed to be found below the 10 kDa molecular weight marker. Instead, we see these bands at nearly the same position as the native sample in lane 5, which itself is consistent with the native protein literature sample (Figure 46B)[129]. As discussed earlier, SDS-PAGE is not the preferred method for samples with extremely low molecular weights: to visualise these bands, a higher acrylamide percentage would be preferable. Future repeats with varying increase acrylamide percentages would be worthwhile to attempt to visualise

RNAse A and lysoszyme. However, as SDS-PAGE was not the focus of this project and served mainly as a comparative tool for ATP-PAGE, this was not done at this time.

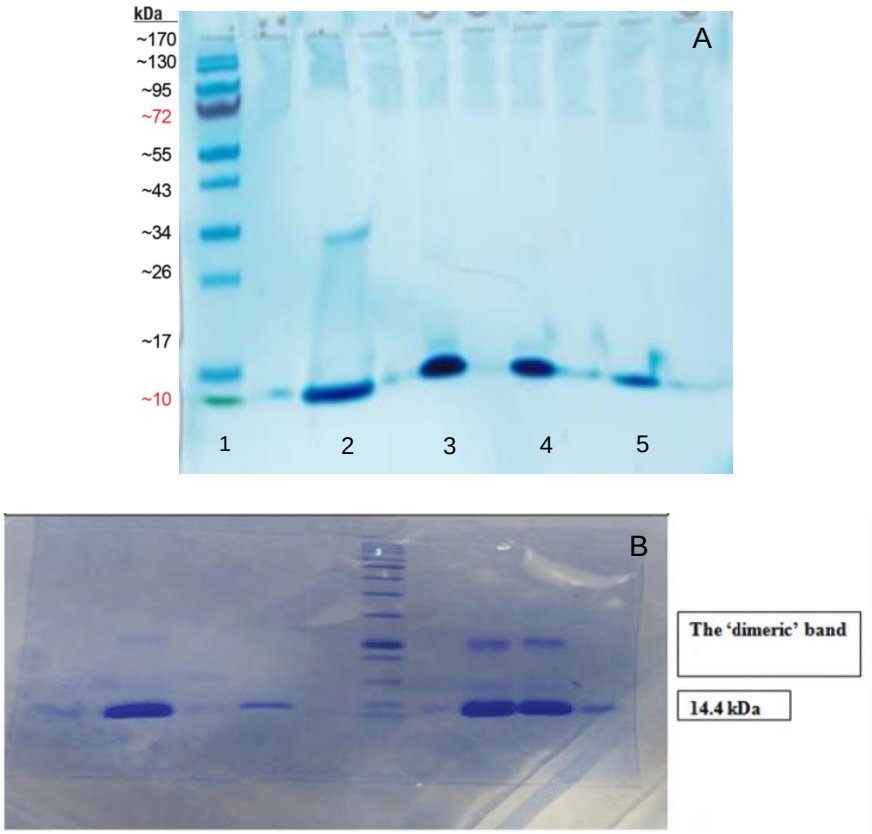

Figure 46: 12% SDS-PAGE of Lysozyme (46A). under different conditions. Lane 1: Molecular weight ladder. Lane 2: Reduced and denatured sample. Lane 3: Only denatured sample. Lane 4: Native protein + loading dye. Lane 5: Native protein. Figure 46B shows a comparison image from literature.[129]

3.3.4 NATIVE POLYACRYLAMIDE GEL ELECTROPHORESIS

With native-PAGE, only anionic proteins were expected to migrate. Insulin for example contains a largely positive surface (see figure 19B in section 2.3.1), which would hinder its migration towards the cathode. The results were needed as a control, to then compare with the SDS and ATP effects on the proteins. Although the BSA sample concentration was too high - as seen by the overloading (Figure 47) – and the insulin and RNAse samples mixed upon loading, the general pattern seen is suitable. As there was no denaturation involved, larger proteins such as BSA were not expected to migrate far and can be seen at the 100 kDa mark. Although, with both BSA and BLG, separation of the bands due to the dimer conformation is noticeable. The more intense band seen above the BLG dimer is likely the GST band. It is common that after sample loading, they may move out of the wells and mix into the neighbouring wells. This would explain the streaky band seen where the GST was loaded in the third lane, and the actual band showing in the first lane. The streaky pattern is a consequence of sample overloading.

Sample mixing occurred in the 8th lane, with RNAse and insulin samples. Two intense bands and two less intense band alternating with these can be seen. The more intense bands and the one in between them are likely the insulin tetramer bands. The lighter band above these is the RNAse band. Insulin, although being a tetramer, would be expected to move further. However, native PAGE does not involve any negative charge added to the protein surface. Similarly. RNAse is expected to have little movement down the gel, thus explaining the bands towards the top. Lastly, the lysozyme band can be seen still in the well. Although mostly negative (Figure 19B), the strong disulphide bonds

contained create a large molecule, unlikely to move far in the gel without denaturing conditions.

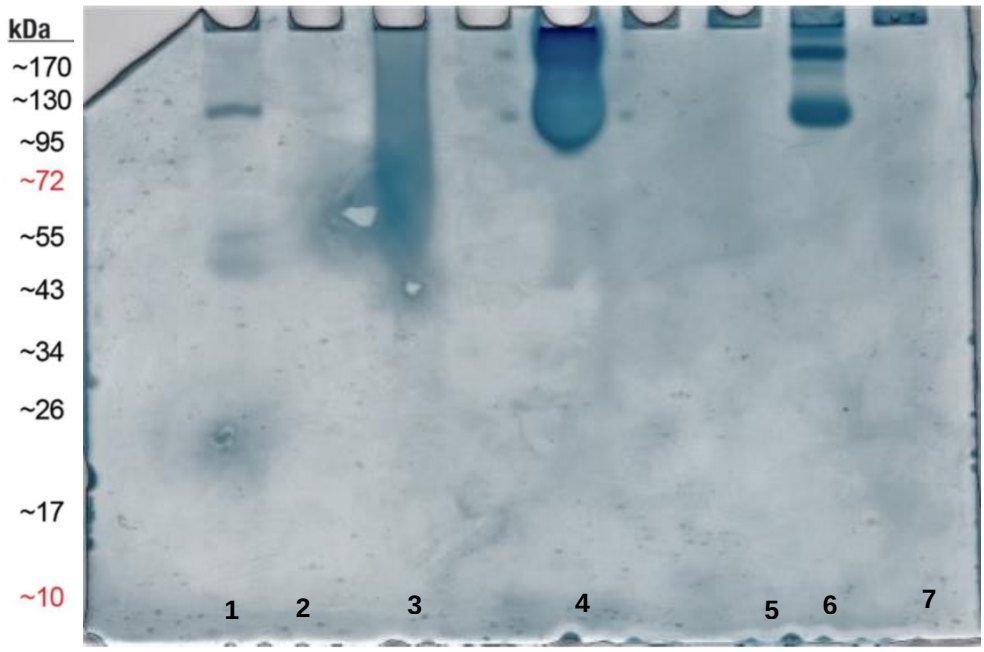

Figure 47: 12% Native polyacrylamide gel with samples in native conditions. Lane 1: molecular weight ladder; Lane 2: GST; Lane 3: BLG; Lane 4: BSA; Lane 5: Insulin; Lane 6: RNAse A; Lane 7: Lysozyme. Results here were poor, due to overloading for GST and BSA. Some mixing occurred with insulin and RNAse A in the sample well, causing overlapping of the bands. Good migration of proteins in this trial was not expected due to the lack of sample manipulation required for optimal results seen with SDS-PAGE.

To assess whether including ATP in the gel hindered or improved the results, ATP treated samples were tested on a native 12% polyacrylamide gel (Figure 48). The results are noticeably improved compared to those seen in Figure 47 and are similar to the ATP-PAGE trials seen later on in Figure 49. Although fainter, a single band for GST can be seen in lane 2, at circa 95kDa. In lane 3, two very intense bands can be seen; below this, two clear bands are also present. The top bands are due to overloaded BSA, where the concentration was too high, possible in a dimer conformation. The bands below these are very likely also BSA, but at a more desirable concentration and possibly in a monomeric structure (Figure 42B). Compared to the previous results, these have also travelled further down the gel. Some sample mixing occurred between BLG and insulin. These results are more favourable compared to the native PAGE, as the cationic proteins moved further. RNAse A (Figure 48) can be slightly visualised in lane 6, having travelled further down

compared to Figure 47. This could be due to the ATP providing a small increase in negative charge, enough to allow for augmented migration. Lysozyme, however, is not visualised at all in lane 7. This could be both due to the need for denaturation as discussed previously, or increased concentration. It is also possible the majority remained in the well as seen before. In conclusion, this gel showed better band separation and migration compared to the native gels. Therefore, improved band separation can be seen with BSA, BLG and insulin.

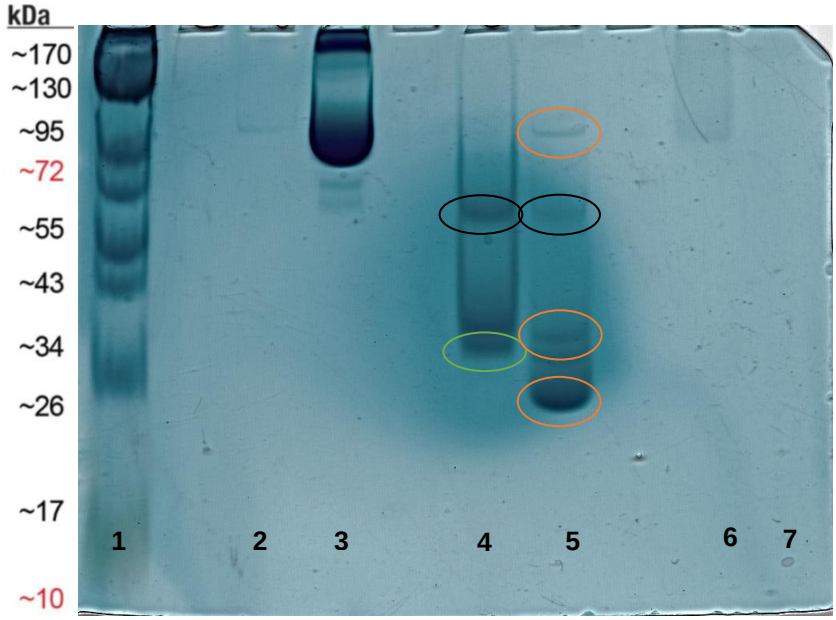

Figure 48: 12% polyacrylamide native gel with ATP treated samples. Lane 1: molecular weight ladder; Lane 2: GST-ATP; Lane 3: BSA-ATP; Lane 4: Insulin-ATP; Lane 5: BLG-ATP; Lane 6: RNAse A-ATP; Lane 7: Lysozyme-ATP. The orange circles highlight the BLG octamer, dimer and monomer bands. The black circles is likely to be residual BSA that had moved into the neighbouring wells when the sample was loaded, due to the same exact band location as seen in Lane 3 at the 55-72kDa mark. Finally, the green circle indicates the insulin hexamer band, consistent with literature results at the 34kDa mark.

3.3.5 ATP POLYACRYLAMIDE GEL ELECTROPHORESIS

The addition of ATP to the gel varied the results, although to a lesser extent than hypothesised (Figure 49). However, the presence of dimer and trimer bands expected was significant: although the ATP does not denature the proteins, it still separates them by molecular weight. As postulated, some proteins saw interacted with the ATP more efficiently. Figure 49 shows multiple bands in Lanes 3, 4 and 5. Lane 3, with the BSA

samples, has overloading in the well, marked by the irregular, saturated bands; the neighbouring well shows a much clearer result, as the sample would have spilled over into the loading buffer, usually leading to it mixing into adjacent wells. Therefore, the two bands seen in Lane 3 found at above 170 kDa and 130 kDa are possibly not representative of BSA but could be a mixture of other high molecular weight compounds formed as a result of the addition of ATP. However, below the overloaded bands, there are two bands more consistent with the BSA dimer seen in literature, below 95kDa (Figure 49 and literature reference, Figure 42B). Similar to the sample mixing seen with BSA, the same issue is encountered in Lane 4 and 5: here, due to the proximity of the wells, the BLG and insulin mixed. To analyse the results in Figure 49 in a clearer way, the bands of interest have been highlighted in different colours, with each colour representing one type of protein. The yellow protein is BSA, the orange is BLG and the black is insulin (Figure 49). Consequently, we can see the following: both lane 4 and 5 show the BLG octamer (140kDA) and dimer conformation encountered also in previous trials (Figure 48 with native polyacrylamide gel and BLG-ATP, Figure 43A for the SDS-PAGE). Lane 5 (Fig 49) also shows the BLG monomer. Although some proteins did migrate well in the gel, some did not migrate as far as expected, such as GST and BSA. They were seen at 140kDa and between 95 and 72kDa respectively (Figure 49), whilst their literature references showed 25kDa and 65kDa. Others, such as RNAse A and lysozyme were not visualised well. These latter two proteins were anticipated to interact well with ATP, due to the Chimera studies completed prior (Figure 19B and 20B) showing a mostly hydrophilic and positive surface. However, they are also quite small proteins (≈10kDa), therefore they are not easily visualized with gel electrophoresis, as discussed previously. The “slowing down” of the protein migration may be explained by the addition of ATP to the gel. Furthermore, the disodium salts contained in the ATP are present in the gel, which may deter the protein movement. A band for RNAse can be seen in lane 8, such as in Figure 48, at a similar distance. As discussed previously, RNAse is a mostly positive protein: it would need a large amount of negative charge to be provided to it for further movement. Lysozyme is again not visualised. Due to the consistent

result seen with lysozyme and ATP in previous research[93], it is unlikely ATP has enough negative charge to provide to the protein. Furthermore, it is probable lysozyme will need a thermal denaturation for appropriate visualisation with PAGE. In conclusion, however, overall, there was a significant increase of protein migration with the addition of ATP compared to the native PAGE, particularly seen with insulin and β- lactoglobulin. In other trials, a similar pattern in results was seen, although with less clear band separation.

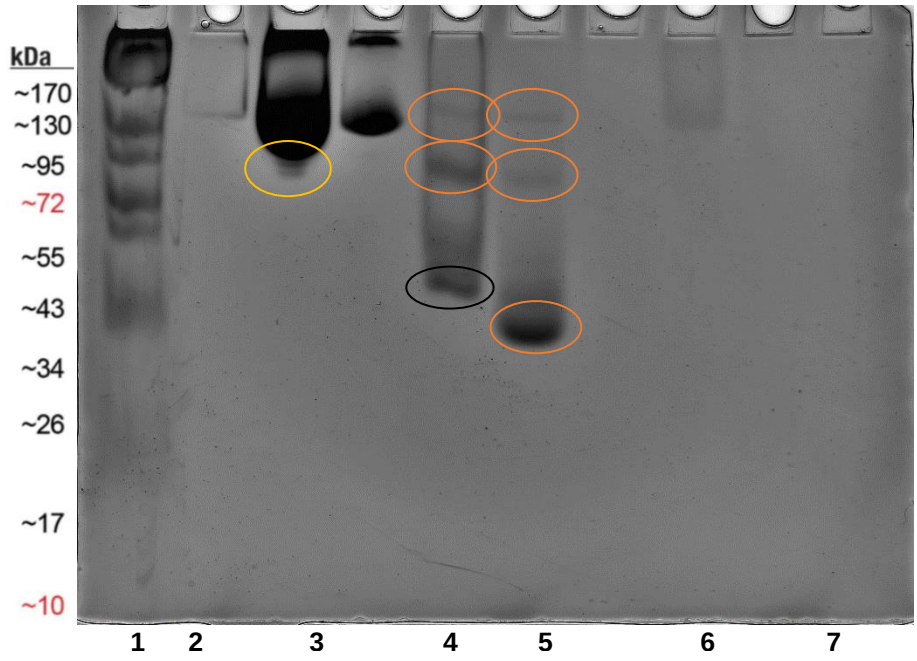

Figure 49: 10% ATP polyacrylamide gel with ATP treated samples. Lane 1: molecular weight ladder; Lane 2: GST-ATP; Lane 3: BSA-ATP; Lane 4: Insulin-ATP; Lane 5: BLG-ATP; Lane 6: RNAse A-ATP; Lane 7: Lysozyme-ATP. For better visualization, some bands have been highlighted above. The BSA bands are highlighted in yellow. The BLG octamer (140kDa) and dimer (36 kDa) are highlighted in orange; the octamer band present in Lane 4 as well as Lane 5 indicate there was some sample mixing between the neighbouring wells. The band seen between 72-95 kDa in Lanes 4 and 5 was also present in the SDS-PAGE trials for BLG, therefore they are likely representative of the BLG dimer structure. The insulin band is highlighted in black to discern it from the BLG.

Another issue encountered throughout experiment repetition was the buffer hydrolysing and therefore not working. This applied both to running buffers and sample buffers: therefore, without functioning sample buffer, little to no movement could be seen. The ATP buffer shelf life was found to be up to a week. The addition of magnesium acetate, which has been shown to increase the effect of ATP *in vivo*, yielded poor results.

There was overall no amelioration of the results (Figure 50) seen previously (Figure 48 and Figure 49), and the bands seen showed poor results. BSA showed as a monomer, which is an important discrepancy compared to the previous results discussed (Figure 42B,48 and 49). Similarly, BLG showed a monomeric instead of a dimeric band. Analogously, insulin showed as a single band. A weak band can be seen also for RNAse. There are no bands seen for GST or lysozyme. A possible explanation for this is the $Mg(OAc)_2$ counteracting ATP's negative charge to such an extent where it would have little to no effect on the proteins analysed. Due to the poor results and time constraints, this was not trialled further as the ATP-PAGE results were already found to be satisfactory. However, future work on ATP-PAGE is required, especially with trials at various protein concentrations, and sample preparation. For example, varying the pH of the sample and running buffers until a more consistent protein visualisation is seen. Furthermore, increasing the polyacrylamide percentage to 18%[127] to visualise the smaller proteins would be valuable to see the extent of their interaction with ATP. Repeating these trials on separate gels for higher and lower molecular weight proteins could also be useful in the method development stage, until a consistently desirable common acrylamide percentage is found.

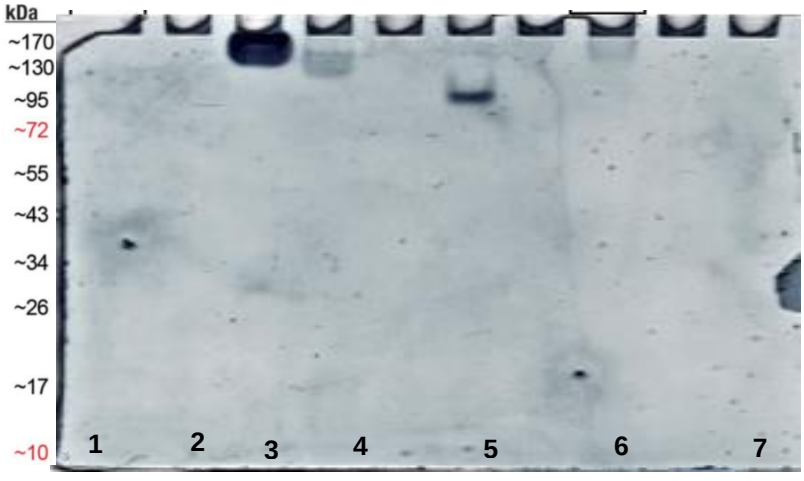

Figure 50: 10% ATP polyacrylamide gel with ATP-$Mg(OAc)_2$ treated samples. Lane 1: molecular weight ladder; Lane 2: GST-ATP $Mg(OAc)_2$; Lane 3: BSA-ATP $Mg(OAc)_2$; Lane 4: BLG-ATP $Mg(OAc)_2$; Lane 5: Insulin-ATP $Mg(OAc)_2$; Lane 6: RNAse A-ATP $Mg(OAc)_2$; Lane 7: Lysozyme-ATP $Mg(OAc)_2$. The black circles highlight BLG bands.

3.3.6 AMP POLYACRYLAMIDE GEL ELECTROPHORESIS

Varying concentrations of AMP were trialled. The first one tested, based on the ATP literature and results, was 8mM. Next, 4mM was trialled. The other concentrations tested with ATP (16, 2 and 1 mM) were not tested due to the poor results these yielded with ATP. As seen below (Figure 51), AMP also yielded poor results. The only bands seen are those of BSA, which can be seen in two lanes as they moved out of the well during pipetting. Due to these poor results, AMP was not trialled further.

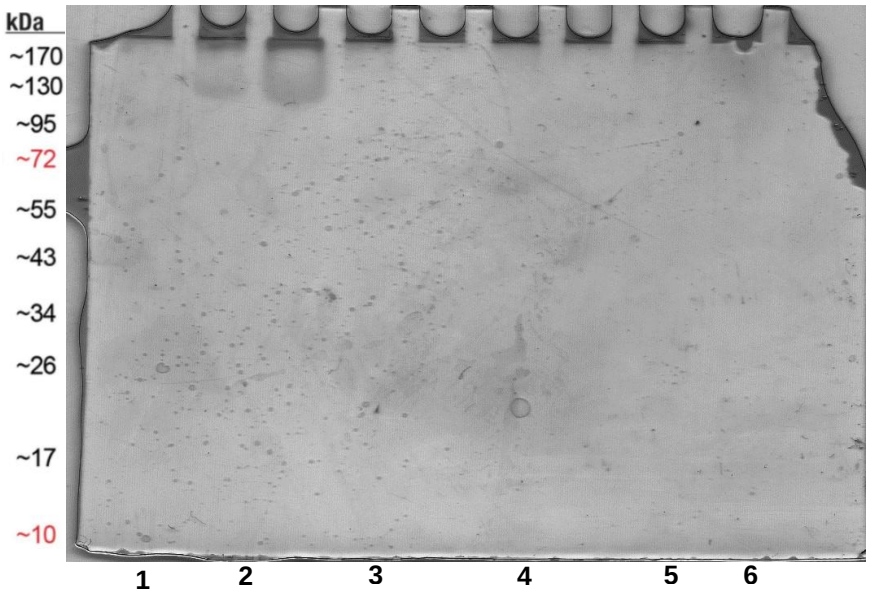

Figure 51: 10% polyacrylamide gel with 8mM AMP addition. Trialled with AMP treated samples. Lane 1: GST-AMP; Lane 1: BSA-AMP; Lane 3: BLG-AMP; Lane 4: Insulin-AMP; Lane 5: RNAse A-AMP; Lane 6: Lysozyme-AMP.

3.3.7 ATP Polyacrylamide Gel Electrophoresis with Cell Lysate Studies

Cell lysate is a mixture which contains all the components of a denatured cell. As seen in Figure 52, best dilution was that of 1:2 demonstrated by the better band separation than seen in further dilutions. A few bands can be discerned well, although not all. However, this may be due to the limited amount of negative charge provided by the ATP, combined with the large molecular size. Due to time constraints this was not investigated further, although the result above is very promising and further investigation would be required to improve results. If an ATP result comparable to a typical SDS PAGE result could be obtained, the applications in biomedical research could be numerous.

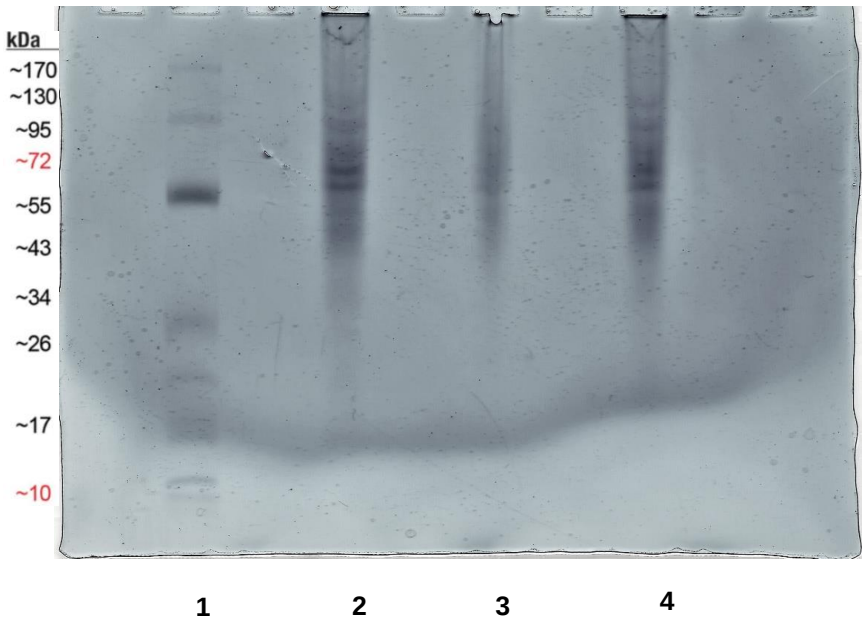

Figure 52: Cell lysate dilution series studies. Lane 1: molecular weight ladder; Lane 2: Cell lysate 1:2 dilution with MilliQ water; Lane 3: 1:4 dilution; Lane 4: 1:8 dilution.

3.4: CONCLUSION

In conclusion, the polyacrylamide gels were characterised and analysed successfully. Rheology provided insight into the viscoelastic response, showing longer polymerisation time for ATP gels may be required for a more desirable gel. SEM showed interesting variations in gel architectures, providing some explanations for the different results seen with ATP PAGE. Finally, the PAGE analysis was done. Native PAGE with ATP samples showed results more akin to what would be expected with the addition of SDS, which is the technique ATP PAGE aims to replace. However, the lack of lysozyme bands in the results signifies a limit for ATP PAGE: further testing on strongly bound molecules would need to be done. This is essential to verify whether ATP is effective in the presence of robust bonds such as the disulphide bonds present in lysozyme. The addition of $Mg(OAc)_2$ did not provide better results, nor using AMP. The cell lysate studies were promising, although more time was needed to fully investigate these.

CHAPTER 4: CONCLUSIONS AND FUTURE WORK

The aim of this project was mainly to develop ATP-PAGE, and to examine whether it could be a viable substitute for SDS-PAGE. In chapter 2, characterisation of the proteins was carried out, through various techniques. The analytical methods used for this characterisation each had a specific aim: Chimera software, for the computational analysis of hydrophobicity and surface charge, to evaluate the efficacy of the interaction and conformational changes due to the addition ATP; Dynamic Light Scattering, to measure the variation in protein particle size in native state, with SDS and with ATP; Zeta Potential to measure the ATP-protein stability and finally Circular Dichroism to define the α-helix, β-pleated sheets and random coil percentages within the protein samples. Some provided extremely useful insight, such as the "Chimera" studies. From these results, we were able to postulate which proteins would theoretically interact best with ATP via hydrophobic interactions or via attraction between ATP's relatively negative tail and a positive protein surface. Comparing these hypothesized results to the experimental ones, discrepancies were then examined using literature. From the results of Chimera, DLS and Zeta Potential, it was initially put forward the optimal results with ATP would be seen with GST, RNAse A and Lysozyme. However, as discussed with the PAGE studies in Chapter 3, this was not found to be the case, due to very small molecular weight of the proteins, requiring modifications to the electrophoresis protocol. Furthermore, issues were encountered with sample agglomeration upon addition of ATP. This was encountered with DLS and zeta potential. Some proteins gave a good understanding, such as BSA. This is likely due its high stability, as shown by the high volume of literature regarding the characterisation of BSA, which ultimately lead to it being used a protein standard. However, the results for the other proteins need further method development. This may include using higher protein concentrations, different sample buffers to limit protonation or using more positively charged and widely available proteins until a reliable method is achieved.

Zeta potential studies also were hindered by sample agglomeration and would benefit from further method development. As the proteins being used have a wide range of

isoelectric points (pH 4-10), the effect on the surface charge due to increasing or decreasing the solvent pH would be interesting future work. Theoretically, in native conditions and at pH 7.8, GST, BSA, BLG and INS should all be negatively charged, as their isoelectric points are between 4 and 5.5. RNAse A and lysozyme should instead be positively charged. Due to time constraints, zeta potential analysis at different pH values could not be completed; this could be an interesting test to carry out to fully characterise the effect of ATP on the surface charge at different pH values. This could be especially interesting at a pH of around 3, as it lays well below the lowest isoelectric point of the proteins analysed. Circular dichroism analysis was successful in quantifying the change in α-helix and anti-parallel β-sheet content across the SDS, native and ATP conditions. Although the native and ATP results were expected to match, there was significant contribution from the ATP in the conformational changes. Furthermore, the signal obtained by the CD represents an average of all the conformations which a protein may form. These may include helical, sheet, random coil or others in the single peak. Therefore, it would be more likely the result seen is a combination of all the secondary structures mentioned. As above, repetition of these trials would be valuable, with increased protein concentrations for samples such as GST, lysozyme and RNAse A, which were a limited resource due to both accessibility and low molecular weights.

In chapter 3, the polyacrylamide gels were characterised. Good results were obtained from the rheological studies, where the viscous and elastic response of the gels was measured. Two ATP gels were compared, formed at different polymerisation times (minutes later and overnight). Overnight polymerisation showed results more akin to the SDS polyacrylamide gels, indicating this could be a preferable method for ATP-PAGE gel casting. Samples from the same rheology batch were used for SEM imaging. The ATP PA response for this was unseen before and showed remarkable results, where the ATP still formed crosslinking, albeit with the addition of salt molecules throughout. With the contribution of these results, it was suggested the addition of ATP within the PAGE gels would not hinder protein migration. To further investigate this, varying polyacrylamide concentrations could be also analysed via SEM and rheological studies. As some of the proteins used in this research had a low molecular weight, combining a low molecular weight PAGE protocol as

discussed previously with ATP, would be of extreme value to the research. This could establish a more successful protocol with proteins such as GST, lysozyme and RNAse A, which as discussed above were the proteins which yielded the poorer results.

Subsequently, polyacrylamide gel electrophoresis was conducted with native, SDS and ATP gels. A good result was obtained for this: five of the six proteins examined were seen on the ATP-polyacrylamide gel. An improved result was obtained by combining native and ATP PAGE, by using a native gel and ATP samples. However, in neither of the trials were RNAse A and lysozyme visualised properly. As discussed previously, issues with lysozyme separation with electrophoresis are not uncommon in literature, and as many of the gels showed incomplete separation of BSA – the largest protein analysed – but no bands for lysozyme, it is a reasonable assumption to make that lysozyme had already run off the gel by the time the run had finished. Future experiments could also include decreasing polyacrylamide concentration in the gel or separating the trials into a low molecular weight and a higher molecular weight protocol. The method established in this research with 12% polyacrylamide could be kept for the heavier proteins. However, separating the gels into lower and higher weighing proteins could eliminate any issues with running times altogether as the protocol would be tailored to the proteins being analysed. This was not considered at the time of when the research was conducted as the initial aim was to try a direct replacement for SDS with ATP: the universal application of SDS to proteins was therefore mimicked here by analysing all the samples on one gel.

Furthermore, supplementary method development could yield better results with the cell lysate studies in ATP-PAGE. Examining the functionality of the other enzymatic proteins (GST and lysozyme) in ATP conditions would also further justify the purpose of ATP-PAGE as a novel method, as the applications would widen to biochemistry.

BIBLIOGRAPHY

1 B. Alberts, A. Johnson, J. Lewis, M. Raff, K. Roberts and P. Walter, *Molecular Biology of the Cell - Protein Function*, Garland Science, New York, 2002.

2 A. T. Kopylov, V. G. Zgoda, E. V. Ilgisonis, E. A. Ponomarenko, A. V. Lisitsa, E. V. Poverennaya, M. A. Pyatnitskiy and A. I. Archakov, *Int. J. Anal. Chem.*, 2016, **2016**, 1–6.

3 M.-S. Kim, S. M. Pinto, D. Getnet, R. S. Nirujogi, S. S. Manda, R. Chaerkady, A. K. Madugundu, D. S. Kelkar, R. Isserlin, S. Jain, J. K. Thomas, B. Muthusamy, P. Leal-Rojas, P. Kumar, N. A. Sahasrabuddhe, L. Balakrishnan, J. Advani, B. George, S. Renuse, L. D. N. Selvan, A. H. Patil, V. Nanjappa, A. Radhakrishnan, S. Prasad, T. Subbannayya, R. Raju, M. Kumar, S. K. Sreenivasamurthy, A. Marimuthu, G. J. Sathe, S. Chavan, K. K. Datta, Y. Subbannayya, A. Sahu, S. D. Yelamanchi, S. Jayaram, P. Rajagopalan, J. Sharma, K. R. Murthy, N. Syed, R. Goel, A. A. Khan, S. Ahmad, G. Dey, K. Mudgal, A. Chatterjee, T.-C. Huang, J. Zhong, X. Wu, P. G. Shaw, D. Freed, M. S. Zahari, K. K. Mukherjee, S. Shankar, A. Mahadevan, H. Lam, C. J. Mitchell, S. K. Shankar, P. Satishchandra, J. T. Schroeder, R. Sirdeshmukh, A. Maitra, S. D. Leach, C. G. Drake, M. K. Halushka, T. S. K. Prasad, R. H. Hruban, C. L. Kerr, G. D. Bader, C. A. Iacobuzio-Donahue, H. Gowda and A. Pandey, *Nature*, 2014, **509**, 575–81.

4 T. Kondo, *Biochim. Biophys. Acta - Proteins Proteomics*, 2019, **1867**, 2–8.

5 A. Patel, L. Malinovska, S. Saha, J. Wang, S. Alberti, Y. Krishnan and A. A. Hyman, *Science (80-.).*, 2017, **356**, 753–756.

6 R. J. Fritsch and I. Krause, *Encycl. Food Sci. Nutr.*, 2003, 2055–2062.

7 K. Weber and M. Osborn, *J. Biol. Chem.*, 1969, **244**, 4406–4412.

8 I. M. Rosenberg, *Protein Analysis and Purification : Benchtop Techniques*, Birkhäuser, 2005.

9 T. Maniatis, A. Jeffrey and H. Van deSande, *Biochemistry*, 1975, **14**, 3787–3794.

10 D. Rodbard and A. Chrambach, *Anal. Biochem.*, 1971, **40**, 95–134.

11 D. Hanold and G. Vadamalai, in *Viroids and Satellites*, Elsevier, 2017, pp. 357–367.

12 W. H. Voige, *J. Chem. Educ.*, 1999, **76**, 35.

13 H. Schägger and G. von Jagow, *Anal. Biochem.*, 1987, **166**, 368–379.

14 C. Kachuk and A. A. Doucette, *J. Proteomics*, 2018, 175, 75–86.

15 M. M. Faas, T. Sáez and P. de Vos, *Mol. Aspects Med.*, 2017, 55, 9–19.

16 I. H. CHAUDRY, *Ann. N. Y. Acad. Sci.*, 1990, **603**, 130–140.

17 J. Hannig, B. Greenebaum, C. S. Carrillo and R. C. Lee, 2000, 60637.

18 J. L. Gordon, *Biochem. J.*, 1986, **233**, 309–19.

19 A. Johri and M. Flint Beal, *J. Pharmacol. Exp. Ther.*, 2012, **342**, 619–630.

20 C. Park and S. K. Park, *Mol. Cells*, 2012, **33**, 105.

21 J. K. Kimball, Biology Pages: ATP, https://www.biology-pages.info/A/ATP.html, (accessed 27 June 2019).

22 J. Zhang, *Encycl. Membr.*, , DOI:10.1007/978-3-642-40872-4_1789-1.

23 J. Zhang, eds. E. Drioli and L. Giorno, Springer Berlin Heidelberg, 2015, pp. 1–4.

24 M. E. Zoghbi, R. S. Cooper and G. A. Altenberg, , DOI:10.1074/jbc.M115.698498.

25 D. L. Nelson and M. M. Cox, *Lehninger Principles of Biochemistry*, 2008.

26 A. Dominguez, A. Fernandez, N. Gonzalez, E. Iglesias and L. Montenegro, *J. Chem. Educ.*, 1997, **74**, 1227–1231.

27 H. Jakubowski, BC Online: CHAPTER 1 - B. Lipids in Water, https://employees.csbsju.edu/hjakubowski/classes/ch331/lipidstruct/ollipidwater.html , (accessed 27 June 2019).

28 T. K. Hodgdon and E. W. Kaler, *Curr. Opin. Colloid Interface Sci.*, 2007, **12**, 121–128.

29 R. Guo, M. E. Compo, S. E. Friberg and K. Morris, *J. Dispers. Sci. Technol.*, 1996, **17**, 493–507.

30 V. Dhapte and P. Mehta, *St. Petersbg. Polytech. Univ. J. Phys. Math.*, 2015, **1**, 424–435.

31 A. von Saint André-von Arnim and J. McLaughlin, *Pediatr. Crit. Care*, 2011, 1058–1072.

32 H. Liu, P. Yin, S. He, Z. Sun, Y. Tao, Y. Huang, H. Zhuang, G. Zhang and S. Wei,

Biochem. Biophys. Res. Commun., 2010, **397**, 598–602.
33 J. D. Kaspersen, A. Søndergaard, D. J. Madsen, D. E. Otzen and J. S. Pedersen, *Biophys. J.*, 2017, **112**, 1609–1620.
34 Y. Moriyama, Y. Kawasaka, C. Kobayashi and K. Takeda, *Seibutsu Butsuri*, 2017, **44**, S200.
35 A. Ito and T. Ito, *Photochem. Photobiol.*, 1986, **44**, 355–8.
36 H. J. Cleaves, in *Encyclopedia of Astrobiology*, Springer Berlin Heidelberg, Berlin, Heidelberg, 2011, pp. 858–858.
37 E. R. Taylor, University of Kent, 2017.
38 P. Reinemer, L. Prade, P. Hof, T. Neuefeind, R. Huber, R. Zettl, K. Palme, J. Schell, I. Koelln, H. D. Bartunik and B. Bieseler, *J. Mol. Biol.*, 1996, **255**, 289–309.
39 J. D. Hayes, J. U. Flanagan, I. R. Jowsey and H. Flanagan Jowsey, *Annu. Rev. Pharmacol. Toxicol*, 2005, **45**, 51–88.
40 D. Sheehan, G. Meade, V. M. Foley and C. A. Dowd, *Biochem. J.*, 2001, **360**, 1–16.
41 D. M. Townsend and K. D. Tew, *Oncogene*, 2003, **22**, 7369–7375.
42 K. A. Majorek, P. J. Porebski, A. Dayal, M. D. Zimmerman, K. Jablonska, A. J. Stewart, M. Chruszcz and W. Minor, *Mol. Immunol.*, 2012, **52**, 174–182.
43 U. Anand and S. Mukherjee, *Phys. Chem. Chem. Phys*, 2013, **15**, 9375.
44 Horiba Scientific, *DT-Series Particle Characterization Analyzer ZETA POTENTIAL OF BOVINE SERUM ALBUMIN (BSA) PROTEIN*, 2009.
45 L. Vijayalakshmi, R. Krishna, R. Sankaranarayanan and M. Vijayan, *Proteins Struct. Funct. Bioinforma.*, 2008, **71**, 241–249.
46 G. Kontopidis, C. Holt and L. Sawyer, *J. Dairy Sci.*, 2004, **87**, 785–796.
47 B. Y. Qin, M. C. Bewley, L. K. Creamer, H. M. Baker, E. N. Baker and G. B. Jameson, *Structural Basis of the Tanford Transition of Bovine-Lactoglobulin †, ‡*, 1998.
48 D. E. W. Chatterton, G. Smithers, P. Roupas and A. Brodkorb, *Int. Dairy J.*, 2006, **16**, 1229–1240.
49 C. S. Tai, Y. Y. Chen and W. L. Chen, *Biomed Res. Int.*, 2016, **2016**, 1–12.
50 S. I. O'Donoghue, X. Chang, R. Abseher, M. Nilges and J. J. Led, *J.Biomol.NMR*, 2000, **16**, 93–108.
51 S. Culina, V. Brezar and R. Mallone, *Eur. J. Endocrinol.*, 2013, **168**, 19–31.
52 G. Van den Berghe, P. Wouters, F. Weekers, C. Verwaest, F. Bruyninckx, M. Schetz, D. Vlasselaers, P. Ferdinande, P. Lauwers and R. Bouillon, *N. Engl. J. Med.*, 2001, **345**, 1359–1367.
53 A. K. Niazi and S. K. Niazi, *Indian J. Endocrinol. Metab.*, 2012, **16**, S57.
54 C. Damyanov, M. Radoslavova, V. Gavrilov and D. Stoeva, *Low dose chemotherapy in combination with insulin for the treatment of advanced metastatic tumors. Preliminary experience*, 2009.
55 K. Kurpiewska, J. Font, M. Ribó, M. Vilanova and K. Lewiński, *Proteins Struct. Funct. Bioinforma.*, 2009, **77**, 658–669.
56 A. Karuturi, RNase A - 17 Need to Know Facts about Ribonuclease A - AG Scientific, http://agscientific.com/blog/2019/05/rnase-a-faq/, (accessed 7 June 2019).
57 V. A. Mitkevich, O. N. Ilinskaya and A. A. Makarov, *Cell Cycle* , 2015, **14**, 931–932.
58 V. A. Proctor, F. E. Cunningham and D. Y. C. Fung, *C R C Crit. Rev. Food Sci. Nutr.*, 1988, **26**, 359–395.
59 B. K. Shoichet, W. A. Baase, R. Kuroki and B. W. Matthews, *Proc. Natl. Acad. Sci.*, 1995, **92**, 452–456.
60 S. A. Ragland and A. K. Criss, *PLoS Pathog.*, 2017, 13.
61 T. Wu, C. Wu, S. Fu, L. Wang, C. Yuan, S. Chen and Y. Hu, *Carbohydr. Polym.*, 2017, **155**, 192–200.
62 C. Pleyer, J. Flesche and F. Saeed, *Clin. Nephrol. Case Stud.*, 2015, **3**, 42–45.
63 N. Alkudaisi, B. A. Russell, D. J. S. Birch and Y. Chen, *J. Photochem. Photobiol. B Biol.*, 2019, **197**, 111540.
64 V. Gdovinová, N. Tomašovičová, I. Batko, M. Batková, L. Balejčíková, V. M. Garamus, V. I. Petrenko, M. V. Avdeev and P. Kopčanský, *J. Magn. Magn. Mater.*, 2017, **431**, 8–11.
65 Malvern Instruments Ltd., *Dynamic Light Scattering: An introduction in 30 minutes.*, .
66 J. Stetefeld, S. A. Mckenna and T. R. Patel, *Biophys. Rev.*, 2016, **8**, 409–427.

67 J. Panchal, J. Kotarek, E. Marszal and E. M. Topp, *AAPS J.*, 2014, **16**, 440–51.
68 D. Fairhurst, An Overview of the Zeta Potential - Part 2: Measurement | American Pharmaceutical Review - The Review of American Pharmaceutical Business & Technology, https://www.americanpharmaceuticalreview.com/Featured-Articles/134634-An-Overview-of-the-Zeta-Potential-Part-2-Measurement/, (accessed 24 August 2019).
69 N. J. Adamson and E. C. Reynolds, *J. Chromatogr. B Biomed. Sci. Appl.*, 1997, **699**, 133–147.
70 Applied Photophysics, *An introduction to circular dichroism spectroscopy*, .
71 A. J. Adler, N. J. Greenfield and G. D. Fasman, *Methods Enzymol.*, 1973, **27**, 675–735.
72 B. Kumar Paul, D. Ray and N. Guchhait, *Phys. Chem. Chem. Phys*, 2013, **15**, 1275.
73 N. J. Greenfield, *Nat. Protoc.*, 2006, **1**, 2876–90.
74 T. D. Goddard, C. C. Huang and T. E. Ferrin, *J. Struct. Biol.*, 2007, **157**, 281–287.
75 W. Kabsch and C. Sander, *Biopolymers*, 1983, **22**, 2577–2637.
76 *Chimera User's Guide*, .
77 E. Gasteiger, C. Hoogland, A. Gattiker, S. Duvaud, M. R. Wilkins, R. D. Appel and A. Bairoch, in *The Proteomics Protocols Handbook*, ed. J. M. Walker, Humana Press, Totowa, NJ, 2005, pp. 571–607.
78 S. Salgın, U. Salgın and S. Bahadır, *Zeta Potentials and Isoelectric Points of Biomolecules: The Effects of Ion Types and Ionic Strengths*, 2012, vol. 7.
79 E. Kenndler and N. M. Maier, *Capill. Electromigr. Sep. Methods*, 2018, 69–111.
80 Lonza, *Mol. Biol. Res. Prod. Cat. Sourceb. Electrophor.*, 2001, 195–202.
81 A. Adel, M. Nadia, O. Mohamed and G. Abdelhafidh, *Mater. Sci. Eng. C*, 2008, **28**, 594–600.
82 D. I. Lipin, L. H. L. Lua and A. P. J. Middelberg, *J. Chromatogr. A*, 2008, **1190**, 204–214.
83 R. W. Murphy, B. E. Farkas and O. G. Jones, *J. Colloid Interface Sci.*, 2017, **505**, 736–744.
84 S. I. Takata, T. Norisuye, N. Tanaka and M. Shibayama, *Macromolecules*, 2000, **33**, 5470–5475.
85 H. Komatsu, A. Kitajima, Y. Nakata and S. Okada, *Chem. Pharm. Bull.*, 1996, **44**, 1966–1969.
86 S. Falke, K. Dierks, C. Blanchet, M. Graewert, F. Cipriani, R. Meijers, D. Svergun and C. Betzel, *Multi-channel in situ dynamic light scattering instrumentation enhancing biological small-angle X-ray scattering experiments at the PETRA III beamline P12*, .
87 Y. Zhang, E. Farrell, D. Mankiewicz and Z. Weiner, Study of Protein Hydrodynamics with Light Scattering: Size and Charge of Lysozyme - Brookhaven Instruments, https://www.brookhaveninstruments.com/study-of-protein-hydrodynamics-with-light-scattering-size-and-charge-of-lysozyme/, (accessed 4 March 2021).
88 C. Di Ilio, A. Aceto, R. Piccolomini, N. Allocati, A. Faraone, L. Cellini, G. Ravagnan and G. Federici, *Biochem. J.*, 1988, **255**, 971–975.
89 S. Paul, N. Sepay, S. Sarkar, P. Roy, S. Dasgupta, P. Saha Sardar and A. Majhi, *New J. Chem.*, 2017, **41**, 15392–15404.
90 F. Ye, Y. An, D. Qin, L. Yang, L. She and R. Xing, *Guang Pu Xue Yu Guang Pu Fen Xi*, 2007, **27**, 321–324.
91 K. Takeda, M. Miura and T. Takagi, *J. Colloid Interface Sci.*, 1981, **82**, 38–44.
92 M. I. Viseu, T. I. Carvalho and S. M. B. Costa, .
93 D. Hamada, S. Segawa and Y. Goto, *Nat. Struct. Biol. 1996 310*, 1996, **3**, 868–873.
94 S. P. WOOD, T. L. BLUNDELL, A. WOLLMER, N. R. LAZARUS and R. W. J. NEVILLE, *Eur. J. Biochem.*, 1975, **55**, 531–542.
95 S. W. Provencher and J. Glöckner, *Biochemistry*, 1981, **20**, 33–37.
96 R. T. Raines, *Chem. Rev.*, 1998, **98**, 1045–1065.
97 T. Knubovets, J. J. Osterhout, P. J. Connolly and A. M. Klibanov, *Proc. Natl. Acad. Sci. U. S. A.*, 1999, **96**, 1262–1267.
98 A. Mirazimi and L. Svensson, *ATP Is Required for Correct Folding and Disulfide Bond Formation of Rotavirus VP7 Downloaded from*, 2000, vol. 74.
99 H. Schägger, *Nat. Protoc.*, , DOI:10.1038/nprot.2006.4.

100 C. A. Grattoni, H. H. Al-Sharji, C. Yang, A. H. Muggeridge and R. W. Zimmerman, *J. Colloid Interface Sci.*, 2001, **240**, 601–607.
101 (No Title), https://people.clarkson.edu/~skrishna/DHR_Rheology_Theory.pdf, (accessed 4 March 2021).
102 S. Carrara, Universite de Marseille, 2017.
103 C. Cao, Z. L. Zhou, L. D. Cao, L. Zheng, J. Xu, F. M. Li and Q. L. Huang, *Soft Matter*, 2018, **14**, 6070–6075.
104 M. Lebendiker and H. Shagger, PAGE-SDS Laemmli Protocol, http://wolfson.huji.ac.il/purification/Protocols/Tricine.html, (accessed 5 January 2019).
105 E. Gout, F. Rébeillé, R. Douce and R. Bligny, , DOI:10.1073/pnas.1406251111.
106 D. Khyati, City University of New York, 2012.
107 J. C. Quintanilla de Stéfano, V. Abundis-Correa, S. D. Herrera-Flores and A. J. Alvarez, *Polymers (Basel).*, 2020, **12**, 1974.
108 Amplitude sweeps :: Anton Paar Wiki, https://wiki.anton-paar.com/uk-en/amplitude-sweeps/, (accessed 4 March 2021).
109 H. E. Park, N. Gasek, J. Hwang, D. J. Weiss and P. C. Lee, *Phys. Fluids*, 2020, **32**, 033102.
110 R. Rucher and M. D. Brager, *Anal. Biochem.*, 1975, **6**, 415–428.
111 S. Stamova, I. Michalk, H. Bartsch and M. Bachmann, *Methods Mol. Biol.*, 2012, **869**, 433–436.
112 B. B. Samal, *Anal. Biochem.*, 1987, **163**, 42–44.
113 G. D. Heda, *Biotechniques*, 2021, **70**, 54–57.
114 M. Scimeca, S. Bischetti, H. K. Lamsira, R. Bonfiglio and E. Bonanno, *Eur. J. Histochem.*, 2018, **62**, 89–99.
115 P. Damberg, J. Jarvet and A. J. Gräslund, in *Methods in Enzymology*, Academic Press Inc., 2001, vol. 339, pp. 271–285.
116 M. Okubo, M. Fujimura and T. Mori, *Colloid Polym. Sci.*, 1991, **269**, 121–123.
117 P. J. Fitzpatrick, T. O. B. Krag, P. Hojrup and D. Sheehan, *Biochem. J.*, 1995, **305**, 145–150.
118 M. Ono, H. Watanabe, Y. Ikehata, N. Ding, M. Yoshimura, K. Sano and H. Saji, *Sci. Rep.*, 2017, **7**, 1–11.
119 L. K. Creamer, S. M. Loveday and L. Sawyer, in *Encyclopedia of Dairy Sciences: Second Edition*, Elsevier Inc., 2011, pp. 787–794.
120 S. M. Loveday and L. Sawyer, in *Reference Module in Food Science*, Elsevier, 2016.
121 C. J. Fee, J. M. Billakanti and S. M. Saufi, in *Separation, Extraction and Concentration Processes in the Food, Beverage and Nutraceutical Industries*, Elsevier Ltd, 2010, pp. 450–482.
122 C. E. Olivier, S. L. S. Lorena, C. R. Pavan, R. A. P. G. Dos Santos, R. P. D. S. Lima, D. G. Pinto, M. D. Da Silva and R. D. L. Zollner, *Allergy Asthma Proc.*, 2012, **33**, 432–436.
123 M. F. Dunn, in *BioMetals*, Springer, 2005, vol. 18, pp. 295–303.
124 M. Weiss, D. F. Steiner and L. H. Philipson, *Insulin Biosynthesis, Secretion, Structure, and Structure-Activity Relationships*, MDText.com, Inc., 2000.
125 C. Manoharan and J. Singh, *Polymers (Basel).*, 2015, **7**, 836–850.
126 G. Thiagarajan, J. Lakshmanan, M. Chalasani and D. Balasubramanian, *Investig. Ophthalmol. Vis. Sci.*, 2004, **45**, 2115–2121.
127 C. Rivera, J. Rosales, J. Freites-Perez and E. Rodriguez, *BIO-PROTOCOL*, , DOI:10.21769/bioprotoc.3093.
128 A. Rath, F. Cunningham and C. M. Deber, *Proc. Natl. Acad. Sci. U. S. A.*, 2013, **110**, 15668–15673.
129 S. Thakur K and E. SV, *J. Anal. Bioanal. Tech.*, 2017, **08**, 1–7.

APPENDIX

Section 1: Dynamic Light Scattering: Intensity by Number, by Volume and Correlation Function

1. Glutathione S – Transferase

Frequency by Volume (%)

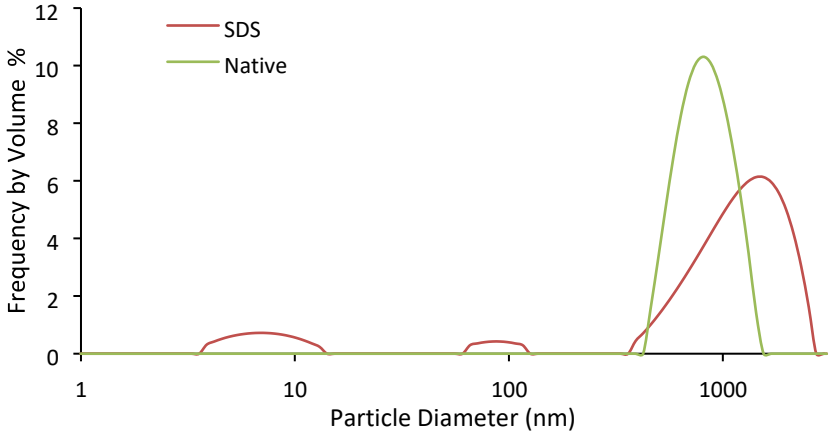

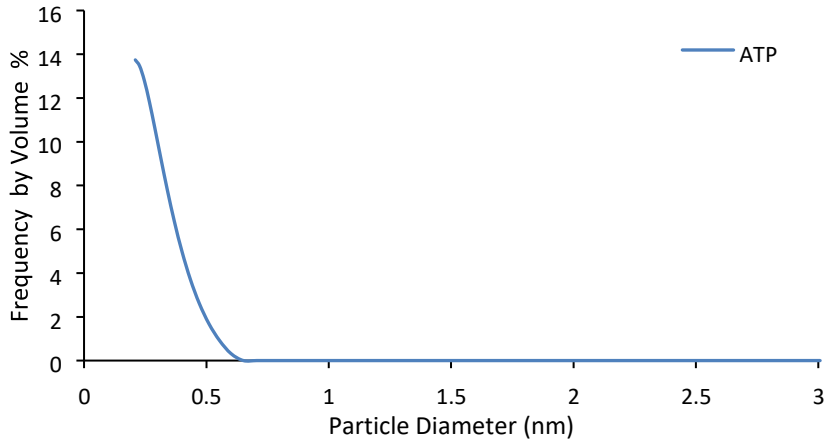

Frequency by Intensity (%)

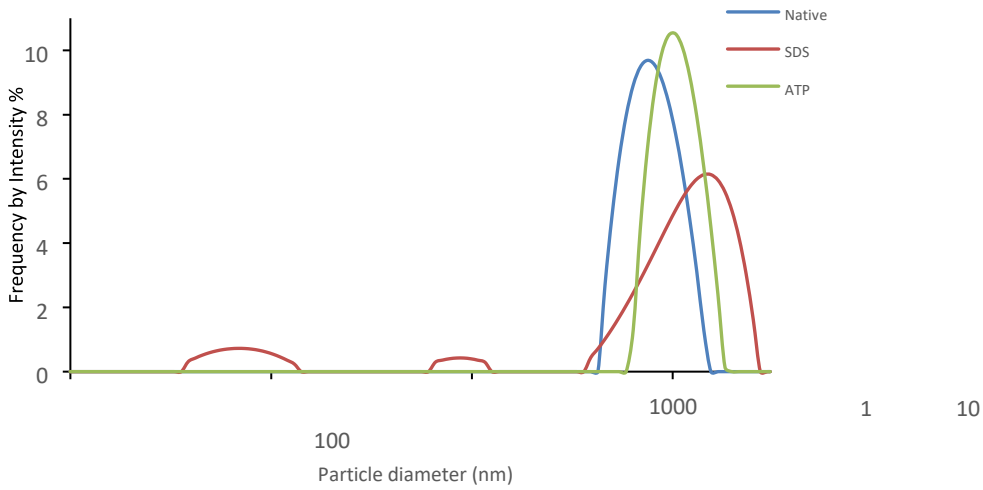

Native GST Correlation Function

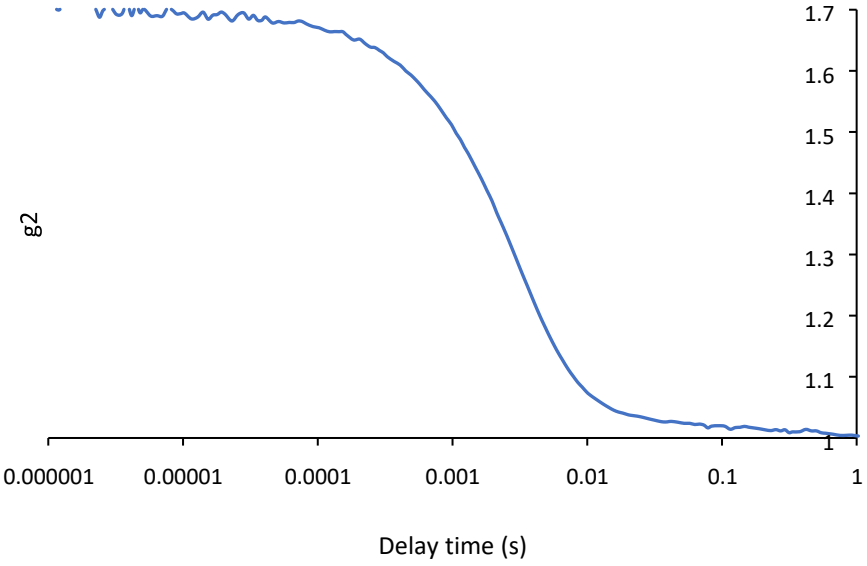

SDS GST Correlation Function

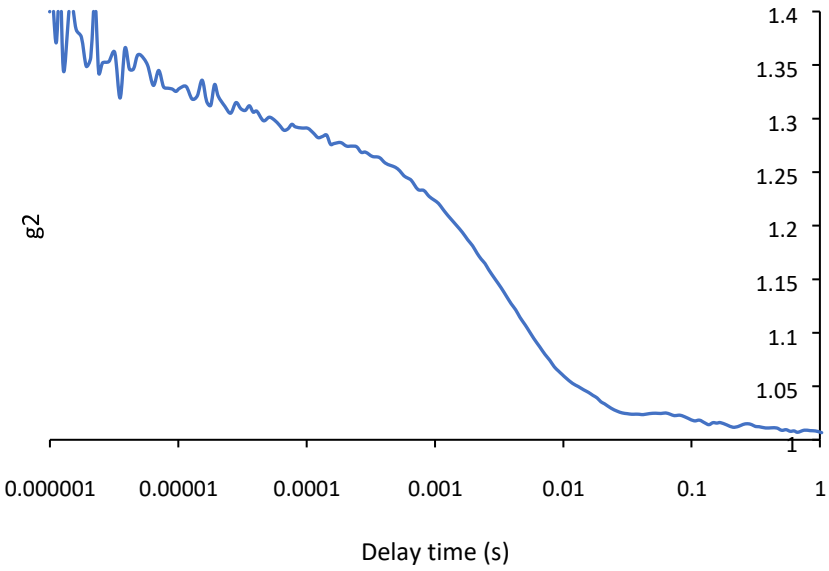

ATP GST Correlation Function

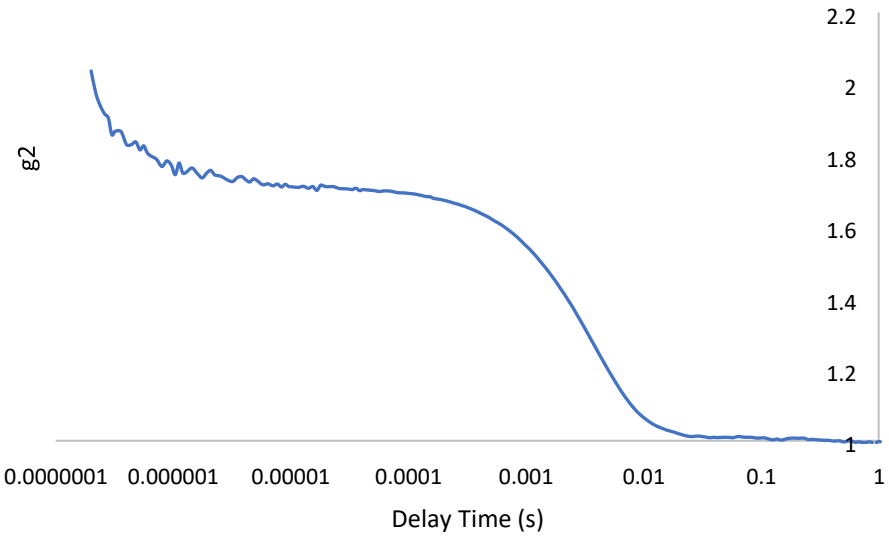

2. Bovine Serum Albumin

Frequency by Volume (%)

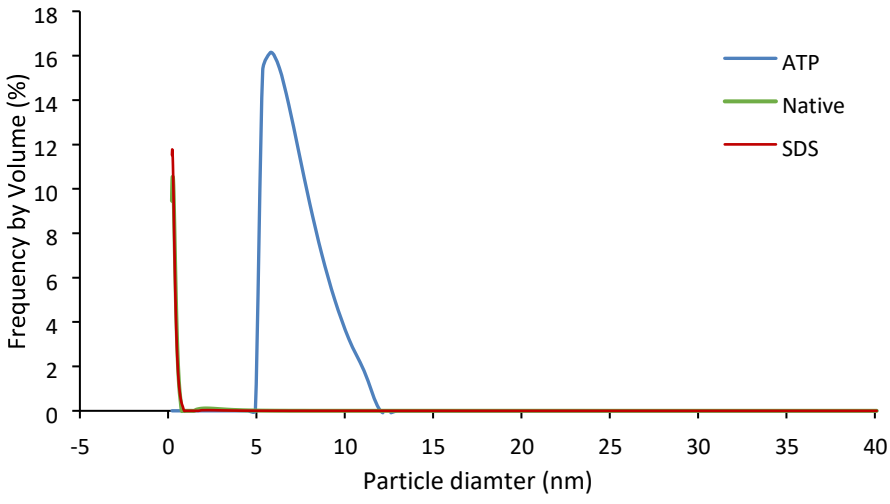

Frequency by Intensity (%)

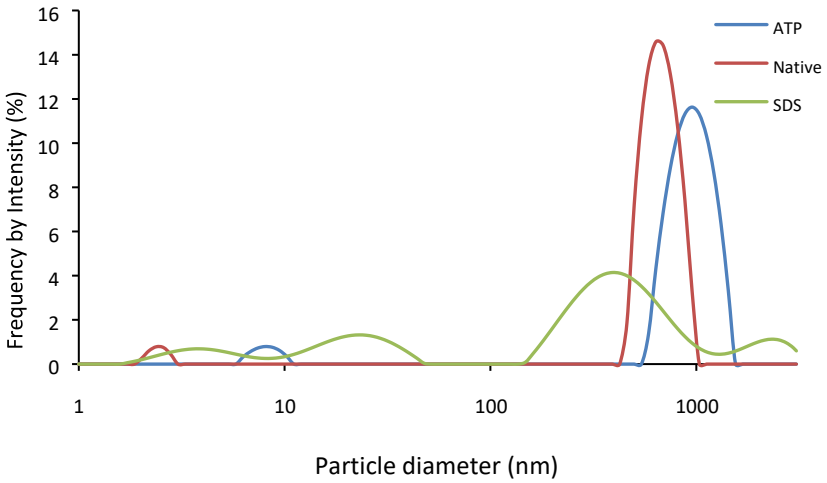

Native BSA Correlation Function

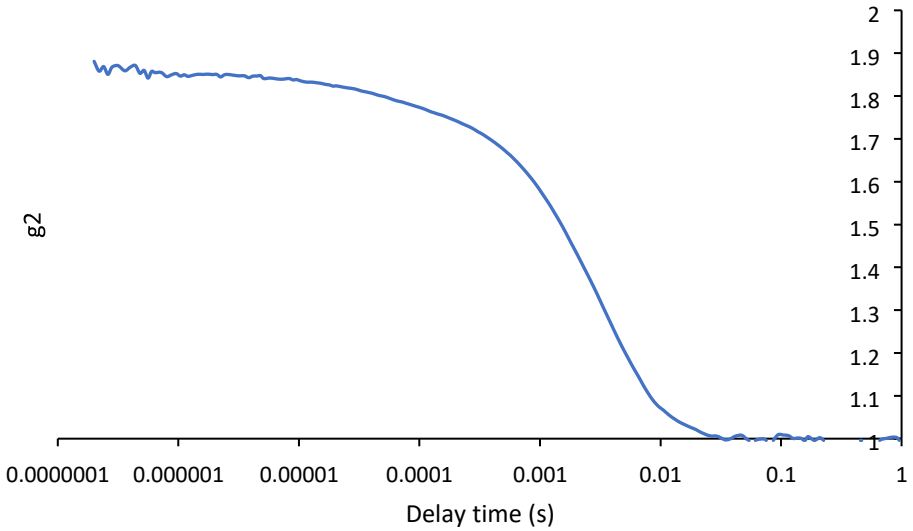

ATP BSA Correlation Function

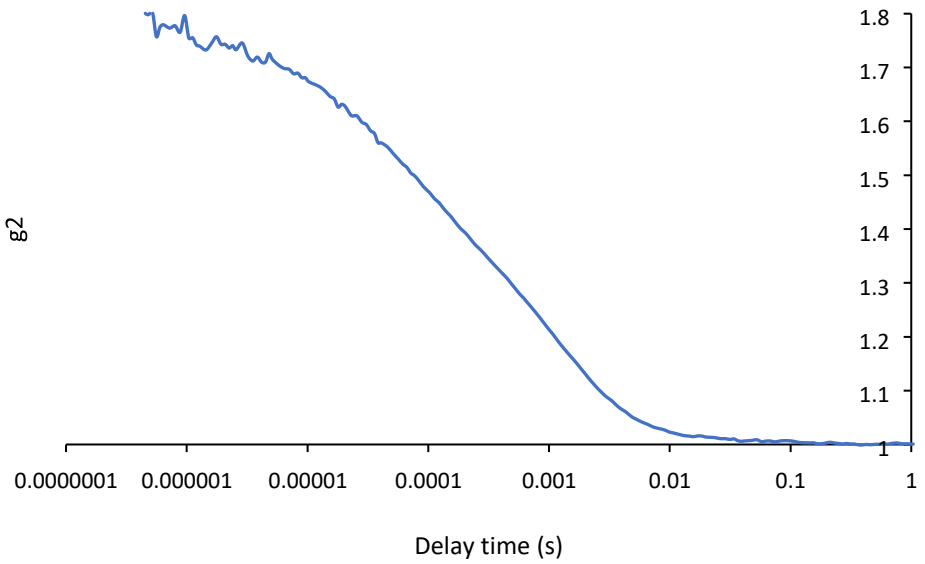

SDS BSA Correlation Function

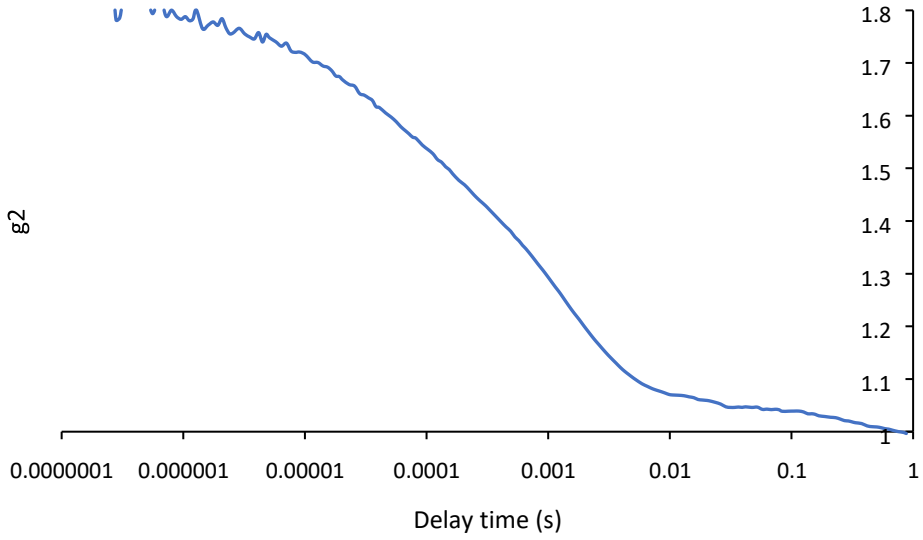

3. β- Lactoglobulin

Frequency by Volume (%)

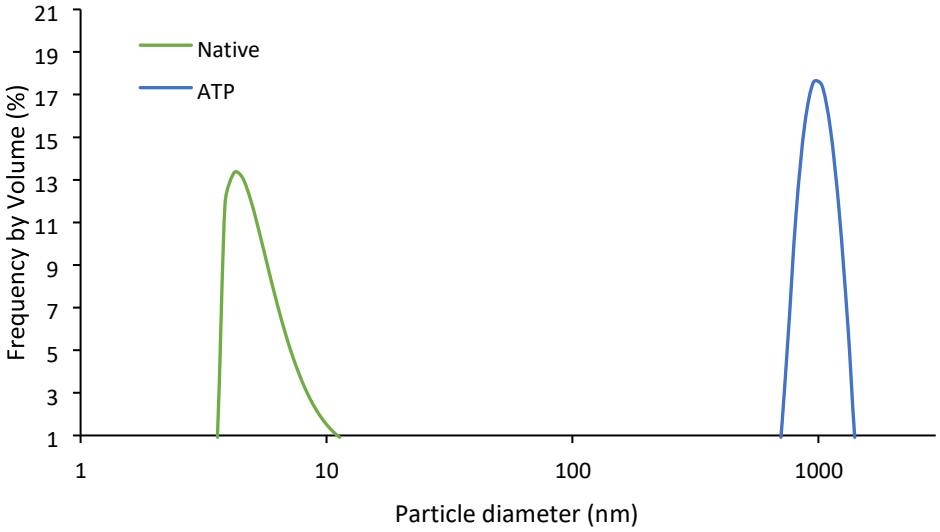

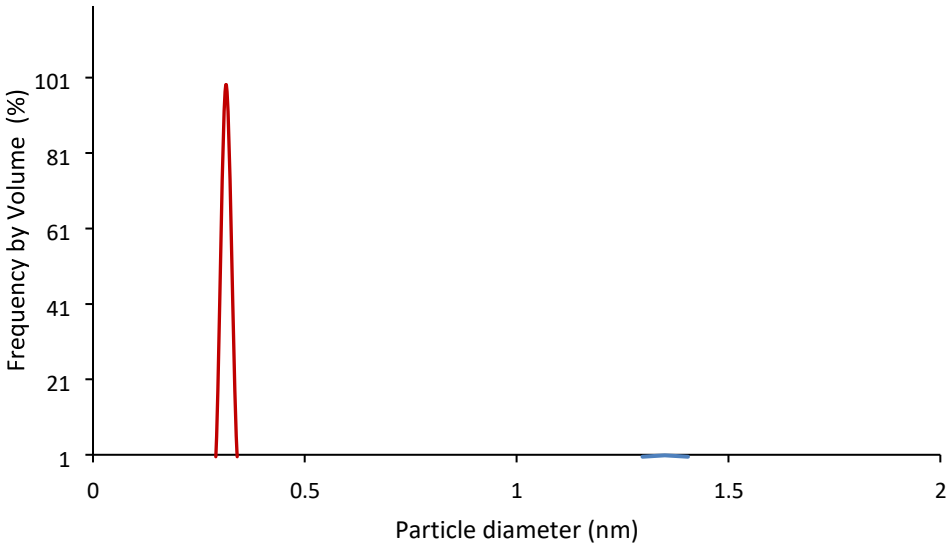

Frequency by Intensity (%)

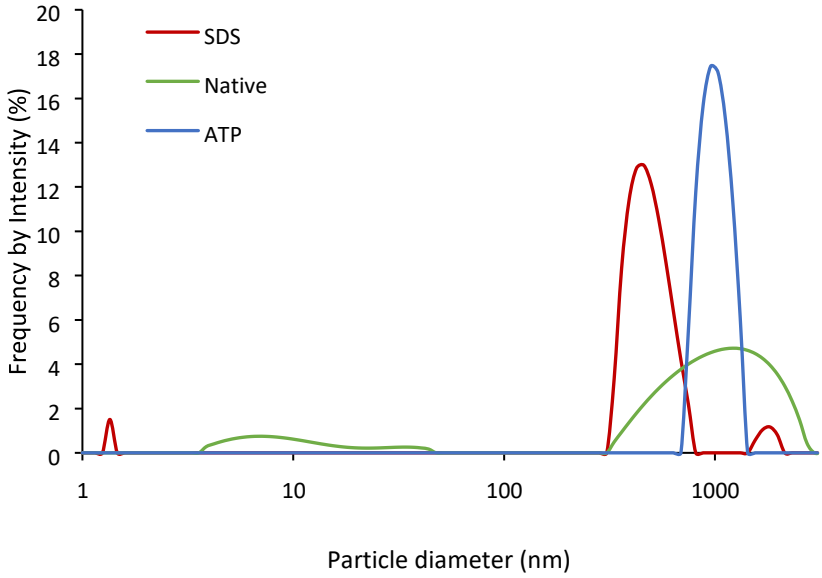

Native BLG Correlation Function

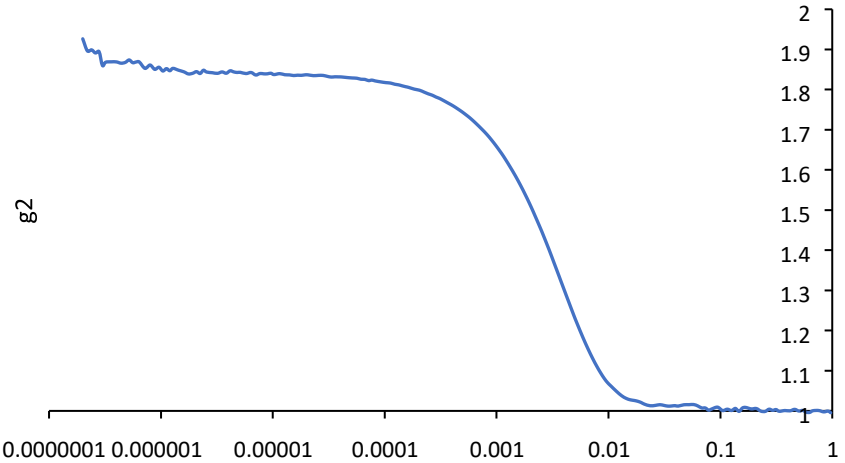

ATP BLG Correlation Function

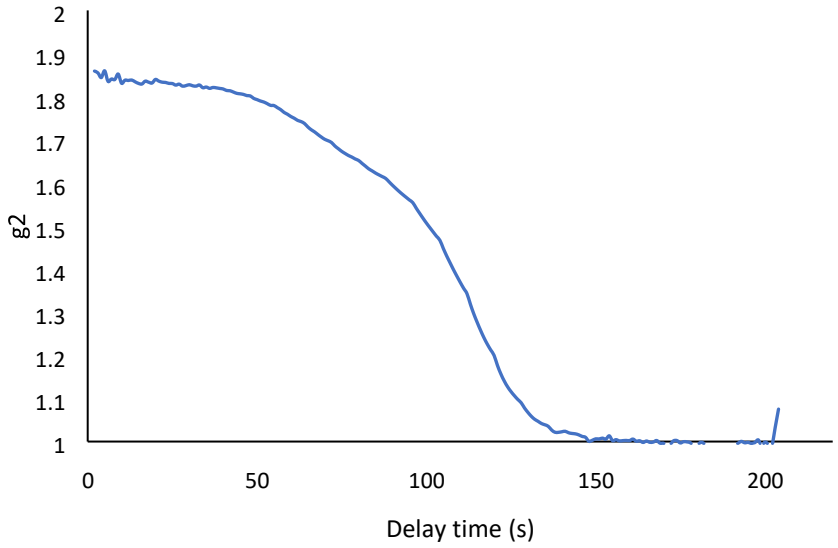

SDS BLG Correlation Function

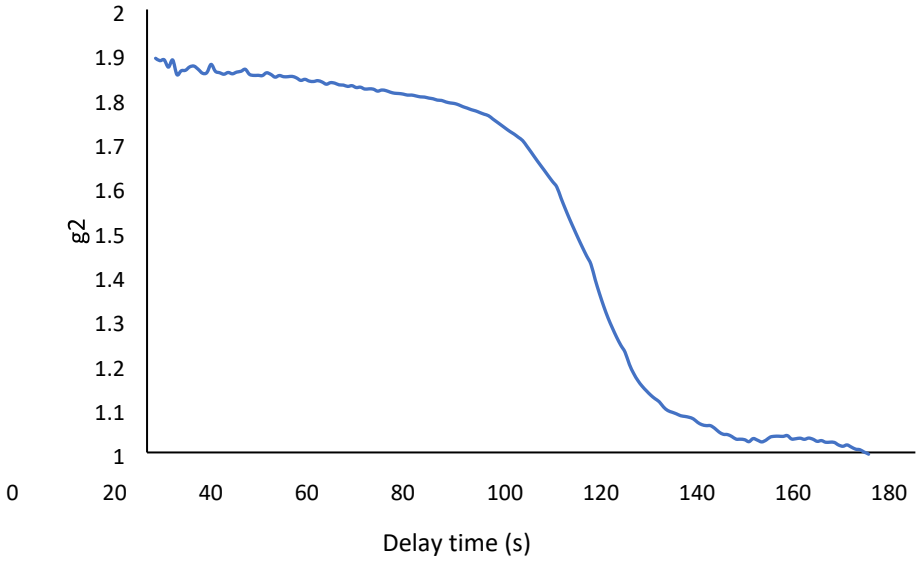

4. Insulin

Frequency by Volume (%)

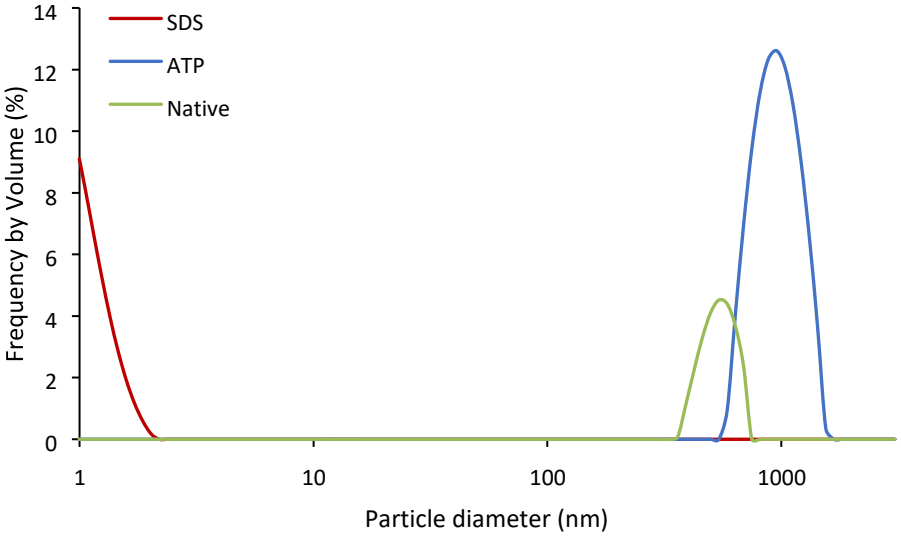

Frequency by Intensity (%)

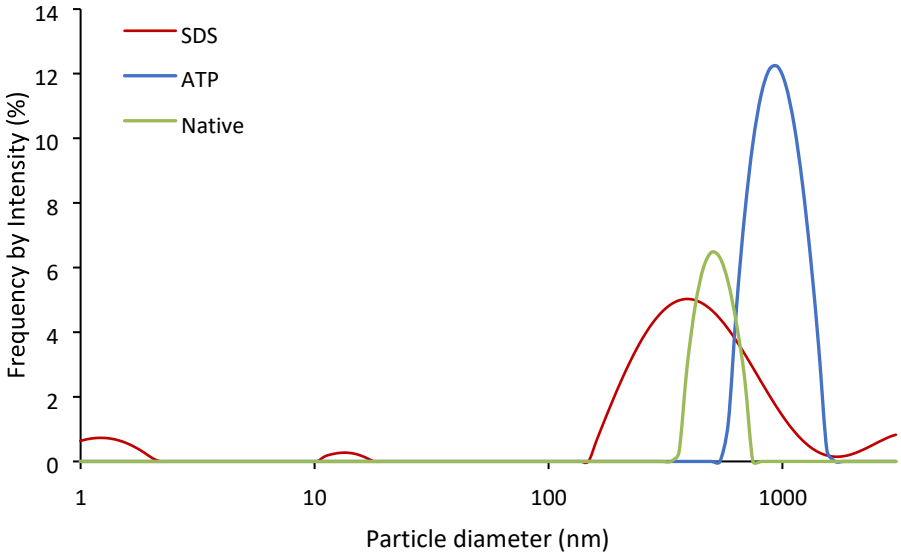

Native INS Correlation Function

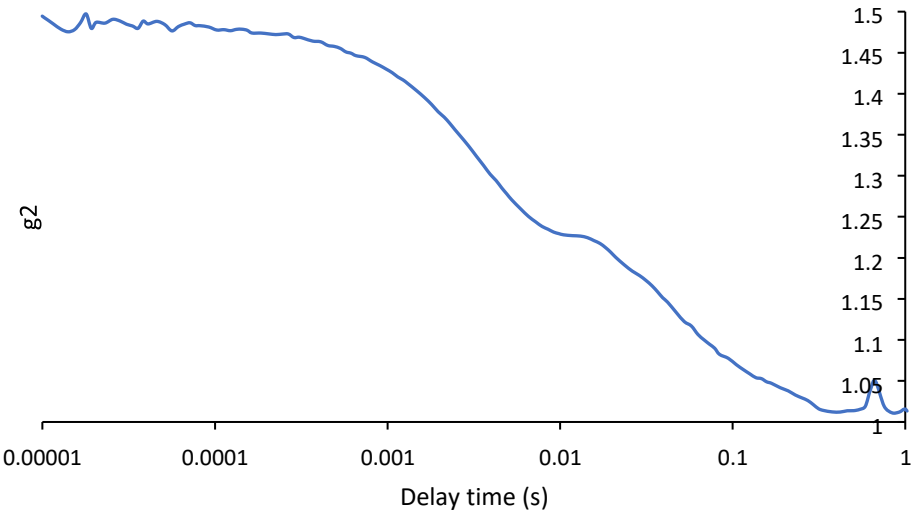

ATP INS Correlation Function

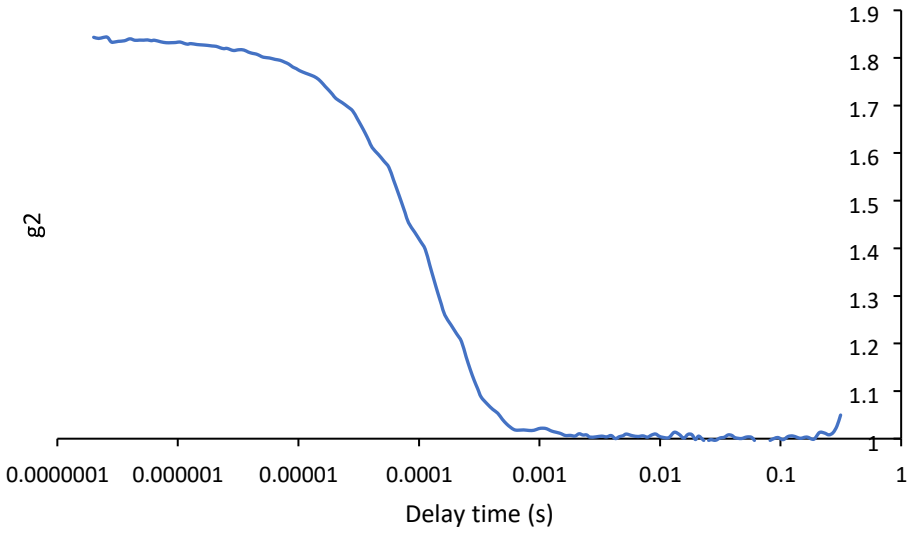

SDS INS Correlation Function

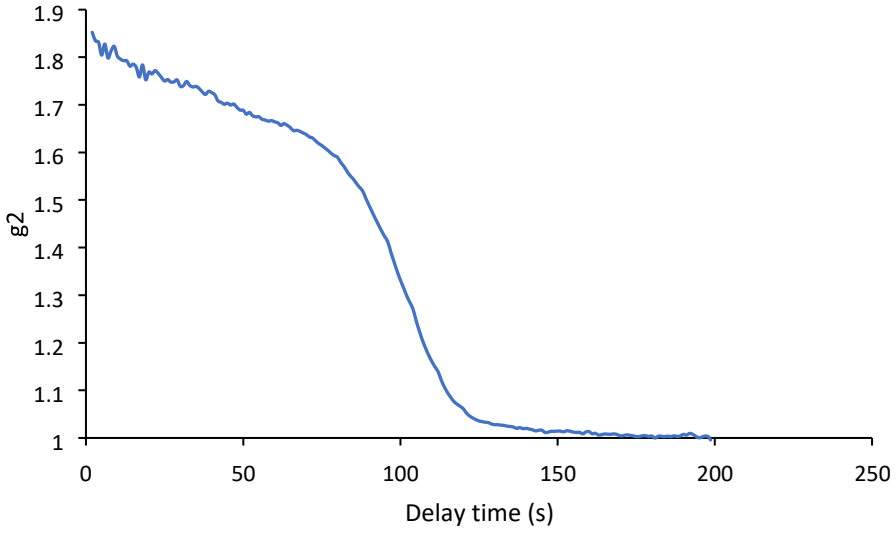

5. RNAse A

Frequency by Volume (%)

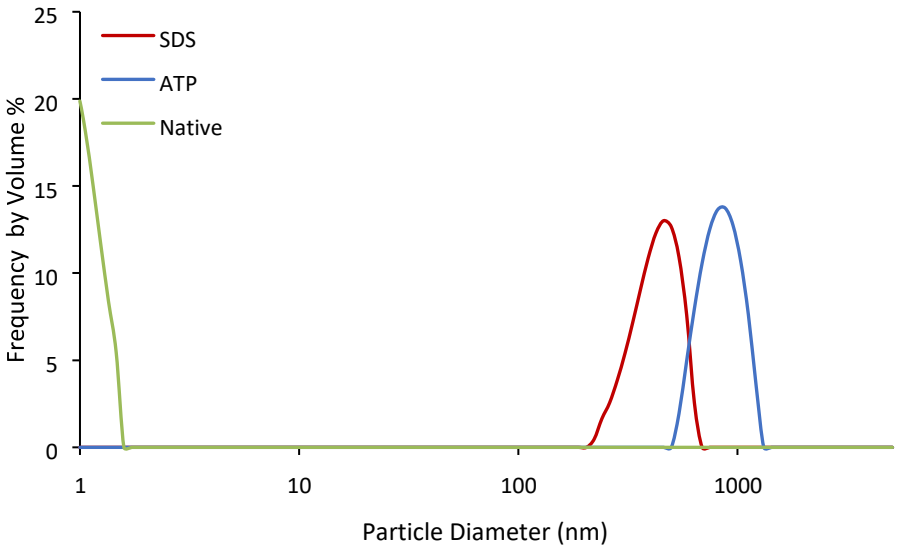

Frequency by Intensity (%)

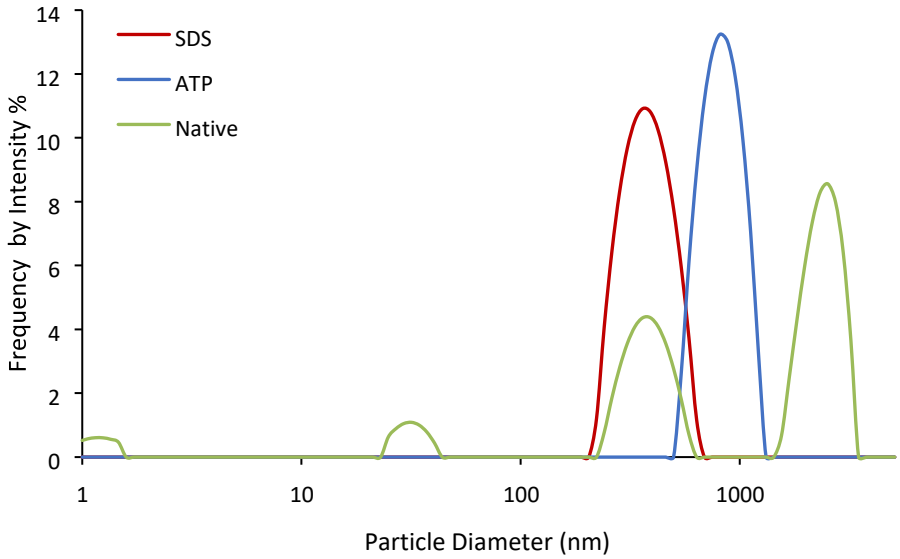

Native RNase A Correlation Function

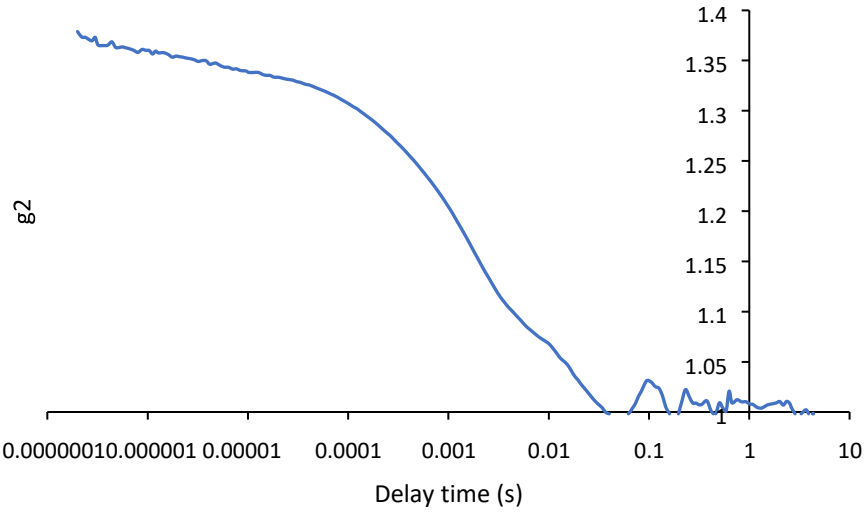

ATP RNAse A Correlation Function

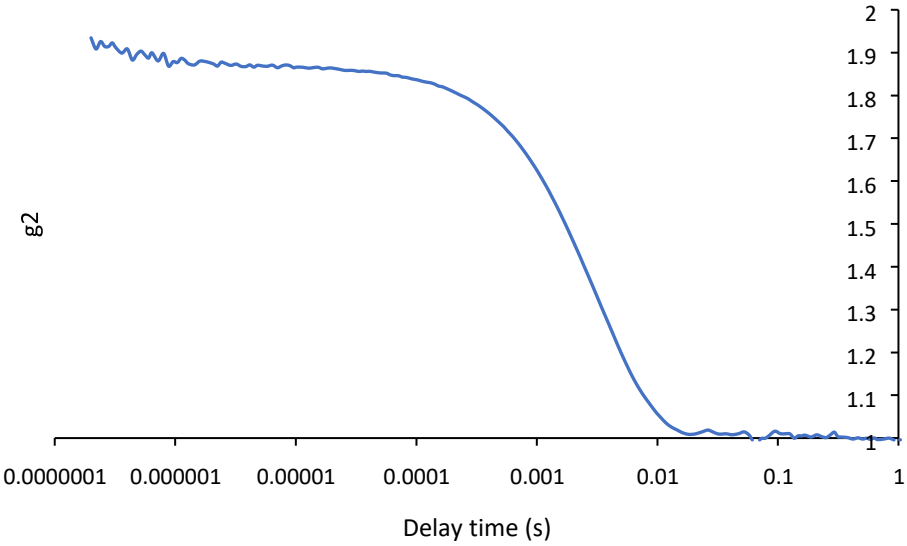

SDS RNase A Correlation Function

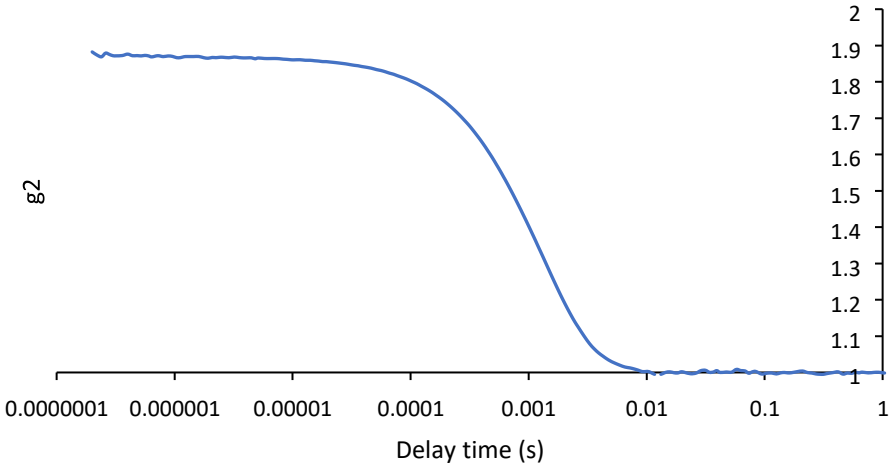

6. Lysozyme

Frequency by Volume (%)

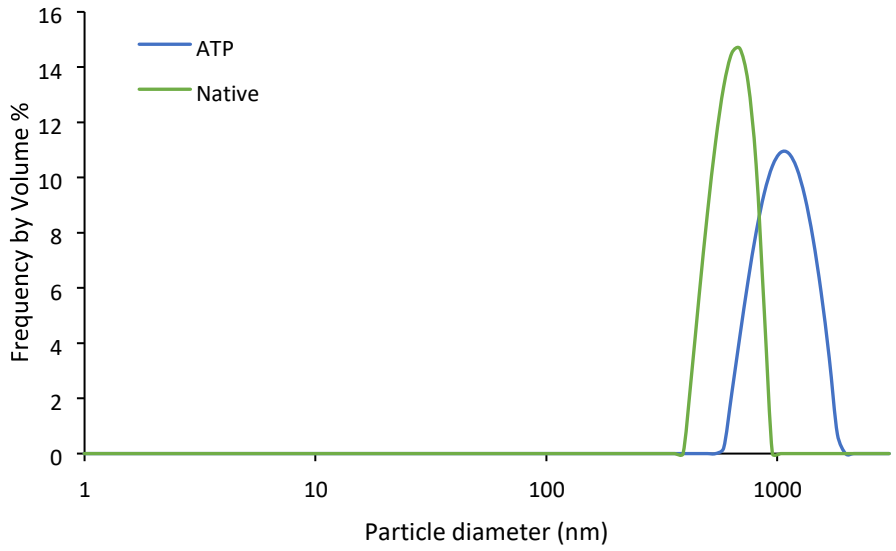

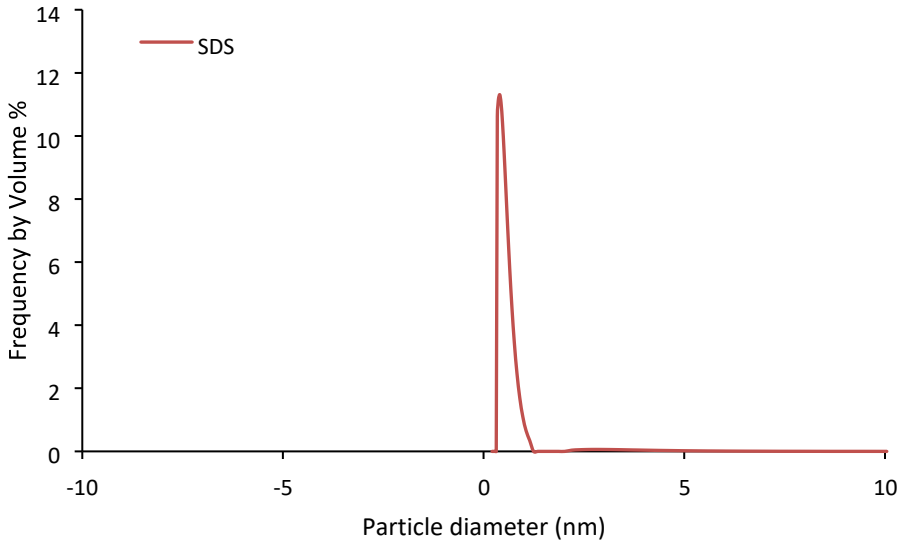

Frequency by Intensity (%)

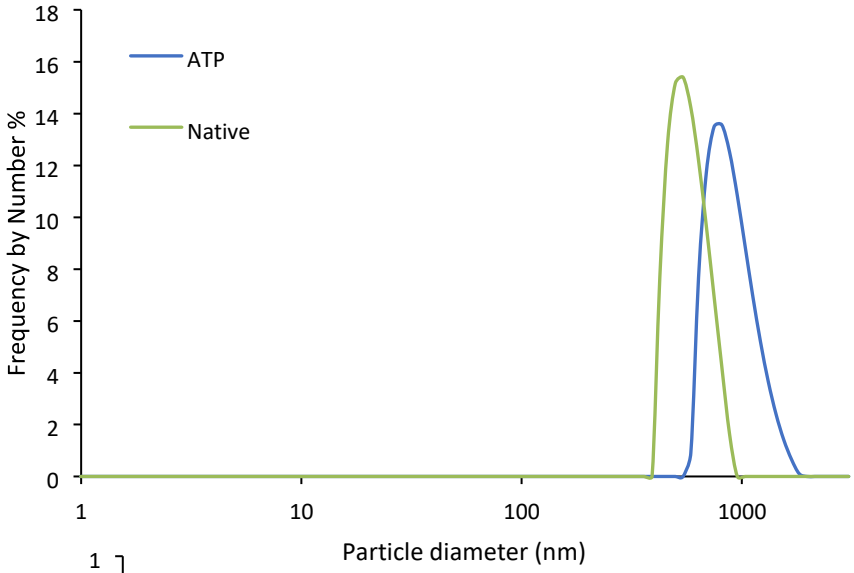

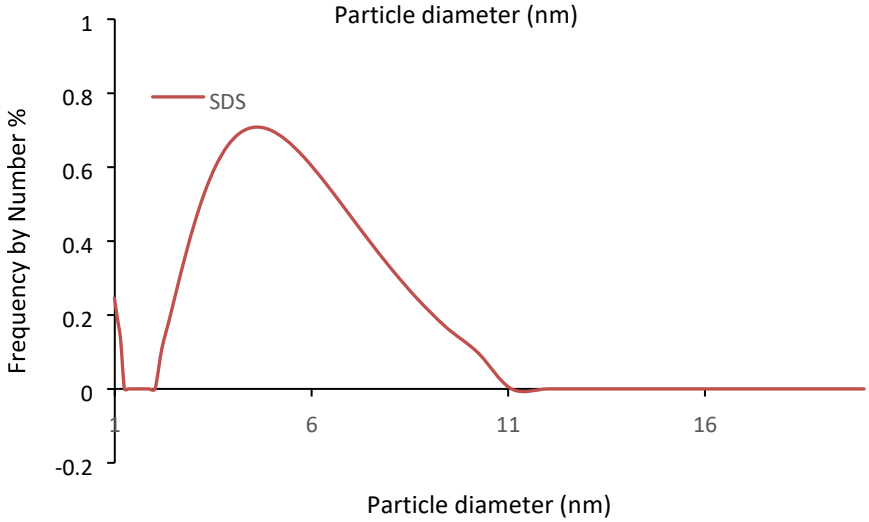

Native Lysozyme A Correlation Function

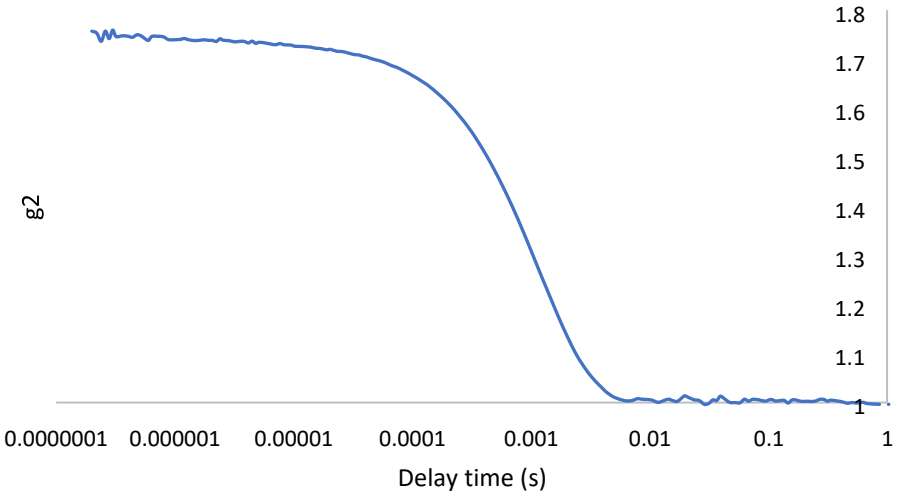

ATP Lysozyme Correlation Function

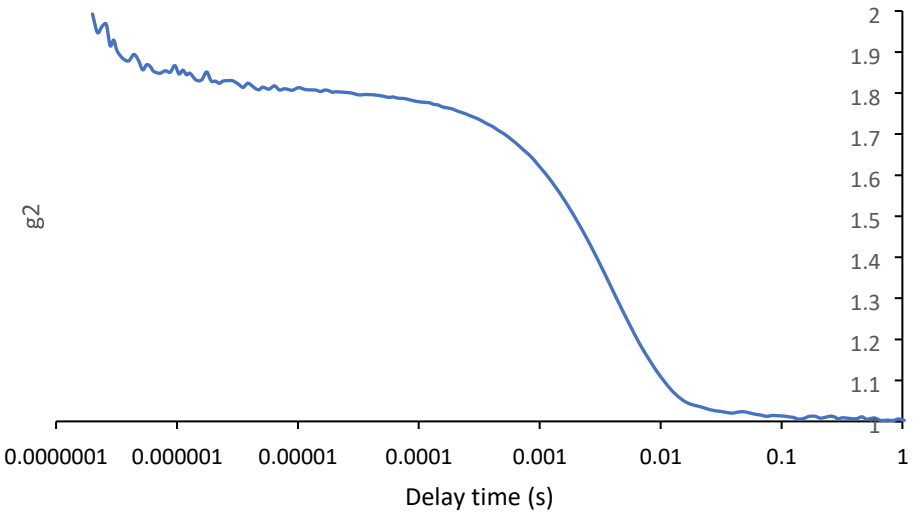

SDS Lysozyme Correlation Function

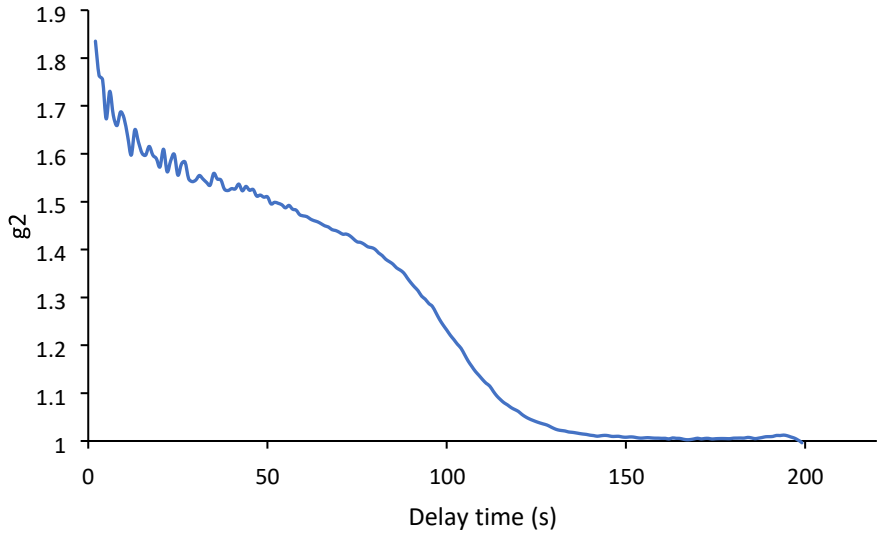

Section 2: RNA-RNAse A Binding Assay Method 1

This assay was done on both a 10% and 20% TBE denaturing gel. The 10% gel was made by adding 2.5 mL of 20% TBE stock, 2.5 mL 1x TBE fresh buffer, 5 µl TEMED and 10 µl of 40% APS in a 15mL Falcon tube, and then pouring into glass plates and allowing to polymerise with the well comb inserted. The 20% gel was made by mixing 5 mL 20% TBE Stock with 5 µl TEMED and 10 µl 40% APS into a Falcon tube, followed by pouring into glass plates and allowing to polymerise after placing the well comb. The RNA strand used was 15 bases long and bought from Integrated DNA Technologies (IDT), with the following sequence:

5' - rCrUrC rUrCrU rCrUrC rUrCrU rCrUrC - 3'

The samples loaded onto the gels were the same, and in the following order: Low Molecular Weight Ladder (5-300bp), four controls consisting of DNA T5, RNA, RNA + SDS and RNA + ATP and finally the RNA+RNAse complexes, in native form, with SDS and with ATP. The addition of a native and SDS samples was done to provide not only a control for the assay, but to provide comparability with the sample conditions used throughout the project.

The DNA2 T5 sequence was as follows:

5' TTT TTC AGT TGA CCA TAC AG 3'

The gels were run at constant 15mAmps, 300V for 1 hour.